RECENT ADVANCES IN NATURAL AND ENGINEERING SCIENCES

Editors

Murat Oduncuoglu
Halil Ibrahim Kurt

Natural Sciences

RECENT ADVANCES IN NATURAL AND ENGINEERING SCIENCES

Editors
Murat Oduncuoglu
Halil Ibrahim Kurt

LIVRE DE LYON
Lyon 2023

RECENT ADVANCES IN NATURAL AND ENGINEERING SCIENCES

Editors
Murat Oduncuoglu
Halil Ibrahim Kurt

LIVRE DE LYON
Lyon 2023

Recent Advances in Natural and Engineering Sciences

Editors • Prof. Dr. Murat Oduncuoglu • Orcid: 0000-0002-3130-5646
Assoc. Prof. Dr. Halil Ibrahim Kurt • Orcid: 0000-0002-5992-8853
Cover Design • Motion Graphics
Book Layout • Motion Graphics
First Published • March 2023, Lyon

ISBN: 978-2-38236-529-8

Publisher • Livre de Lyon
Address • 37 rue marietton, 69009, Lyon France
website • http://www.livredelyon.com
e-mail • livredelyon@gmail.com

PREFACE

Recently the growing interest in interdisciplinary studies has brought scientists together from Science and Engineering and increased the demand for these studies. Disciplinary and/or interdisciplinary studies allow for synthesis of ideas and the synthesis of characteristics from many disciplines. At the same time it addresses scientists, engineers and students' individual differences and helps to develop important, transferable skills. These skills, like critical thinking, communication, analysis, interpretation and discussion are important and continually developing at all stages of life.

This book is intended to provide a comprehensive works of the science and engineering studies in the multi-disciplines. One of the major aims of this book is to present evidence and gathers together the results of research and development carried out on the engineering applications during recent years. It includes discussion of the factors that affect those properties. It is also beyond the scope of this book to provide more than generalized properties- of the different application. The book project brought together scientists and engineers involved in assessing the various engineering areas, with particular emphasis on academic studies, applications and opinions.

Prof. Dr. Murat Oduncuoglu
Assoc. Prof. Dr. Halil Ibrahim Kurt

CONTENTS

CHAPTER I

SODIUM LAURYL SULFATE AS A SURFACTANT USED TO ENHANCE THE SOLUBILITY OF POORLY WATER-SOLUBLE DRUGS BY MICELLAR SOLUBILIZATION

ABDULKADER ALHUSAINI[1] & MUSTAFA SINAN KAYNAK[2]

[1]Department of Pharmaceutical Technology, Institute of Health Sciences Anadolu University, e-mails:abdulkaderalhusaini@anadolu.edu.tr, abdelqader.alhusini@gmail.com ORCID: 0009-0006-5408-4280

[2](Assoc. Prof. Dr.), Department of Pharmaceutical Technology, Faculty of Pharmacy, Anadolu University, e-mail:msk@anadolu.edu.tr ORCID: 0000-0003-2917-2407

1. Introduction

Due to its high patient compliance and low manufacturing cost, the oral route is the most widely used and convenient method of drug administration. However, the major challenge of developing an oral dosage form is the low oral bioavailability of many drugs due to their low solubility or permeability. In the pharmaceutical industry, most of the chemical substances (more than 40%) which is under development are practically insoluble in water (Savjani et al., 1957). one of the most common techniques used to improve the solubility of poorly water-soluble drugs is using surfactants, which are responsible to form what is called the micelles (colloidal-sized clusters in solutions), which by turn increase the solubility of drugs with low-solubility in water (de Oliveira Rangel Yagui et al., 2005; Torchilin, 2006).

2. The Solubility and Dissolution Rate

The solubility of a material in a solvent is defined as the maximum quantity of the compound in its most stable crystalline form which can remain in the solution under equilibrium conditions in a certain volume of the solvent and at a certain temperature and pressure (Jain & Yalkowsky, 2001; Yalkowsky & Valvani, 1980).

There are numerous techniques have been used to improve the solubility of poorly water-soluble drugs, including the use of certain organic solvents (Jouyban, 2008), adding surfactants to the formulations (Chaudhari & Dugar, 2017), adjustment of the formulation pH, formation of salts of drug compounds (Allen & Ansel, 2013), using liposomes (Lasic & Papahadjopoulos, 1998), microemulsions (Constantinides et al., 2000), and cyclodextrins (Vyas et al., 2008).

Dissolution of the drug from the oral dosage form is often the rate-limiting step of absorption of drugs from the gastrointestinal (GI) tract. Many factors affect the dissolution rate of the drugs including the drug solubility in GI fluids, and the particle size of the drug which determines the drug's surface area which in turn demonstrates its ability to be wetted by GI fluids, In addition to the viscosity of the GI fluids. Solubility of the drug in the GI fluids is affected by aqueous solubility, crystalline and amorph form, the lipophilicity of the drug, solubilization by biosurfactants and co-ingested foodstuffs, and pKa of drugs (Hörter & Dressman, 1997).

3. The Micelles in Pharmaceuticals

Micelles in Pharmaceutical industries are Known as drug carriers, which provide several advantages for drugs since they can minimize drug degradation and loss, increase drug bioavailability by increasing its solubility or permeability through the biological barriers, prevent drug molecules from enzymatic degradation or hydrolysis, and decrease the harmful side-effect of the drug (Torchilin, 2001). Micelles have been used also to deliver various biomolecules including proteins, plasmid DNA, antisense DNA, short interfering RNA (siRNA), and genes (Kataoka et al., 2001; Lee & Kataoka, 2009; Nishiyama & Kataoka, 2006).

Micelles are widely used in pharmaceutical industries. There are many advantages of using the micelles as a drug delivery system that drive manufacturers to use this technique including easy loading of hydrophobic drugs, drug release can be regulated by polymers structure, easy and cheap preparation, and there no need for surface functionalization (Ghezzi et al., 2021).

3.1. Micelles Formation and Structure

One of the most fundamental properties of surfactants is micelle formation. Micelle formation, or micellization, is an important phenomenon due to several important interfacial phenomena, such as detergency and solubilization and other different useful phenomena. this phenomenon occurs when the concentration of the surfactants in the solution reaches a certain concentration. The concentration at which this phenomenon occurs is called the critical micelle concentration (CMC). To determine the CMC value many methods can be used, such as detection of the breaks in the electrical conductivity, surface tension, light scattering, or fluorescence spectroscopy (Rosen & Kunjappu, 2012).

When surfactant molecules are dissolved in water at concentrations above the critical micelle concentration (CMC), they form micelles by gathering the hydrophobic tails to the interior (to minimize their contact with water), and assembly the hydrophilic heads on the outer surface (to maximize their contact with water). In this way, the surfactants aggregate and form the micelles (Chevalier & Zemb, 1990).

Micelle structure is composed of two different domains, a hydrophobic core, and a hydrophilic shell. Amphiphilic copolymers (surfactants) are used in producing the micelles. the micelles are formed through spontaneous self-assembly of the copolymers (surfactants) as a result of hydrophobic interactions in aqueous solutions (Miyata et al., 2011).

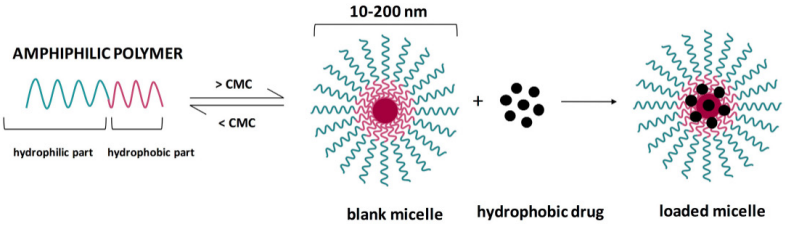

Figure 1. Schematic illustration of micelles (Ghezzi et al., 2021).

3.2. Micelles Preparation

Several methods have been established to produce drug-loaded micelles including dialysis, solvent evaporation, and film sonication. In the dialysis method, an organic solution of the drug and copolymer mixture is placed in a dialysis device immersed in water or an aqueous buffer. A slow replacement of the organic medium with water occurs through dialysis, therefore, micelles are formed. In solvent evaporation, a mixture of the drug and copolymer in an organic solvent or a mixture of solvents is added to water under forceful mixing.

Then, the micelles are formed by slow evaporation of the organic solvent (4–24 hours) (Aliabadi et al., 2007). In the film sonication method, mixtures of drug and copolymer are dissolved in an organic solvent and waited to dry and form a mixed film. Then polymeric micelles are formed by hydrating the film in water and sonicating it using an ultrasonic mixer. The chosen organic solvent(s) in all methods is vital for forming stable, uniformly sized micelles with high drug-loading content (H. Chen et al., 2011).

4. Micellar Solubilization

Micelles have many distinguishing features, one of the most key features is their ability to increase the solubility of compounds that exhibit poor solubility in the solvent (Micellar Solubilization). This occurs since the micelle has a core that is incompatible with the solvent, which by turn provides a convenient microenvironment for the solute, which is also (the solute) incompatible with the solvent. Consequently, the extent of dissolution of the solute in micellar systems is significantly enhanced when compared to the extent of dissolution of the solute in pure solvents. This phenomenon known as micro emulsification or solubilization forms the basis of several different applications of surfactants (Nagarajan & Ganesh, 1989).

5. Surfactants

Surfactants are amphiphilic molecules, composed of a hydrophilic or polar head and a hydrophobic or nonpolar tail. Some surfactants have a charge due to their head may be charged (anionic or cationic), dipolar (zwitterionic), and some are non-charged (nonionic) (de Oliveira Rangel Yagui et al., 2005).

Surfactants have several uses in pharmaceutical industries and drug developments including increasing the solubility of hydrophobic drugs in aqueous solution, as vehicles for oral and transdermal drug delivery, as plasticizers in semisolid dosage forms delivery systems, as co-factor in the formatting of emulsions, and as drug absorption and penetration enhancer (Sekhon, 2014).

6. Sodium Lauryl Sulfate

Sodium lauryl sulfate (known also as sodium dodecyl sulfate) is an anionic surfactant utilized in different pharmaceutical formulations, cosmetics, as a detergent, and wetting agent. Recently it has been used in an analytical electrophoretic technique which is called SDS (sodium dodecyl sulfate)

polyacrylamide gel electrophoresis, which is nowadays one of the most commonly used techniques for the analysis of proteins. For different uses the SDS has been used with different concentrations, 0.5-2.5% as an emulsifier, 10% as a detergent in shampoos, concentration more than CMC (>0.00025%) as solubilizer to great micelles, and 1.0-2.0% as a lubricant in tablets and wetting agent in dentifrices (Kanzaki, n.d.).

6.1. Structural formula, Empirical Formula, and Molecular Weight

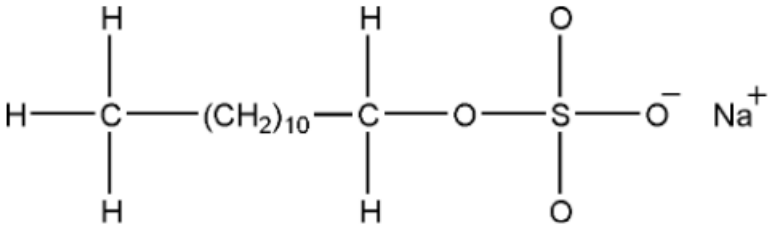

Figure 2. Structural formula of Sodium Lauryl Sulfate (Kanzaki, n.d.).

The empirical formula of SLS is $C_{12}H_{25}NaO_4S$, and its molecular weight is (288.38).

6.2. SLS in Pharmacopoeias

In The USP (*USP_41_NF_36_The_United_States_Pharmacop*, n.d.) SLS has been defined as a "Mixture of sodium alkyl sulfates consisting chiefly of sodium lauryl sulfate ($C_{12}H_{25}NaO_4S$). It contains NLT 85.0% of sodium alkyl sulfates calculated as sodium lauryl sulfate ($C_{12}H_{25}NaO_4S$)". Whereas European Pharmacopeia (*European_Pharmacopoeia_10th_Edition_2019*, n.d.) defines the SLS as a "Mixture of sodium alkyl sulfates consisting mainly of sodium dodecyl sulfate ($C_{12}H_{25}NaO_4S$; M_r 288.4)".

6.3. SLS Properties

Sodium lauryl sulfate consists of crystals, flakes, or powder that have the following physical traits, white or cream to pale yellow color, a smooth feel, a faint odor of fatty materials, and a soapy bitter taste. It has a free solubility in water, forming an opalescent solution, while it is practically insoluble in both ether and chloroform. The pH of sodium lauryl sulfate Solutions is between 9.5 and 10.0, which is slightly corrosive to the metals like steel, bronze, copper,

and aluminum. Indeed, it is also incompatible with lead and potassium salts and precipitates with it (Kanzaki, n.d.).

Sodium lauryl sulfate has bacteriostatic action against Gram-positive microorganisms; however, it is ineffective against a considerable number of Gram-negative microorganisms. It boosts the fungicidal effect of certain drugs such as sulfathiazole and sulfanilamide.

Sodium lauryl sulfate interacts with cationic surfactants, causing loss of activity even in low concentrations. it has high compatibility with dilute acids and calcium and magnesium ions.

It is classed as a moderate toxic substance with acute toxic effects such as irritation to the skin, upper respiratory tract, eyes, mucous membranes, and stomach. it may cause drying and cracking of the skin by repeated and prolonged exposure to its dilute solutions. Furthermore, this drying and cracking can be developed into contact dermatitis (Wigger-Alberti et al., 2000). As a result of using cosmetics and pharmaceutical formulations containing sodium lauryl sulfate in its formulations, adverse reactions represented by irritation of the skin (Blondeel et al., 1978; Bruynzeel et al., 1982; Eubanks & Patterson, 1984) or eyes (Grant & Thomas, 2008) following topical application have been reported. Intravenous preparations which are designed to be given to humans should be free of Sodium lauryl sulfate. The human lethal oral dose is between 0.5–5.0 g/kg.

Sodium lauryl sulfate can be synthesized by sulfation of lauryl alcohol and neutralizing the produced compound with sodium carbonate.

6.4. Applications of SLS in Pharmaceutical Formulations

Many formulations have been developed using SLS as a surfactant that provides micellar solubilization to enhance the solubility of poorly water-soluble drugs. Amidon et al. (Granero et al., 2008) found that the solubility of fenofibrate has been enhanced in a 2% w/v SLS solution 2000 times higher than the solubility of fenofibrate in an aqueous phosphate buffer solution without SLS, and SLS also enhanced the intrinsic dissolution rate 500-fold.

Dave et al. (Dave et al., 2012) studied the effect of SLS on the solubility of indomethacin when added in different ways. They prepared a binary system consisting of indomethacin with PVP of ratio 1:1(SD) and three different ternary systems with a different drug: polymer: surfactant ratios and different methods including Physical Mixtures (PM)(simple mixing of contents in a mortar and pestle), Solid Dispersion External (SDE) (adding and mixing SLS

to solid dispersion of drug: polymer (1:1)) and Solid Dispersions Internal (SDI) (dissolving SLS, drug, and polymer together in ethanol and evaporating the mixture to obtain a dry powder mixture [Micelles formation]). Then they prepared a tablet using the former systems by direct compression method and studied the effect of SLS in increasing the solubility of indomethacin by Saturation solubility studies and Dissolution test studies. They found that (SDI) system in which drug-loaded micelles have been formed, has a drastic impact on the enhancement of the solubility of the drug shown by increasing the drug release in the Dissolution test.

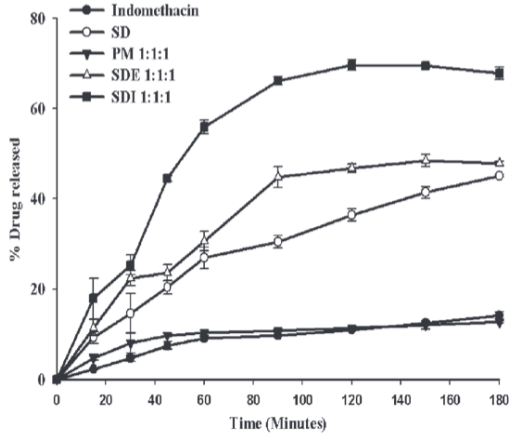

Figure 3. The dissolution profile of SDI, SDE, PM, SD, and indomethacin of ratio 1:1:1 in purified water (Dave et al., 2012).

Y. Chen et al. (Y. Chen et al., 2016) studied the effect of adding SLS to the formulation of a parenteral dosage form of Posaconazole. They observed that adding SLS to the formulation enhanced the solubility extremely. Interpreting that by dissolving the non-polar moiety of the drug in the interior side of the micelle, while the positively charged moiety of the drug in the outer side of the micelle. Therefore, decreasing the repulsive forces between the heads group of SLS, decreasing the CMC, increasing aggregation number and volume of micelles thereby increasing the solubility of the drug extremely. By that, the volume of solvent required to prepare the dosage form of the drug is decreased, so they recommended using these useful findings in the development of parenteral dosage forms of Posaconazole.

The impact of SLS in the enhancement of the solubility of all sulfathiazole (Dave et al., 2013), Carvedilol (Hamed et al., 2020), β-lactam antibiotics (Tsuji

et al., 1982), Piroxicam (Amidon et al., 1995), valdecoxib (Desai & Park, 2004), Enrofloxacin (Seedher & Agarwal, 2009), carbamazepine (Crison et al., 1996) and oxazepam (Stewart & Liu, 2002) has been detected too.

Using SLS to increase the solubility of drugs is not restricted just to oral dosage forms, Nokhodchi et al. and Shokri et al.(Nokhodchi et al., 2003; Shokri et al., 2001) studied the enhancement of the aqueous solubility and skin permeability of Diazepam and Lorazepam respectively, using sodium lauryl sulfate.

The purity of used SLS also has a significant impact on the ability of SLS to enhance the solubility of poorly water-soluble drugs. The higher the purity of SLS, the higher the solubility has been obtained (Crison et al., 1997; Qiang et al., 2010).

Table 1. studies using SLS on the solubility enhancement of drugs.

Authors	Year	Administration route	API
Granero et al.	2008	Oral	Fenofibrate
Dave et al.	2012	Oral	Indomethacin
Dave et al.	2013	Oral	Sulfathiazole
Hamed et al.	2020	Oral	Carvedilol
Stewart & Liu	2002	Oral	Oxazepam
Crison et al.	1996	Oral	Carpamazepine
Amidon et al.	1995	Oral	Piroxicam
Seedher & Agarwal	2009	Oral	Enrofloxacin
Tsuji et al.	1982	Oral	*β*-lactam antibiotics
Desai & Park	2004	Oral	*Valdecoxib*
Y. Chen et al.	2016	Parenteral	Posaconazole
Nokhodchi et al.	2003	Topical-Skin	*Diazepam*
Shokri et al.	2001	Topical-Skin	*Lorazepam*

7. Conclusion

The low bioavailability is one of the biggest challenges in the development of new oral dosage forms. Since more than 40% of newly developed drugs are poorly soluble in water. Sodium lauryl sulfate, an anionic surfactant can be used effectively and safely to enhance the aqueous solubility of various poorly water-soluble drugs by the Micellar Solubilization technique. Therefore, enhance the oral bioavailability of these drugs. In addition to the ability to enhance the permeability of the topical drugs through the skin.

References

Aliabadi, H. M., Elhasi, S., Mahmud, A., Gulamhusein, R., Mahdipoor, P., & Lavasanifar, A. (2007). Encapsulation of hydrophobic drugs in polymeric micelles through co-solvent evaporation: The effect of solvent composition on micellar properties and drug loading. *International Journal of Pharmaceutics*, *329*(1–2), 158–165. https://doi.org/10.1016/J.IJPHARM.2006.08.018

Allen, L., & Ansel, H. C. (2013). *Ansel's pharmaceutical dosage forms and drug delivery systems*. Lippincott Williams & Wilkins.

Amidon, G. L., Lennernas, H., Shah, V. P., & Crison, J. R. (1995). A theoretical basis for a biopharmaceutic drug classification: the correlation of in vitro drug product dissolution and in vivo bioavailability. *Pharm Res*, *12*, 413–420.

Blondeel, A., Oleffe, J., & Achten, G. (1978). Contact allergy in 330 dermatological patients. *Contact Dermatitis*, *4*(5), 270–276. https://doi.org/10.1111/J.1600-0536.1978.TB04557.X

Bruynzeel, D. P., van Ketel, W. G., Scheper, R. J., & von Blomberg-van der Flier, B. M. E. (1982). Delayed time course of irritation by sodium lauryl sulfate: Observations on threshold reactions. *Contact Dermatitis*, *8*(4), 236–239. https://doi.org/10.1111/J.1600-0536.1982.TB04205.X

Chaudhari, S. P., & Dugar, R. P. (2017). Application of surfactants in solid dispersion technology for improving solubility of poorly water soluble drugs. *Journal of Drug Delivery Science and Technology*, *41*, 68–77. https://doi.org/10.1016/J.JDDST.2017.06.010

Chen, H., Khemtong, C., Yang, X., Chang, X., & Gao, J. (2011). Nanonization strategies for poorly water-soluble drugs. *Drug Discovery Today*, *16*. https://doi.org/10.1016/j.drudis.2010.02.009

Chen, Y., Wang, S., Wang, S., Liu, C., Su, C., Hageman, M., Hussain, M., Haskell, R., Stefanski, K., & Qian, F. (2016). Sodium Lauryl Sulfate Competitively Interacts with HPMC-AS and Consequently Reduces Oral Bioavailability of Posaconazole/HPMC-AS Amorphous Solid Dispersion. *Molecular Pharmaceutics*, *13*(8), 2787–2795. https://doi.org/10.1021/ACS.MOLPHARMACEUT.6B00391/ASSET/IMAGES/MEDIUM/MP-2016-003914_0012.GIF

Chevalier, Y., & Zemb, T. (1990). The structure of micelles and microemulsions. *Reports on Progress in Physics*, *53*(3), 279. https://doi.org/10.1088/0034-4885/53/3/002

Constantinides, P. P., Lambert, K. J., Tustian, A. K., Schneider, B., Lalji, S., Ma, W., Wentzel, B., Kessler, D., Worah, D., & Quay, S. C. (2000). Formulation development and antitumor activity of a filter-sterilizable emulsion of paclitaxel. *Pharmaceutical Research*, *17*, 175–182.

Crison, J. R., Shah, V. P., Skelly, J. P., & Amidon, G. L. (1996). Drug dissolution into micellar solutions: Development of a convective diffusion model and comparison to the film equilibrium model with application to surfactant-facilitated dissolution of carbamazepine. *Journal of Pharmaceutical Sciences*, *85*(9), 1005–1011. https://doi.org/10.1021/js930336p

Crison, J. R., Weiner, N. D., & Amidon, G. L. (1997). Dissolution media for in vitro testing of water-insoluble drugs: Effect of surfactant purity and electrolyte on in vitro dissolution of carbamazepine in aqueous solutions of sodium lauryl sulfate. *Journal of Pharmaceutical Sciences*, *86*(3), 384–388. https://doi.org/10.1021/js960105t

Dave, R. H., Patel, A. D., Donahue, E., & Patel, H. H. (2012). To evaluate the effect of addition of an anionic surfactant on solid dispersion using model drug indomethacin. *Drug Development and Industrial Pharmacy*, *38*(8), 930–939. https://doi.org/10.3109/03639045.2011.633264

Dave, R. H., Patel, H. H., Donahue, E., & Patel, A. D. (2013). To evaluate the change in release from solid dispersion using sodium lauryl sulfate and model drug sulfathiazole. *Http://Dx.Doi.Org/10.3109/03639045.2012.725731*, *39*(10), 1562–1572. https://doi.org/10.3109/03639045.2012.725731

de Oliveira Rangel Yagui, C., Lineu Prestes, A., Rangel-Yagui, C. O., Pessoa-Jr, A., & Costa Tavares, L. (2005). Micellar solubilization of drugs. *J Pharm Pharmaceut Sci (Www.Cspscanada.Org)*, *8*(2), 147–163. www.cspscanada.org

Desai, K. G. H., & Park, H. J. (2004). Solubility studies on valdecoxib in the presence of carriers, cosolvents, and surfactants. *Drug Development Research*, *62*(1), 41–48. https://doi.org/10.1002/DDR.10365

Eubanks, S. W., & Patterson, J. W. (1984). Dermatitis from sodium lauryl sulfate in hydrocortisone cream. *Contact Dermatitis*, *11*(4), 250–251. https://doi.org/10.1111/J.1600-0536.1984.TB00994.X

European_Pharmacopoeia_10th_Edition_2019. (n.d.).

Ghezzi, M., Pescina, S., Padula, C., Santi, P., del Favero, E., Cantù, L., & Nicoli, S. (2021). Polymeric micelles in drug delivery: An insight of the techniques for their characterization and assessment in biorelevant conditions.

Journal of Controlled Release, *332*, 312–336. https://doi.org/10.1016/J.JCONREL.2021.02.031

Granero, G. E., Ramachandran, C., & Amidon, G. L. (2008). Dissolution and Solubility Behavior of Fenofibrate in Sodium Lauryl Sulfate Solutions. *Http://Dx.Doi.Org/10.1080/03639040500272108*, *31*(9), 917–922. https://doi.org/10.1080/03639040500272108

Grant, W. M., & Thomas, C. C. (2008). Toxicology of the eye, third edition. *Http://Dx.Doi.Org/10.3109/15569528709052171*, *6*(2), 155–156. https://doi.org/10.3109/15569528709052171

Hamed, R., Alnadi, S. H., & Awadallah, A. (2020). The Effect of Enzymes and Sodium Lauryl Sulfate on the Surface Tension of Dissolution Media: Toward Understanding the Solubility and Dissolution of Carvedilol. *AAPS PharmSciTech*, *21*(5), 1–11. https://doi.org/10.1208/S12249-020-01683-3/TABLES/5

Hörter, D., & Dressman, J. B. (1997). Influence of physicochemical properties on dissolution of drugs in the gastrointestinal tract. *Advanced Drug Delivery Reviews*, *25*(1), 3–14. https://doi.org/10.1016/S0169-409X(96)00487-5

Jain, N., & Yalkowsky, S. H. (2001). Estimation of the aqueous solubility I: Application to organic nonelectrolytes. *Journal of Pharmaceutical Sciences*, *90*(2), 234–252. https://doi.org/10.1002/1520-6017(200102)90:2<234::aid-jps14>3.0.co;2-v

Jouyban, A. (2008). Review of the cosolvency models for predicting solubility of drugs in water-cosolvent mixtures. *Journal of Pharmacy & Pharmaceutical Sciences*, *11*(1), 32–58.

Kanzaki, Z. (n.d.). *Handbook-of-Pharmaceutical-Excipients 6th Edition*. Retrieved February 1, 2023, from https://www.academia.edu/16731682/Handbook_of_Pharmaceutical_Excipients_6th_Edition

Kataoka, K., Harada, A., & Nagasaki, Y. (2001). Block copolymer micelles for drug delivery: Design, characterization and biological significance. *Advanced Drug Delivery Reviews*, *47*(1), 113–131. https://doi.org/10.1016/S0169-409X(00)00124-1

Lasic, D. D., & Papahadjopoulos, D. (1998). *Medical applications of liposomes*. Elsevier.

Lee, Y., & Kataoka, K. (2009). Biosignal-sensitive polyion complex micelles for the delivery of biopharmaceuticals. *Soft Matter*, *5*(20), 3810–3817. https://doi.org/10.1039/B909934D

Miyata, K., Christie, R. J., & Kataoka, K. (2011). Polymeric micelles for nano-scale drug delivery. *Reactive and Functional Polymers*, *71*(3), 227–234. https://doi.org/https://doi.org/10.1016/j.reactfunctpolym.2010.10.009

Nagarajan, R., & Ganesh, K. (1989). Block Copolymer Self-Assembly in Selective Solvents: Theory of Solubilization in Spherical Micelles. *Macromolecules*, *22*(11), 4312–4325. https://doi.org/10.1021/MA00201A029/ASSET/MA00201A029.FP.PNG_V03

Nishiyama, N., & Kataoka, K. (2006). Current state, achievements, and future prospects of polymeric micelles as nanocarriers for drug and gene delivery. *Pharmacology and Therapeutics*, *112*(3), 630–648. https://doi.org/10.1016/J.PHARMTHERA.2006.05.006

Nokhodchi, A., Shokri, J., Dashbolaghi, A., Hassan-Zadeh, D., Ghafourian, T., & Barzegar-Jalali, M. (2003). The enhancement effect of surfactants on the penetration of lorazepam through rat skin. *International Journal of Pharmaceutics*, *250*(2), 359–369. https://doi.org/10.1016/S0378-5173(02)00554-9

Qiang, D., Gunn, J. A., Schultz, L., & Li, Z. J. (2010). Evaluation of the impact of sodium lauryl sulfate source variability on solid oral dosage form development. *Http://Dx.Doi.Org/10.3109/03639045.2010.488647*, *36*(12), 1486–1496. https://doi.org/10.3109/03639045.2010.488647

Rosen, M. J., & Kunjappu, J. T. (2012). *Surfactants and interfacial phenomena*. John Wiley & Sons.

Savjani, K. T., Gajjar, A. K., & Savjani, J. K. (1957). *Drug Solubility: Importance and Enhancement Techniques*. *2012*. https://doi.org/10.5402/2012/195727

Seedher, N., & Agarwal, P. (2009). Various Solvent Systems for Solubility Enhancement of Enrofloxacin. *Indian Journal of Pharmaceutical Sciences*, *71*(1), 82. https://doi.org/10.4103/0250-474X.51958

Sekhon, B. S. (2014). *Surfactants: Pharmaceutical and Medicinal Aspects*. http://localhost:8080/xmlui/handle/1/48

Shokri, J., Nokhodchi, A., Dashbolaghi, A., Hassan-Zadeh, D., Ghafourian, T., & Barzegar Jalali, M. (2001). The effect of surfactants on the skin penetration of diazepam. *International Journal of Pharmaceutics*, *228*(1–2), 99–107. https://doi.org/10.1016/S0378-5173(01)00805-5

Stewart, P. J., & Liu, J. (2002). The influence of aggregate microenvironment on the dissolution of oxazepam in ternary surfactant interactive mixtures. *The Journal of Pharmacy and Pharmacology*, *54*(9), 1181–1187. https://doi.org/10.1211/002235702320402017

Torchilin, V. P. (2001). Structure and design of polymeric surfactant-based drug delivery systems. *Journal of Controlled Release*, *73*(2–3), 137–172. https://doi.org/10.1016/S0168-3659(01)00299-1

Torchilin, V. P. (2006). Micellar Nanocarriers: Pharmaceutical Perspectives. *Pharmaceutical Research 2006 24:1*, *24*(1), 1–16. https://doi.org/10.1007/S11095-006-9132-0

Tsuji, A., Miyamoto, E., Matsuda, M., Nishimura, K., & Yamana, T. (1982). Effects of surfactants on the aqueous stability and solubility of β-lactam antibiotics. *Journal of Pharmaceutical Sciences*, *71*(12), 1313–1318. https://doi.org/10.1002/jps.2600711203

USP_41_NF_36_The_United_States_Pharmacop. (n.d.).

Vyas, A., Saraf, S., & Saraf, S. (2008). Cyclodextrin based novel drug delivery systems. *Journal of Inclusion Phenomena and Macrocyclic Chemistry 2008 62:1*, *62*(1), 23–42. https://doi.org/10.1007/S10847-008-9456-Y

Wigger-Alberti, W., Krebs, A., & Elsner, P. (2000). Experimental irritant contact dermatitis due to cumulative epicutaneous exposure to sodium lauryl sulphate and toluene: single and concurrent application. *The British Journal of Dermatology*, *143*(3), 551–556. https://doi.org/10.1111/J.1365-2133.2000.03710.X

Yalkowsky, S. H., & Valvani, S. C. (1980). Solubility and partitioning I: Solubility of nonelectrolytes in water. *Journal of Pharmaceutical Sciences*, *69*(8), 912–922. https://doi.org/10.1002/JPS.2600690814

CHAPTER II

GENETIC STUDIES ON NATIVE POPLAR SPECIES IN TÜRKİYE

ASIYE ULUĞ[1] & FUNDA ÖZDEMIR DEĞİRMENCİ[2]

[1](Asst. Prof. Dr.) Kafkas University,
e mail: asya.ulug@kafkas.edu.tr
ORCID: 0000-0001-5524-8431

[2](Asst. Prof. Dr.) Ahi Evran University,
e mail: funda07@gmail.com
ORCID: 0000-0002-8875-0273

1. Introduction

The members of the genus *Populus* (Poplar) have a wide geographical distribution ranging from North Africa, Europe, Asia to North America, thanks to their dioecious nature, wind-pollination behavior, ability to reproduce vegetatively from branches and root shoots, and adaptability to different environments (eFloras.org, 2013). Due to the presence of the entire genome sequence of *Populus trichocarpa*, biological characteristics of the genus such as rapid growth, efficient sexual reproduction and hybridization capacity, poplar species are used as model organisms for genetic studies in many tree species and investigation of their qualitative and quantitative properties against biological stress factors (DiFazio et al., 2011). Today, improvement studies in these tree species are gaining great importance day by day due to usage of poplar as a renewable energy source, raw material, in addition to paper production, wood veneer, sawdust and timber production. Along with willows, poplars are also used for bioremediation due to their deep and rich root systems that penetrate deeply into ground (Guerra et al., 2011; Aghaalikhani et al., 2017; Yer-Çelik et al., 2021). Genetic studies are frequently carried out for the effective usage of poplar trees to meet the demands of the increasing world population

considering the potential of the species (Gaudet et al., 2008; Khasa et al., 2005; Algidras et al., 2019; Stolarski, 2020).

2. *Populus* species in Türkiye

Populus species are naturally distributed in different forest and river ecosystems of Türkiye. Poplar trees have been grown traditionally and economically in Anatolia for many years. There are 260,681 hectares of poplar stands naturally distributed in seven regions of Türkiye (Velioğlu et al., 2020). Planting poplar is considered a sacred work in Turkish culture, and it is a tradition in villages to plant poplar when a new baby is born (Işık, 2019). There are five poplar species that are naturally distributed in Türkiye. These; aspen (*Populus tremula* L.), white poplar (*Populus alba* L.), gray poplar (*Populus x canescens* Smith), Euphrates poplar (*Populus euphratica* Oliv.), and black poplar (*Populus nigra* L.). In addition, American black poplar (*Populus deltoides* Marsh.) and hybrid poplar (*Populus x canadensis* Moench) are cultivated extensively in the temperate regions of the country.

2.1. Populus tremula

Aspen (*Populus tremula*) which is in the Leuce section together with white poplar is known as a common tree that grows in the colder, temperate, and boreal regions of Europe and Asia (Euforgen, 2022). It is a species with a Euro-Siberian element and has a wide distribution area of approximately 133,716.98 hectares, spreading in all forest areas, along streams and in open forests, except the steppe region in Türkiye (eFloras.org, 2013; Anşin and Özkan, 2006). This medium-sized trees are known to have dioecious, deciduous, and fast-growing nature. As the wood of aspen is not very strong, it is generally used for veneer, matches, toothpick and paper production as well as quality charcoal and chip wood (Öner and Aslan, 2002). Due to its rapid growth, it plays an important role in bioenergy production. Aspen has an important ecological value in terms of biodiversity as it provides habitat for various mammals and birds, as well as many insects and fungi. It also contributes to important ecosystem services such as the protection of watersheds, pollution reduction and soil stabilization (Euforgen, 2022).

2.2. Populus alba

White poplar (*Populus alba*) known as an invasive tree has a distribution ranging from the Mediterranean to Central Asia. The species grows well in

alluvial, filled soils, especially along rivers, between 1100 m altitudes above sea level (eFloras.org, 2022). White poplar is found in different regions of Türkiye either individually or together with *Populus x canescens*, a hybrid formed with *P. tremula*. Like aspen, white poplar is also a medium-sized, fast-growing, deciduous, and dioecious species. The wood of white poplar is not durable for construction, but is useful to produce biomass, pulp, and pellets for energy production due to its rapid growth and strong regeneration ability (Euforgen, 2022). In addition to having an important role in soil stabilization and watershed protection by forming windbreaks in coastal areas, white poplar is an important ecological component of riparian forest systems, where it contributes to biodiversity.

2.3. Populus x canescens

Gray poplar (*Populus x canescens*), a spontaneous hybrid of white poplar and aspen, is a broad-topped tree that can grow up to 35 m. They are distributed in moist forest areas and waterfronts in Western Asia, Europe, and T**ü**rkiye (eFloras, 2022). It is naturally grown in Edirne, Ankara, Muş, Van, Hakkari and Muğla. This species is frequently used in seaside afforestation (Yaltırık, 1993; Yaltırık and Efe, 2000).

2.4. Populus euphratica

Euphrates poplar (*Populus euphratica*) placed in the Turanga section has a distribution in Africa, Asia, Middle East and Türkiye. The natural populations of Euphrates poplar in Türkiye are located on the banks of the Tigris River and Botan Stream (Browicz and Yaltırık, 1982). It is an average-sized, deciduous, mostly shrub-like tree with its greenish matte blue leaves having different sizes and forms (Browicz and Yaltırık, 1982). The species can grow in low humidity, summer drought, and high salinity (Kansu and Kaya, 2020). Even though, the species has no economic value, Euphrates poplar is important as a fuel and timber source for the local people in the Eastern Mediterranean and Southeastern Anatolia regions.

2.5. Populus nigra

Black poplar (*Populus nigra*) belonging to Aigeiros section spreads along riverbanks in Europe, North Africa, Central and Western Asia (eFloras.org, 2022). The species is one of the common trees of the eastern and central regions of Türkiye, so black poplar breeding efforts have been concentrated

in these parts of the country. Like other member of genus *Populus*, it has deciduous and dioecious nature with higher heights. Black poplar is used as a model tree for breeding programs in different regions of the world due to its excellent ability of hybridization, vegetative regeneration and rapid growth for bioenergy and raw material production (Vanden Broeck, 2003). Thanks to its environmental plasticity, afforestation is carried out by using black poplar to clean soil in industrial areas where chemical wastes are found (Jelic et al., 2015). Ecologically, it contributes to biodiversity as it is home to many insects, small mammals, and bird species. The species is also a pioneer tree, especially in riparian woodlands, thanks to its tolerance to high water levels, soil stabilization and protection of watersheds. However, habitat degradation and reduction in genetic diversity due to anthropogenic effects have threaten the species in its natural habitat (Euforgen, 2022).

1.6. Populus deltoides and Populus x canadensis

Populus deltoides (Eastern cottonwood) is widely distributed from the Eastern, Central, and Southwestern USA to Southern Canada(Kartesz and Meacham, 1999). It shares the *Aigeiros* subgenus with *P. nigra*. The species with quick growing and drought tolerant characteristics has been introduced to different regions of the world (Zhang et al., 2020). Eastern cottonwood has been widely cultivated for short rotation industrial timber production in the mid-latitude regions of the world. It can hybridize with *P. nigra,* and their genetic resources have been used effectively for producing new poplar cultivars (Smulders et al., 2008b).

Populus x canadensis, a hybrid of *P. nigra* and *P. deltoides*, is the best known commercially cultivated poplar species in the world with its good growth performance, adaptability, and strong hybrid viability (Smulders et al., 2008b). The hybrid has been produced in Türkiye since the 1960s (Toplu, 2005). After many field trials, hybrid clones with outstanding success have been identified and cultured in different regions of T**ü**rkiye and grown in large plantations (Velioğlu et al., 2020). It has been reported that hybrid clones grown on plantations in Europe effectively spread to river ecosystems and suppress development of native stands of *P. nigra* (Khasa et al., 2005; Jelic et al., 2015).

3. Genetic studies on Populus species in Türkiye

Poplar cultivation, which has economic, social, ecological, and environmental importance in Türkiye, must be sustainable to meet the needs of

the country. The studies related with conservation and breeding of poplar species in Türkiye have been performed by colloboration between the European Forest Genetic Resources Program (EUFORGEN) and Poplar and Fast-Growing Forest Trees Research Institute (Kocaeli, Türkiye). Poplar and Fast-Growing Forest Trees Research Institute monitors the scientific and technical developments and changes seen in poplar, willow, and fast-growing species in 4-year periods and provide national reports to International Poplar Commission (IPC) (Velioğlu et al., 2020).

Genetic diversity is recognized as an important character in species survival, evolution, and adaptation to changing environmental conditions. This diversity allows a population to gain ability to resist natural events (emerging diseases, epidemics, bottleneck etc.) and anthropogenic effects (habitat fragmentation, isolation, overexploitation) (Klug et al., 2019). To protect genetic diversity of poplar species that grow naturally in Türkiye and have economic importance all over the world, the determination of gene sources and their usage in breeding programs gain great importance. Effective gene conservation requires for accurate identification and genetic characterization of trees for all phases of poplar breeding and conservation studies by reliable genetic markers (Heinze, 2008).

There are many studies investigating genetic diversity of poplar species to evaluate genetic structure of their populations, to protect and restore destroyed populations for the different countries of the world. When looking genetic studies related with poplar species in Türkiye, a few studies are present. Between 2010 and 2013, the project titled by "Genetic characterization of Turkish black poplar genetic resources and development of molecular black poplar breeding program" was carried out between Middle East Technical University (Ankara) and Poplar and Fast-Growing Forest Trees Research Institute (Kocaeli). With this project, the 297 black poplar trees sampled from seven regions of T**ü**rkiye and grown in Behiçbey clone bank was identified genetically by studying microsatellite DNA markers. The results of the project indicated that high level of clonal duplication and admixture were observed with reduced genetic diversity. The existing genetic resources of natural *P. nigra* populations were not represented by clone collections of Behiçbey (Çiftçi et al., 2013; Çiftçi et al., 2017).

Taşkıran (2014) also studied with 297 *P. nigra* trees cultivated in Behiçbey clone bank to examine cellulose, lignin and D-glucose content. The genotypes were determined with high cellulose to low lignin contents by comparing wood and growth traits to obtain high quality of wood for industry of paper

manufacturing and bioenergy production. Taşkıran (2020) evaluated the specific activities of cellulose (SuSy and UGPase) and lignin pathway related (PAL, 4CL, and CAD) enzymes in 285 *P. nigra* trees represented by 4 ramets and replicated twice. Even though, a positive correlation was found among enzymes of phenylpropanoid pathway (PAL, 4CL, and CAD), there was no relationships between lignin content and these enzymes.

Zeybek (2014) determined the expression of antioxidant enzymes (ascorbate peroxidase (APX), glutathione reductase (GR), and catalase (CAT) and dehydroascorbate reductase (DHAR)) during one year seasonal changes in *P. nigra* trees grown in Behiçbey clone bank. The activities of GR, APX and DHAR were found to be increased with low air temperatures. The author reported that the genes related with sugar transport activities and carbohydrate metabolism were significantly up-regulated in a cold resistant genotype in the microarray analysis. This genotype could be cultivated in poplar plantations of low temperature areas of the country.

Yıldırım and Uylaş (2016) examined the tolerance of *P. nigra* to Boron toxicity and accumulation by considering physiologic and gene regulation responses. They performed a transcriptome experiment on the leaves and roots of a poplar genotype that has tolerance to Boron accumulation. According to obtained results, *P. nigra* could be used for elimination of Boron pollution because the species can tolerate highly toxic concentrations of Boron (15 ppm soil Boron content and >1500 ppm Boron in leaves). Yıldırım and Kaya (2017) identified drought adaptation strategies for tree species by using poplar as a model organism. They tested 300 black poplar trees in a field trial by considering Stress tolerance Index and Mean Relative Performance. The obtained values were used to determine the adaptive responses of trees under drought stress. They investigated the drought escape, avoidance and tolerance adaptations of *P. nigra* genotypes by microarray based transcriptomic analysis. Storage protein production was found positively correlated with secondary metabolite biosynthesis in drought resistance. Special bark storage proteins was inducted under drought stress. Also, the genes expressed in secondary metabolite production was found to be effectively up regulated in a tree with the highest leaf water content and growth performance under drought stress. Higher enzyme activates were accepted as a strategy to prevent the negative effect of drought in the study.

Çiftçi and Kaya (2019) studied genetic diversity structure of native *P. nigra* populations from Göksu and Kızılırmak rivers. They revealed that due to

anthropogenic effect (habitat loss) and natural events (hybridization), the genetic diversity of the natural populations has been reduced dramatically. Çiftçi and Kaya (2019) found that hybrid poplar trees identified along the Göksu River are products of mating among *P. x canadensis* clones cultivated on commercial plantations. Hybrid trees naturally reproduce and disperse seeds and threat the genetic resources of native *P. nigra* (Cagelli and Lefevre 1995; Smulders et al., 2008b). They emphasized that it is crucial to implement efficient conservation strategies for prevent further genetic pollution and maintain remaining genetic variation of the species. Çiftçi, Yelmen, Değirmenci and Kaya (2020) evaluated genetic diversity of *P. nigra* by considering gender. The authors investigated the possible effects of biased sex ratio by studying microsatellite DNA loci for male and female members of *P. nigra* sampled from five geographical regions in T**ü**rkiye. They detected that 60 clones of the same genotype were both in females and males phenoytpe. This result indicated the occurrence of biased sex ratio and deviation of *P. nigra* from dioecism with reduced genetic diversity.

To detect the presence of hybridization and its effect on the genetic structure of native *P. nigra*, Uluğ (2022a) performed a study including detection of diagnostic alleles for *P.nigra* and *P. deltoides* to examine their hybrid. The author analyzed one native population of *P. nigra*, EUFORGEN core collection of *P. nigra*, cultivated *P. deltoides* trees and morphologically identified hybrids. Introgression between the native trees of *P. nigra* and cultivated hybrids (*P x canadensis*) or *P. deltoides* trees in the surrounding area was observed. Some hybrid trees were morphologically misidentified as *P. nigra*. Another study with hybrid poplar trees detected the genetic identity of ten hybrid trees sampled from Seyhan River with 17 microsatellite markers. Presence of seven hybrid trees with different genotype showed that hybrid trees reproduce sexually and disperse their seeds far from plantation sites (Uluğ, 2022b). The author suggested that more rigorous standards should be applied for reliable identification and registration of poplar clones with large sample size for conservation of the native *P. nigra* in their natural habitat.

The genetic diversity structure of native populations of Euphrates poplar sampled from G**ö**ksu and Euphrates rivers were studied by Kansu and Kaya (2020). Genetic characterization of 21 microsatellite DNA loci indicated reduced genetic diversity and increased level of gene exchange among the populations of two river. Authors emphasized that continued habitat loss and fragmentation caused to gene pool shrinkage in the species which seemed to be marginal.

The genetic diversity structure of male and female trees of *P. euphratica* sampled from the Göksu river were examined with seven microsatellite markers selected by considering previous sex determination studies related with different Poplar species (Nebioğlu, 2021). The author didnt find significant genetic variation between populations of male and female trees. The studied microsatellite loci, which indicated low level of variation in male and female trees of *P. euphratica* was found to be unsutiable for gender determination in the study. Çelik (2021) detected the genetic diversity of old and young stands of *P. euphratica* populations sampled from upstream, midstream, and downstream parts of the Göksu River by 15 microsatellite markers. The author determined the amount of sharing of genetic diversity between mature and young stands taking into account the generative regeneration capacity of natural populations. Mature and young populations exhibited the low and moderate level of genetic diversity. Age based genetic differentiation was not observed between mature and young age groups due to high-degree gene flow in the same locality.

Although, many genetic studies related with *P. nigra* and *P. euphratica* are present in the literature, there is not any genetic study on natural populations of *Populus tremula*, *Populus alba* and *Populus x canescens* in Türkiye.

4. Conclusion

To protect natural populations of poplar species for their ecological and economical importance, genetic resources of the species should be accurately determined, and this heritage should be conserved in the perspectives of *in situ* and *ex situ* conservation in Türkiye. Studying genetic structure of native populations of *P. alba*, *P. tremula* and *P. x canescens* species whose genetic structure has never been studied in Türkiye will be a good start point. For the *P. nigra* and *P. euphratica* species which their genetic diversity structure was mainly determined, the effective conservation and breeding studies should be implemented to protect the remaining genetic resources for future generations. Allelic combination in hybrid species which gain importance for commercial cultivation of poplar in the world, must be revealed. Related information also must be gained about the reproduction and propagation strategies of hybrid trees to protect native stands of other poplar species from genetic pollution.

Kaynakça

Aghaalikhani, A., Savuto, E., Di Carlo, A., and Borello, D. (2017), Poplar from Phytoremediation as a Renewable Energy Source: Gasification Properties and Pollution Analysis, *Energy Process*, 142, 924–931.

Algidras, J., Banioniene, V., Jotautiene, E., Ziemelis, I. (2019), Investigation of black poplar (*Populus nigra* L.) preparation and utilization for energy conversion, Conference: 18th International Scientific Conference Engineering for Rural Development.

Anderson, E.C., Thompson, E. A. (2002), A model-based method for identifying species hybrids using multilocus genetic data, *Genetics*, 160(3), 1217–1229.

Arnaud-Haond, S., Belkhir, K. (2007), GENCLONE: a computer program to analyse genotypic data, test for clonality and describe spatial clonal organization, *Molecular Ecology Notes*, 7, 15–17.

Anşin, R. ve Özkan, Z.C. (2006), *Tohumlu Bitkiler Ders Kitabı*, Trabzon: Karadeniz Teknik Üniversitesi Matbaası.

Browicz, K., Yaltırık, F. (1982), The Populus L., *Davis Flora of Turkey*, 7, 716-720.

Brundu, G., Lupi, R., Zapelli, I., Fossati, T., Patrignani, G., Camarda, I.,Sala, F., and Castiglione, S. (2008), The origin of clonal diversity andstructure of *Populus alba* in Sardinia: evidence from nuclear and plastid microsatellite markers, *Annals of Botany*, 102, 997–1006.

Cagelli, L., Lefevre, F. (1995). The conservation of *Populus nigra* and gene flow with cultivated poplars in Europe, *Forest Genetics*, 2:135–144.

Castiglione, S., Cicatelli, A., Lupi, R., Patrignani, G., Fossati, T., Brundu, G., Sabatti, M., van Loo, M., & Lexer, C. (2010), Genetic structure and introgression in riparian populations of *Populus alba* L. *Plant Biosystems*, 144(3), 656–668.

Çelik, M. (2021), Genetic diversity differences between parental and progeny population of *Populus euphratica* populations in a fragmented river ecosystem (Not puplished MS thesis). Middle East Technical University/ The Graduate School of Natural and Applied Sciences, Ankara.

Cortan, D., Schroeder, H., Sijacic-Nikolic, M. et al. (2016), Genetic structure of remnant black poplar (*Populus nigra* L.) populations along biggest rivers in Serbia assessed by SSR markers, *Silvae Genetica*, 65(1),12–19.

Çiftçi, A., Karatay, H., Kücükosmanoğlu, F,, Karahan, A., Kaya, Z. (2017), Genetic differentiation between clone collections and natural populations of European black poplar (Populus nigra L.) in Turkey, *Tree Genetics and Genomes*, 13:69.

Çiftçi, A., Kaya, Z. (2019), Genetic diversity and structure of *Populus nigra* populations in two highly fragmented river ecosystems from Turkey, *Tree Genetics and Genomes*, 15(4), 66.

DeWoody, J., Trewin, H., Taylor, G. (2015), Genetic and morphological differentiation in *Populus nigra* L: isolation by colonization or isolation by adaptation, *Molecular Ecology*, 24(11), 2641–2655.

Difazio, S.P., Slavov, G.T., Joshi, C.P. (2011), *Populus: a premier pioneer system for plant genomics*. In: Joshi, C.P., Difazio, S.P., Kole, C., editors. Genetics, genomics, and breeding of poplar, Lebanon: Science Publishers.

Doyle, J.J., Doyle, J.L. (1990), A rapid total DNA preparation procedure for fresh plant tissue, *Focus*, 12:13–15.

Earl Dent, A., Vonholdt, Bridgett, M. (2012), STRUCTURE HARVESTER: a website and program for visualizing STRUCTURE output and implementing the Evanno method, *Conservation of Genetic Resources*, 4(2), 359–361.

Excoffier, L., Lischer, H.E.L. (2010), Arlequin suite ver 3.5: a new series of programs to perform population genetics analyses under Linux and Windows, *Molecular Ecology Resources*, 10, 564–567,

Fossati, T., Grassi, F., Sala, F., Castiglione, S. (2003), Molecular analysis of natural populations of *Populus nigra* intermingled with cultivated hybrids, *Molecular Ecology* ,12, 2033–2048.

Francis, R.M. (2016), POPHELPER: an R package and web app to analyse and visualise population structure, *Molecular Ecology Resources*, https://doi.org/ 10.1111/1755-0998.12509.

Gaudet, M., Jorge, V., Paolucci, I., Beritognolo, I., Scarascia Mugnozza, G., Sabatti, M. (2008), Genetic linkage maps of *Populus nigra* L. including AFLPs, SSRs, SNPs, and sex trait, *Tree Genetics and Genomes*, 4, 25– 36.

Guerra, F., Gainza, F., Perez, R., and Zamudio, F. (2011), *Phytoremediation ofHeavy Metals Using Poplars (Populus spp.): A Glimpse of the PlantResponses to Copper, Cadmium and Zinc Stress*, in Handbook ofPhytoremediation. Editors I.A. Golubev New York: Nova SciencePublishers. Jakobsson, M., Rosenberg, N.A. (2007), CLUMPP: a cluster matching and permutation program for dealing with label switching and multimodality in analysis of population structure, *Bioinformatics*, 23, 1801–1806.

Jelic, M., Patenkovic, A., Skoric, M., Misic, D., Kurbalija Novicic, Z., Bordacs, S., Varhidi, F., Vasic, I., Benke, A., Frank, G., Siler, B. (2015), Indigenous Forest of European black poplar along the Danube River: genetic structure and reliable detection of introgression, *Tree Genetics and Genomes*, 11, 89.

Jiang, D., Wu, G., Mao, K. (2015), Structure of genetic diversity in marginal populations of black poplar (*Populus nigra* L.), *Biochemical Systematic and Ecology*, 61, 297–302.

Kalia, R.K., Rai M.K., Kalia, S., Singh, R., Dhawan, A.K. (2011), Microsatellite markers: an overview of the recent progress in plants, *Euphytica,* 177, 309–334.

Kansu, Ç., Kaya, Z. (2020), Genetic diversity of marginal populations of *Populus euphratica* Oliv. from highly fragmented river ecosystems, *Silvae Genetica*, 69(1), 139–151.

Kartesz, J.T., Meacham, C.A. (1999), Synthesis of the North American flora In: North Carolinabotanical garden, Cooperation with the nature resources conser-vation Service, and U.S. Fish and wildlife service.

Khasa, D., Pollefeys, P., Navarro-Quezada, A., Perinet, P., Bousquet, J. (2005). Species-specific microsatellite markers to monitor gene flow between exotic poplars and their natural relatives in eastern North America, *Molecular Ecology Notes*, 5, 920–923.

Klug, A., Park, S.C., Krug J. (2019), Recombination and mutational robustness in neutral fitness landscapes, *PLoS Computational Biology*, 15(8), e1006884.

Nebioğlu, N. (2021), Genetic diversity pattern in female and male trees of *Populus euphratica* populations sampled from Göksu river basin (Not puplished MS thesis). Middle East Technical University/ The Graduate School of Natural and Applied Sciences, Ankara.

Öner, N., Aslan, S. (2002). Titrek kavak (*Populus tremula* L.) Odununun teknolojik özellikleri ve kullanım yerleri, *Türkiye Ormancılık Dergisi*, 3(1), 135 – 146.

Peakall, R., Smouse, P.E. (2012), GenALEx 6.5: genetic analysis in Excel. Population genetic software for teaching and research-an update, *Bioinformatics*, 28(19), 2537–2539.

Pritchard, J.K., Stephens, M., Donnelly, P. (2000), Inference of population structure using multilocus genotype data, *Genetics*, 155, 945–959.

Smulders, M.J.M., Van Der Schoot, J.P., Vosman, B. (2001). Trinucleotide repeat microsatellite markers for black poplar (*Populus nigraL.*), *Molecular Ecology Notes*, 1, 188–190.

Smulders, M.J.M., Cottrell, J.E., Lefevre, F., Van Der Schoot, J., Arens, P. et al. (2008a). Structure of the genetic diversity in black poplar (*Populus nigra* L.) populations across European river systems: consequences for conservation and restoration, *Forest Ecology and Management,* 255(5), 1388– 1399.

Smulders, M.J.M., Beringen, R., Volosyanchuk, R., et al. (2008b), Natural hybridisation between *Populus nigra* L. and *P. x canadensis* Moench. Hybrid

offspring competes for niches along the Rhine River in the Netherlands, *Tree Genetics and Genomes*, 4, 663.

Stolarski, M.J., Warminski, K., Krzyzaniak, M. (2020), Energy Value of Yield and Biomass Quality of Poplar Grown in Two Consecutive 4-Year Harvest Rotations in the North-East of Poland, *Energies*, 13(6), 1495.

Taşkıran, B. (2014). Genetic control of cellulose, lignin and glucose contents in European black poplar (*Populus nigra* L.) Populations from Turkey. (Not puplished MS thesis). Middle East Technical University/ The Graduate School of Natural and Applied Sciences, Ankara.

Taşkıran, B. (2020). Genetic differentiation of European black poplar (*Populus nigra* L.) clones and populations with respect to some enzymes involved in biosynthesis of cellulose and lignin. (Not puplished PHD thesis). Middle East Technical University/ The Graduate School of Natural and Applied Sciences, Ankara.

Toplu, F. (2005), Breeding and conservation of black poplar (*Populus nigra*) gene resources in Turkey, *Unasylva*, 221(56), 26–30.

Tuskan, G.A., Gunter, L.E., Yang, Z.K., Yin, T., Sewell, M.M., and DiFazio, S.P. (2004), Characterization of microsatellites revealed by genomic sequencing of *Populus trichocarpa*, *Canadian Journal of Forest Research*, 34, 85-93.

Vanden Broeck, A. (2003), *Genetic conservation and use for European black poplar (Populus nigra)*, Rome: EUFORGEN technical guidelines, International Plant Genetic Resources Institute.

Van Der Schoot, J., Pospiskova, M., Vosman, B., Smulders, M.J.M. (2000), Development and characterization of microsatellite markers in black poplar (*Populus nigra* L.), *Thoeretical Applied Genetics*, 101(1–2), 317–322.

Van Oosterhout, C., Hutchinson, W.F., Wills, D.P.M., Shipley, P. (2004), MICRO-CHECKER: software for identifying and correcting genotyping errors in microsatellite data, *Molecular Ecology Notes*, 4, 535–538.

Velioğlu, E., Bostanci, Y.S., Akgül, S. (2020), *Poplars and willows in Turkey: country progress report of the National Poplar Commission time period: 2016-2019*, Kocaeli: Poplar and fast-growing Forest Trees Research Institute.

Wang, J., Li, Z., Guo, Q., Ren, G., Wu, Y. (2011a), Genetic variation within and between populations of a desert poplar (*Populus euphratica*) revealed by SSR markers, *Annals of Forest Science*, 68, 1143-1149. Wu, G., Lin, W.C., Huang, T., Poethig, R.S., Springer, P.S., Kerstetter, R.A. (2008), KANADI1 regulates adaxial-abaxial polarity in Arabidopsis by directly repressing the transcription of asymmetric leaves, *Proceedings of the National Academic Science*, 105, 16392–16397.

Web site of the International Populus Genome Consortium, 2016. Available at http://www.ornl.gov/sci/ipgc/ssr_resources. htm. Accessed March 2016.

Web site of the efloras. Available at http:// www.efloras.org, Accessed May 2022.

Web site of EUFORGEN, European forest genetic resources programme. Available at http:// www.euforgen.org, Accessed May 2022.

Yaltırık, F. (1993), *Dendroloji*, İstanbul: İ.Ü. Orman Fakültesi.

Yaltırık, F., Efe, A. (2000), Dendroloji, İstanbul: İ.Ü. Orman Fakültesi.

Yer Çelik, E.N., Ayan, S., Baloğlu, C.M. (2021), Bazı kavak (*Populus* L.) taksonlarının kadmiyuma karşı fitoekstraksiyon rolleri, *Turkish Journal of Forest Science*, 5(1), 46-56.

Yıldırım, K., Kaya, Z. (2017), Gene regulation network behind drought escape, avoidance and tolerance strategies in black poplar (*Populus nigra* L.), Plant Physiology and Biochemistry, 115, 183-199.

Yıldırım, K., Kaya, Z. (2017), Identification of adaptive responses of black poplar to drought stress, *Journal of New Results Science*, 12, 12-25.

Yıldırım, K., Uylas, S. (2016), Genome-wide transcriptome profiling of black poplar (*Populus nigra* L.) under boron toxicity revealed candidate genes responsible in boron uptake, transport and detoxification, *Plant Physiological Biochemistry*, 109, 146e155.

Zeng, Y.F., Zhang, J.G., Abuduhamiti, B., Wang, W.T., Jia, Z.Q. (2018), Phylogeographicpatterns of the desert poplar in Northwest China shaped by both geologyand climatic oscillations, *BMC Evolutionary Biology*, 18, 75.

Zeps, M., Voronova, A., Smilga, J., Kanberga-Silina, K., Lubinskis, L., Baders, E., Rungis, D., Jansons, A. (2017), Within- and among-stand genetic diversity of common aspen (*Populus tremula* L.) in Latvia, *Baltic Forestry*, 23(2), 498-506.

Zeybek, E. (2014), Differential expression of cold resistant related genes in *Populus nigra* L. Clones, (Not puplished PHD thesis). Middle East Technical University/ The Graduate School of Natural and Applied Sciences, Ankara.

Zhang, C., Vornam, B., Volmer, K., Prinz, Kathleen., Kleemann, F., Köhler, L., Polle, A., Finkeldey, R. (2015), Genetic diversity in aspen and its relation to arthropod abundance, *Frontiers in Plant Science*, 5, https://www.frontiersin.org/article/10.3389/fpls.2014.00806.

Zhang, B., Xu, Q., Gao, D., Jiang, C., Liu, F., Jiang, J., Wang, T. (2020), Altered water uptake patterns of *Populus deltoides* in mixed riparian forest stands, *Science of The Total Environment*, 706.

CHAPTER III

ASSESSMENT OF THE ROLE OF BIRDS IN SEED DISTRIBUTION: A BIBLIOMETRIC ANALYSIS OF STUDIES ON THIS SUBJECT

EMRAH ÇELİK[1,2*] & LEYLA SARIBOĞA[3]

[1,2](*Asst.Prof.Dr*) *Igdir University,*
[1]Department of Foresty- Hunting and Wildlife Programme
[2]Igdir University, Ornithology Research and Application Centre (ORNITHOCEN)
e-mail: celikemrah822@gmail.com
ORCID : 0000-0003-1274-4122

[3](MSc) Igdir University
[3]Department of Organic Farming Management
e-mail: leyla_yrdkl@hotmail.com
ORCID: 0009-0007-1055-8242

1. Introduction

Birds are known as a group of living beings consisting of winged, feathered, warm-blooded and egg-laying vertebrates. Thanks to their ability to fly, they can be found in almost every part of the world. There are more than 11,000 bird species worldwide, each with unique physical characteristics, behaviors, and habitats (IUCN, 2023). Birds play a critical role in maintaining the balance of ecosystems and provide a range of valuable services known as "ecosystem services." Some bird species, such as hummingbirds, are important pollinators of flowers, fruits, and vegetables.

They play a vital role in the reproductive success of plants and help to conserve biodiversity (Ford, 1985; Kelly ve ark., 2004). Certain species of vultures play an important role in removing dead animal remains and decaying matter from the ecosystem, which helps to prevent the spread of diseases (DeVault et al., 2003; Prakash et al., 2003). Birds serve as an important part of

our natural heritage, providing cultural and aesthetic benefits by contributing to people's enjoyment of nature (Çelik et al., 2021a). Birds act as a natural pest control mechanism by feeding on insects and other small vertebrates. By helping to keep populations of harmful insects and small rodents in check, birds contribute to reducing damage to crops and other plant communities (Mols and Visser, 2002; Van Bael et al., 2003; Perfecto et al., 2004). Birds, as primary consumers, play an essential role in the nutrient cycle by accumulating and distributing nutrients through their droppings, which can improve soil fertility and promote plant growth. This cycling of nutrients from the atmosphere to the soil and back to the atmosphere through the activities of birds and other organisms is a crucial ecological process that contributes to the sustainability of ecosystems ((Sanchez-Pinero ve Polis, 2000; Wolfe ve ark., 2004; Croll ve ark., 2005). Bird-mediated seed dispersal is a critical ecosystem service that plays a crucial role in maintaining plant diversity and ecosystem functioning (Chen et al., 2022; Silva, 2022; Jordano, 2014).

Birds unique ability to transport seeds over long distances can lead to the establishment of new populations of plant species, which is important for maintaining genetic diversity and increasing the resilience of ecosystems to environmental change (Kelly et al., 2004). This process is particularly important in fragmented landscapes, where bird-mediated seed dispersal can help connect isolated patches of habitat and promote landscape connectivity. Numerous studies have been published on the role of birds in seed dispersal in different regions of the world (Scott et al., 1997; Şekercioğlu et al., 2004; Clark et al., 2005; Whelan et al., 2008; Garcia et al., 2010; Rumeu et al., 2022; Peña et al., 2023). Bibliometric analysis is a valuable tool for assessing the scientific literature and identifying research trends and knowledge gaps in a particular field (de Oliveira et al., 2019). The use of content analysis in bibliometric studies can provide insights into the key themes and concepts addressed in the literature, as well as the geographic and temporal distribution of research (Çelik et al., 2021b) By using bibliometric analysis methods to examine the literature on bird-mediated seed dispersal, this study contributes to our understanding of the current state of research in this field and highlights areas where further investigation is needed.

2. Methodology

2.1. Analysis supported by bibliometrix for dimensionality reduction

Environmental conditions are dynamic, and as a result, it is likely that there will be an increase in the number of reports related to changes. In some research

fields, there are numerous review articles that propose new research approaches or identify gaps in the literature. However, there are fewer bibliometric analysis review studies compared to descriptive or narrative review articles. As a result, the theoretical framework in this section focuses on bibliometric analysis that includes document collection and dimension reduction approaches. To conduct an analysis on the topic, we utilized Bibliometrix, a free online software based on R-Studio (https://www.bibliometrix.org/home/). After optimizing the program's operating conditions and generating a BibTeX file version of the SCOPUS documents, we utilized Bibliometrix to perform our analysis.

2.2. Approach to information retrievel

This title refers to the process of obtaining information or data for research or analysis purposes. The search strategy component includes the methods and techniques used to identify and locate relevant data sources, such as databases, literature, or websites (Chen, 2017). The data collection component includes the process of collecting and compiling the identified data in a usable format. This may involve activities such as data entry, data coding, or data processing to ensure that the data is accurate and usable for the intended research or analysis (Kulak, 2018; Çelik et al., 2021b). The purpose of the search strategy and data collection is to obtain accurate, relevant, and high-quality data that can be used to answer research questions and support results (Ramalho et al., 2020)

The process of search strategy and data collection is a critical component of many research projects, as it is necessary to ensure the validity and reliability of the obtained findings. To scan the SCOPUS database for the keywords relevant to the research topic, the following steps were taken:

1. A search was conducted using the query "TITLE-ABS-KEY (seed dispersal" AND "animals")", which yielded 2,827 documents.
2. Another search was performed using the query "(LIMIT-TO (EXACTKEYWORD, "Aves") OR LIMIT-TO (EXACTKEYWORD, "Bird") OR LIMIT-TO (EXACTKEYWORD, "Birds"))" (Accessing Date: 13.02.2023). This search produced 634 documents that were used for bibliometric analysis.

3. Results and Discussion

3.1. Descriptive analyzes

Table 1 presents the key information of the documents extracted through bibliometric analysis. According to the SCOPUS database, a total of 634

documents were identified between the years 1986-2024. Our primary aim during the publication search process was to obtain a larger number of documents. Therefore, we opted for the SCOPUS database, as we did in our previous studies (Çelik et al., 2021b). The SCOPUS database provides researchers with access to publications scanned from a wide range of sources (Kulak et al., 2019; Ramalho et al., 2020). With a total of 44,034 resources scanned as of the access date of February 13, 2023, SCOPUS includes a diverse array of resources such as journals, printed conference booklets, books, and more across various disciplines.

Based on our bibliometric analysis, we found that 1705 authors have published research papers, with a total of 1899 keywords being used across these papers. On average, each document received 10.3 citations. One interesting finding from our analysis is that the annual growth rate of publications on this topic is 0%. This implies that the number of studies published on this topic has remained constant over time, indicating either a lack of new developments or a sustained level of interest in the subject. Further interpretations of this result are possible and warrant further investigation.

Our study will focus on the keywords used in documents published on the subject of bird-seed transport, which were identified through our analysis. These keywords will form the basis of our investigation in the subsections of the study. In addition, we conducted various analyses, including the productivity of countries in publishing related works, the most commonly used keywords, a thematic map of keywords, word cloud analyses of keywords, titles, and abstracts used in related documents, trend analyses of keywords, and conceptual structure map analyses. These analyses will help us to gain a comprehensive understanding of the current state of research on bird-seed dispersal

Table 1. Synthesis of Relevant Document Information

Description	Results
Timespan	1986:2024
Sources (Journals, Books, etc)	164
Documents	634
Annual Growth Rate %	0
Document Average Age	10,3
Average citations per doc	47,53
Keywords Plus	3097
Author's Keywords	1899
Authors	1705
Authors of single-authored docs	40
Article	597
Conference paper	2
Letter	9
Note	3
Review	21
Short survey	2

3.2. Author and country analysis for the retrieval documents

As shown in Figure 1, the top 10 authors who have published the most documents on seed dispersal and birds are presented. Notably, "Böhning-Gaese, K" and "Jordano, P" occupy the first and second places, respectively, with each author contributing 23 articles.

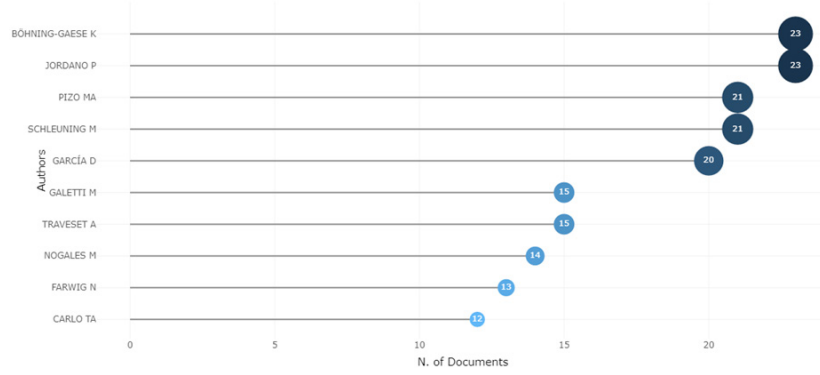

Figure 1. Most relevant authors

The authors' "Production over Time" analysis indicates that "Böhning-Gaese, K" did not publish any articles after 2020, whereas "Jordano, P" contributed regularly every year from 2014 to 2023, as shown in Figure 2. "Böhning-Gaese, K" contributed the most articles to the field from Germany, and "Jordano, P" from Spain. In the analysis, "Böhning-Gaese, K" and "Jordano, P" were identified as the top authors who made significant contributions to the field, followed by "Pizo, MA (n=21)" from Brazil and "Schleuning, M (n=21)" from Germany. Both of these authors have consistently published relevant documents, confirming their significant contributions to the field. The author named "Schleuning, M" has been publishing documents related to the subject on a regular basis since 2011, as revealed by the analysis (Figure 2). Recent research has shown that the contributions of "Böhning-Gaese, K" and "Jordano, P" to the field of ecological interactions have been particularly influential in advancing our understanding of mutualistic relationships between plants and animals. For example, Böhning-Gaese and colleagues have conducted numerous studies exploring how frugivorous birds impact the fitness of plants through seed dispersal, while Jordano's research has focused on the coevolutionary dynamics between figs and their pollinators. By elucidating the ecological and evolutionary mechanisms that underlie these interactions, their work has provided important insights into how biodiversity is generated and maintained in natural systems. Furthermore, the contributions of "Pizo, MA" and "Schleuning, M" have been instrumental in highlighting the importance of considering spatial and temporal variation in ecological interactions, as well as the potential impacts of global change on these dynamics.

Overall, the work of these authors has significantly advanced our understanding of the ecological and evolutionary processes that shape interactions between species, and their continued contributions to the field will undoubtedly be valuable for informing conservation and management efforts.

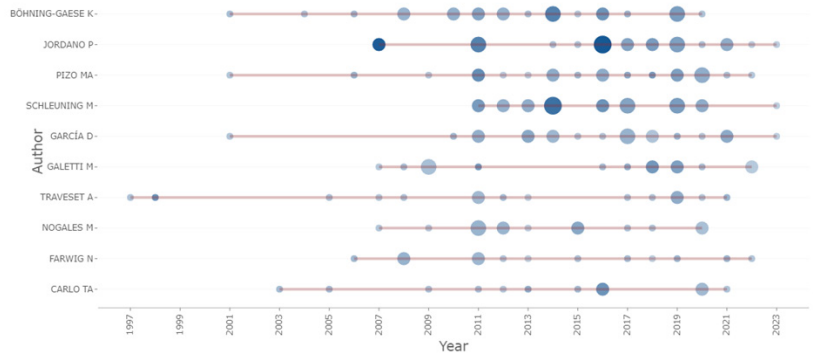

Figure 2. Authors' production over Time

Our analysis also included an examination of the scientific output on the subject by country, revealing that the United States of America (USA) has the highest number of publications (n=451 out of 634 documents included in the analysis; see Figure 3). However, when considering the location of publications related to the topic, there is a tight author collaboration between countries according to the "Collaboration World Map" analysis (see Figure 4). This means that, for example, in a study conducted within the borders of the United States, co-authors may be from different countries and their institutional addresses may indicate different countries. This situation contributes to the publication count of each country involved in the study. Of course, this example also applies to other countries that have published documents related to the topic. When examining the scientific output of countries, the United States ranked first, Spain ranked second, and Germany ranked third.

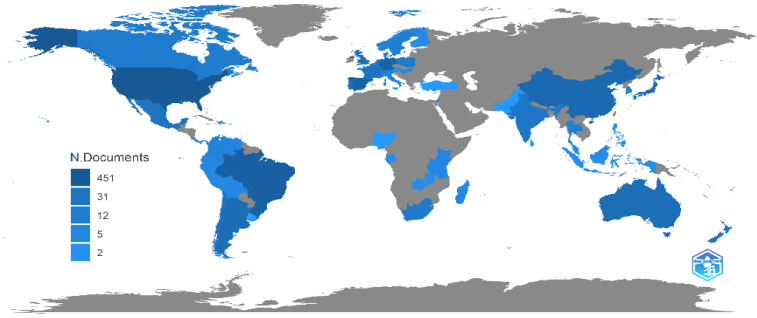

Figure 3. Country scientific production

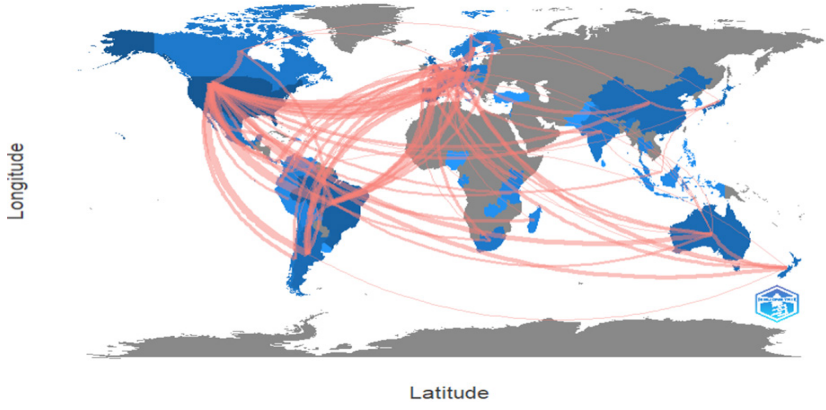

Figure.4. Collaboration World Map

Based on the number of citations received, the USA is ranked first with 10,495 citations, followed by Spain with 3,627 citations and Germany with 2,325 citations, as shown in Figure 5. The dominance of the USA in terms of the number of citations received can be attributed to the large number of research institutions and funding available for research in the country. Spain and Germany also have strong research systems and funding, which is reflected in their relatively high numbers of citations. However, it is worth noting that citation patterns can also vary across different fields of study and disciplines, and should be interpreted in context.

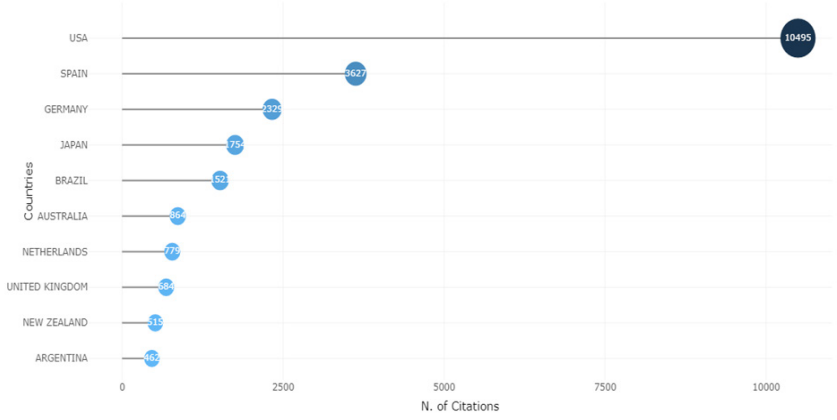

Figure 5. Most cited countries

The author applied the "Lotka Law" to the analyzed documents. This empirical formula describes the relationship between the frequency of publications in a specific field and the number of authors who contribute to those publications (Lotka, 1926). The results presented in Figure 6 indicate that the majority of authors (79.3%, N=1351) in this study have made at least one contribution to the body of literature being analyzed. However, it is noteworthy that a relatively small proportion of authors (11.9%, N=203) have made multiple contributions, suggesting that a subset of authors may be responsible for a significant portion of the research output in this area.

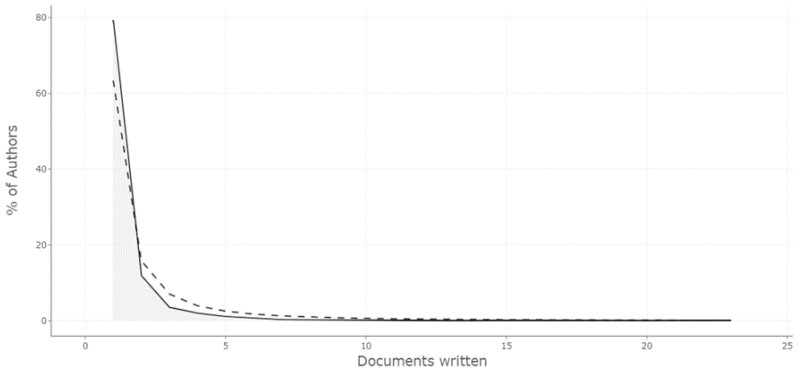

Figure 6. Author productivity through Lotka's Law

The h-index is considered as a measure of a researcher's productivity and impact in a specific field, based on their publication records and the number of citations their work has received (Baldock et al., 2009). However, there are some limitations in determining the h-index, and a possible issue is self-citation, which can artificially inflate a author's h-index. Excluding self-citations may enable a more accurate evaluation of a author's impact in the field. Figure 7 presents the h-index values of the authors, which may be associated with the number of documents they produced as shown in Figure 1. Among the authors included in the analysis, "Böhning-Gaese, K" ranked first with an h-index of 20, followed by "Jordano, P" and "Schleuning, M" with h-index values of 17 and 16, respectively. These results provide insights into the relative impact and productivity of individual authors within the field and may guide future research on scientific authorship and collaboration. Changes observed in authors' h-index values may not always be due to the sheer number of documents produced. Rather, factors such as the impact factor and reputation of the journals in which an author publishes their work and the number of citations their work receives can have a significant influence on the determination of the h-index. Publishing in high-impact journals that are widely read and cited by others can give researchers an advantage in achieving a higher h-index compared to researchers who publish in lower-impact or lesser-known journals. Similarly, access options and regional disparities in access to research can affect the visibility and citation rates of authors' work, which in turn can impact their h-index.

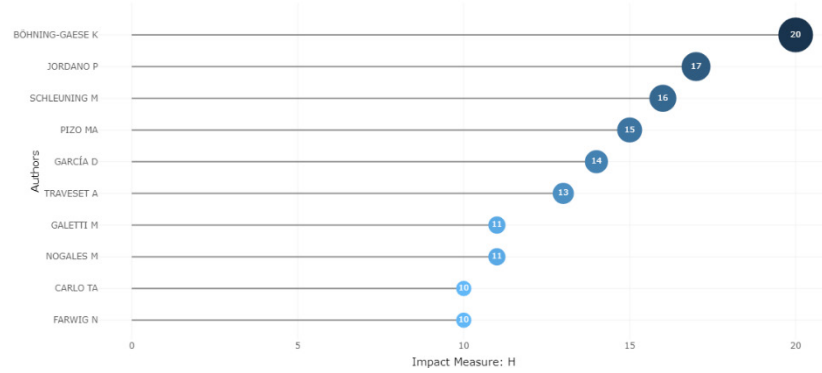

Figure 7. Author local impact

Figure 8 shows the countries of the relevant authors. Analyzing the countries of the relevant authors can provide an idea about the number of publications and collaborations within and between countries. By analyzing the authors' geographic locations, we can determine patterns and trends in scientific collaboration and publication outputs, and how they vary across different fields and regions. The relevant collaboration assessment is based on intra-country (SCP) and inter-country (MCP) collaboration during the period of 1986-2023.

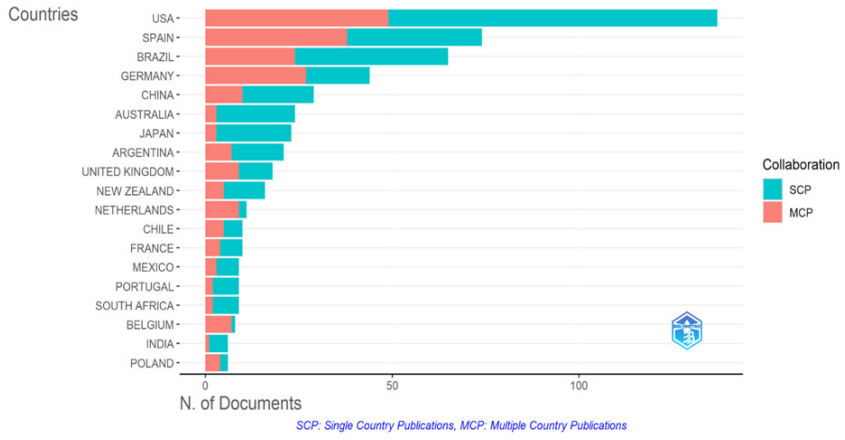

Figure 8. Corresponding author's country

Figure 8 shows the top 20 countries. According to this, the top three countries are the USA (SCP: 88, MCP: 49), Spain (SCP: 36, MCP: 38), and Brazil (SCP: 41, MCP: 24), respectively. When considering the MCP_{ratio}, the top three countries are Germany (MCP_{ratio}: 0.614; documents: 44; SCP: 17; MCP: 27), Spain (MCP_{ratio}: 0.514; documents: 74; SCP: 36; MCP: 38), and Brazil

(MCP_{ratio}: 0.369; documents: 65; SCP: 41; MCP: 24). It is interesting to note that the top three countries based on SCP (total number of documents) differ slightly from the top three based on MCP (number of international collaborations normalized by total number of collaborations). This highlights the importance of considering international collaborations when evaluating the scientific impact and productivity of a country or region. Furthermore, analyzing the changes in the top countries over time can provide valuable information on the evolving landscape of scientific research and collaboration.

3.3. Sources

The identification of the most relevant sources in Bibliometrics studies can aid researchers in gaining a deeper understanding of a field's knowledge base and intellectual structure, as well as in identifying significant research trends and influential authors.

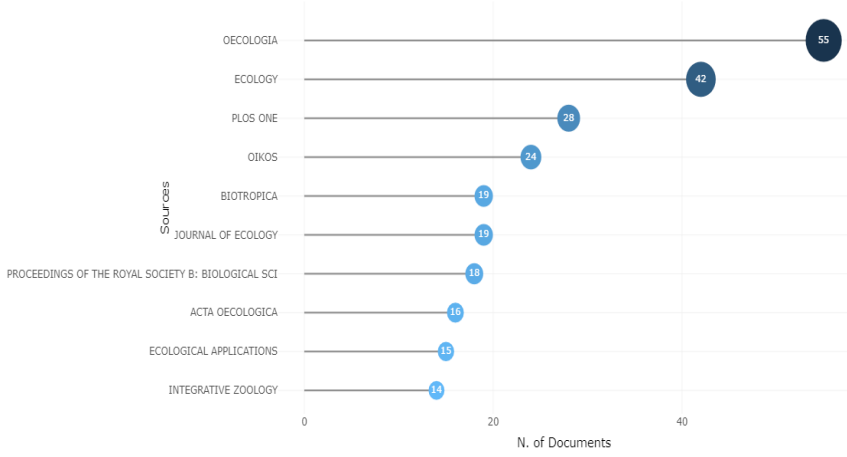

Figure 9. Most relevant sources

Figure 9 shows the most relevant publication sources, with "Oecologia (Springer)" ranking first with 55 documents. Following this journal are "Ecology (n=42, Wiley)" and "Plos One (n=28, Taylor & Francis)". "Oecologia" and "Ecology" are peer-reviewed scientific journals that publish research related to all aspects of ecology. PLOS ONE (Public Library of Science ONE) is a peer-reviewed, open-access scientific journal that publishes original research from all areas of science and medicine.

3.4. Bradford's law

Bradford's Law is a principle in the field of library and information science that describes the distribution of scientific and technical journals in a given field of study (Black, 2004). According to Bradford's Law, the literature of a subject can be divided into three zones or groups of journals. The first zone includes core sources, which are the most important and influential journals in the field. These journals constitute a relatively small proportion of the total number of journals in the field, but they publish a significant portion of the most important and influential articles. In our analysis, we obtained three zones corresponding to 164 sources. The first zone consisted of 8 sources. Figure 10 shows 8 out of 20 sources in this zone. The second and third zones contained 25 and 131 sources, respectively.

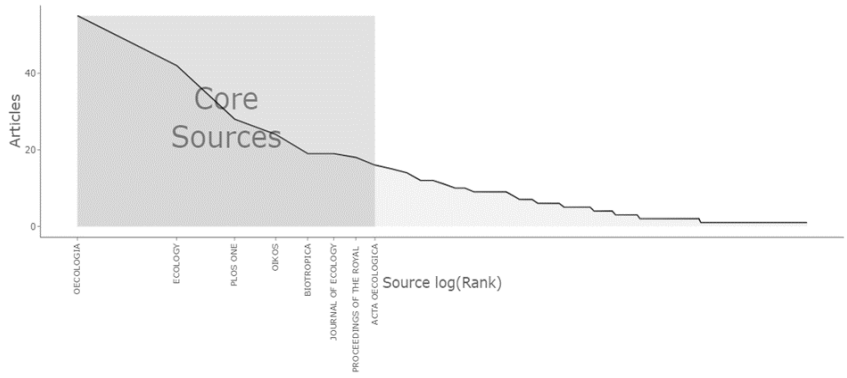

Figure 10. Source clustering through Bradford's Law

According to Bradford's Law, the literature on a particular subject can be divided into three zones or groups of journals. The first zone comprises core journals that are the most important and influential in the field. These journals represent a relatively small proportion of the total number of journals in the field, yet they publish a substantial proportion of the most significant and influential articles. The second zone includes secondary journals that have a moderate level of importance and impact, representing a larger portion of the total number of journals in the field but publishing a smaller proportion of the most important articles. The third zone consists of tertiary journals that are the least important and influential in the field, representing the largest proportion of the total number of journals in the field but publishing a very small proportion of the most significant articles. The zones are formed based on the groups of

journals that publish relevant articles on the subject, and some journals in the second and third zones should not be considered insignificant or low-impact. The most critical factor in the formation of these zones is the publication acceptance criteria of the journals.

3.5. Source local impact

The h-indices of the journals that have published the most documents on the topic are shown in Figure 11. According to this, Oecologia ranks first with an h-index of 31, followed by Ecology with an h-index of 26 and Oikos with an h-index of 15 in second and third place, respectively (Table 2). A high h-index of journals can be a motivating factor for authors to increase the visibility of their research (Virú-Vásquez et al., 2022). However, it is important to note that the pursuit of a high h-index may also have negative consequences. For example, it may encourage unethical behaviors such as citation manipulation by authors (Engqvist and Frommen, 2008). Additionally, a high h-index does not necessarily fully reflect the quality of a researcher's work or their impact on the scientific community (van Raan, 2006).

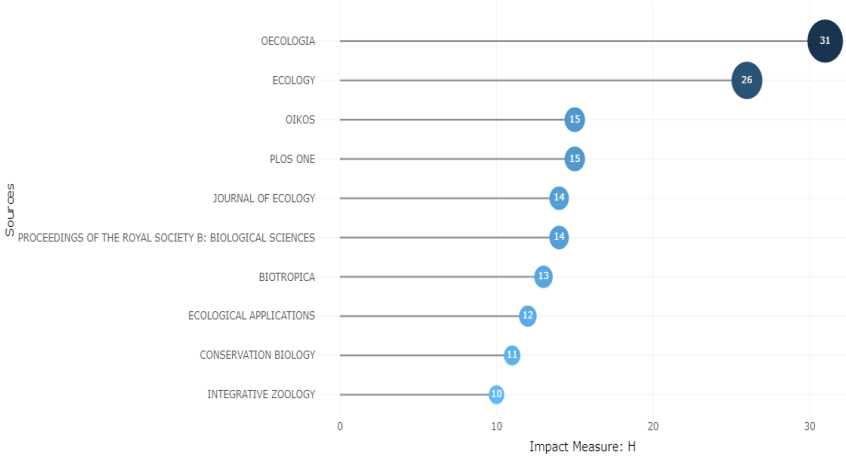

Figure 11. Source local impact

The h-index is a metric that measures the productivity and impact of a researcher's work. It is defined as the highest number of papers that have been cited h or more times (Hirsch, 2005). The g-index is a metric that is similar to the h-index, but places more emphasis on highly cited papers. It is defined as the highest number g such that the top g papers have together received at least

g squared citations (Schreiber, 2008). The m-index is a metric that measures the productivity of a researcher's work, while taking into account the number of co-authors on each paper (Schreiber, 2008). It is defined as the h-index divided by the average number of authors on each paper. These metrics are often used to evaluate the impact and productivity of researchers, but they have their limitations and should not be used as the sole indicator of quality or impact.

Table 2. Source local impact

Sources	h_index	g_index	m_index	TC	ND	ACD
Oecologıa	31	51	0,886	2639	55	1989
Ecology	26	42	1,13	2524	42	2001
Oikos	15	24	0,556	672	24	1997
Plos One	15	26	1	712	28	2009
Journal of Ecology	14	19	0,609	712	19	2001
Proceedıngs of the Royal Socıety B: Bıologıcal Scıences	14	18	0,7	878	18	2004
Biotropica	13	19	0,448	844	19	1995
Ecological Applications	12	15	0,48	860	15	1999
Conservation Biology	11	11	0,647	684	11	2007
Integrative Zoology	10	14	0,769	204	14	2011

ND: Number of Documents **ACD:** Airing Commencement Date, **TC:** Total Citation

3.6. Visualizing keyword frequencies in retrieved documents

WordCloud analysis is a visual representation of the most frequently used words or terms that appear in a series of documents or publications. In bibliometrics, WordCloud analysis can provide insights into the most common topics, themes, or keywords used in a series of publications or in a specific field or discipline (Atenstaedt, 2012). In this context, we conducted a WordCloud analysis using the "Keywords Plus," "Author Keywords," "Titles," and "Abstracts" data obtained from the documents. The top 50 most frequently used words were utilized to generate a WordCloud for each analysis.

Among the "Keywords Plus" words, "seed dispersal (n=791)," "bird (n=482)," and "aves (n=448)" stood out. When considering the results of the WordCloud analysis as a whole, it becomes evident that living groups involved in seed transport and birds, in particular, were frequently mentioned. Additionally, the analysis draws attention to the contributions of seed transport

to the ecosystem, such as pollination, biodiversity, and plant-animal interactions (see Figure 12).

Figure 12. "WordCloud of keywords plus (number of words:50)

WordCloud analysis highlight the importance of seed dispersal in maintaining the biodiversity and ecological balance of natural systems. Specifically, the prominent presence of "seed dispersal," "bird," and "aves" in the Keyword Plus list suggests that birds play a critical role in seed transport and ecosystem functioning. This is consistent with previous studies that have shown birds to be key seed dispersers in many habitats worldwide. Moreover, the identification of pollination, biodiversity, and plant-animal interactions as significant contributions of seed transport underscores the essential ecological services provided by this process.

When a WordCloud is generated from "Keywords Plus" terms that align with the main theme of the research, it suggests that the authors have provided relevant and accurate keywords that reflect the primary topics and themes of their study. This may indicate that the authors conducted a thorough and comprehensive literature review and selected appropriate keywords to describe their research. As illustrated in the thematic map of the word cloud analysis (see Figure 12), the researchers who published documents on the subject utilized keywords that are pertinent to the main theme of the current study. The "Author's keywords" analysis revealed that "seed dispersal (n=221)", "frugivory (n=100)", and "birds (n=44)" were the most commonly used keywords (see Figure 13). Visual examination of the frequently used keywords indicates that the authors frequently mentioned the mechanisms involved in seed transport by birds. It also

highlights the importance of considering the interplay between different species in ecological processes, such as the interactions between birds and plants in seed dispersal through frugivory.

Figure 13. WordCloud of author's keyword (number of words:50)

Based on the WordCloud analysis conducted on the "Titles" used by authors in documents related to the subject, the most frequently occurring words are "seed" (n=274), "dispersal" (n=237), and "birds" (n=98), as depicted in Figure 14. The high frequency of the words "seed" and "dispersal" suggests that research related to the dispersal of seeds is an active area of investigation, which is consistent with the critical role of seed dispersal in shaping plant community dynamics and ecosystem functioning.

Figure 14. WordCloud of titles (number of words:50)

Figure 15. WordCloud of abstract (number of words:50)

Figure 15 depicts a WordCloud analysis of the abstracts of published documents related to the subject. The analysis reveals that the most frequently occurring keywords in these abstracts are "seed" (n=2078), "species" (n=2037), and "dispersal" (n=1584). There could be several reasons why different keywords appeared in each of the word cloud analyses. One possible explanation is that the different sections of the document (e.g., titles, abstracts, keywords) serve different purposes and, therefore, may emphasize different aspects of the research. For example, titles are typically meant to be concise and attention-grabbing, while abstracts are designed to provide a brief summary of the study's main findings and conclusions. As a result, the keywords and language used in each section may vary. Additionally, the methodology used in each analysis may have contributed to the differences in the results. For example, the "Keywords Plus" analysis identifies frequently occurring words from the entire document, including the abstract and the full text, while the "Author's keywords" analysis only includes keywords selected by the authors themselves. The "Titles" analysis, on the other hand, focuses solely on the words used in the document title

3.7. Thematic map of keyword plus

Overall, the thematic maps used in Bibliometrix provide a useful way to explore and analyze the major themes and trends present in bibliographic data. They can be used to identify important research topics, track changes in the field

over time, and compare the research output of different authors, institutions, or journals.

Figure 16 illustrates the thematic map of "Keyword Plus" extracted from documents related to the subject, revealing study topics across all themes. In the "Emerging or Declining Themes" dial, there appears to be a waning interest in research on bird-seed transport in forest ecosystems. Conversely, the "Motor Theme" quadrant indicates an increasing focus on studying the mechanisms of seed transport and the ecosystem services provided by birds. Additionally, research on plant-animal interactions remains a popular area of study. The Motor Theme dial typically showcases the key concepts, theories, and methodologies commonly used in the field.

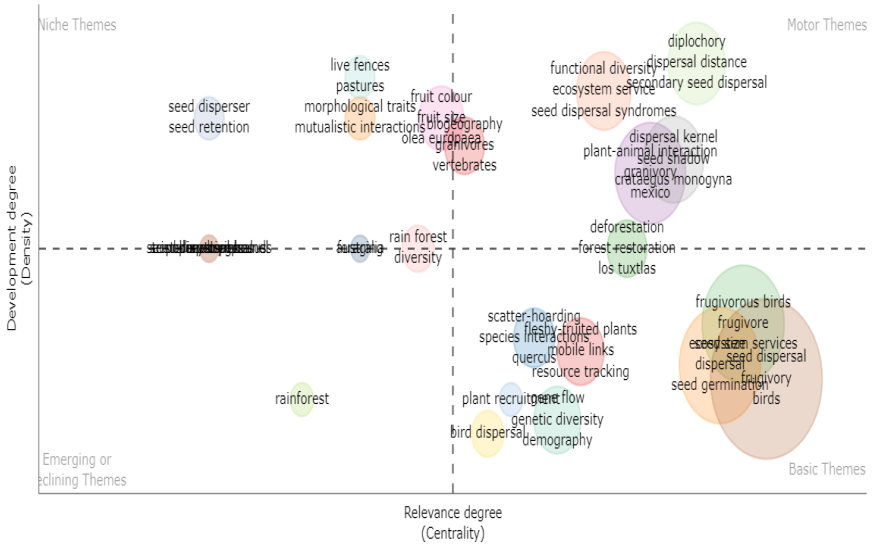

Figure 16. Thematic map of keyword plus

3.8. Co-word analysis

Based on the Multiple Correspondence Analysis (MCA) analysis shown in Figure 17, two main clusters were identified. The blue cluster comprises concepts such as vertebrata (mammalia, birds, rodentia, etc.), plant-animal interactions, frugivory, zoochory, and herbivory. This cluster includes topics related to animal groups that facilitate seed transport and the seed transport mechanisms of birds. The red cluster, on the other hand, contains concepts such as "nonhuman", "biodiversity", "pollination", and "forestry". This cluster focuses on the benefits of seed transport related to ecosystem services.

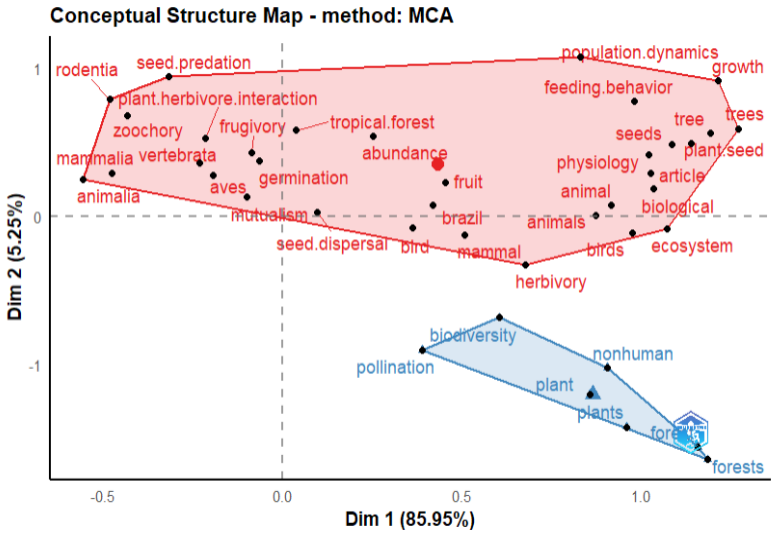

Figure 17. Conceptual structure of the documents

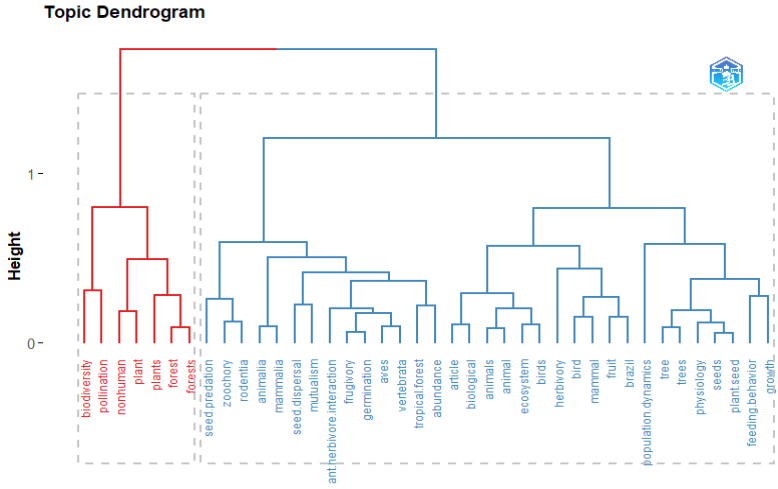

Figure 18. Topic dendogram of the documents

We constructed a topic dendrogram (Figure 18) to better understand the linkages and closeness of the words. This analysis allowed us to classify words and observe their proximity to each other. The topic dendrogram analysis complemented the MCA, revealing two major clusters (which were also observed in the MCA results) with multiple sub-clusters.

4. Conclusıon

The studies reviewed in this analysis primarily focus on the role of birds in seed dispersal and the factors that impact seed dispersal efficiency. It is generally accepted that bird-mediated seed dispersal is an effective way to transport seeds over long distances. Some studies have explored the effect of bird behavior on seed dispersal, including bird diet, feeding behavior, and locomotion patterns. Others have investigated the impact of bird populations and community structure on seed dispersal, such as bird species richness and bird-plant interactions. Overall, research shows that bird-mediated seed dispersal is a powerful and essential process in maintaining plant diversity and dispersal. However, the specific outcome depends on various biotic and abiotic factors. The Bibliometrix study yielded important findings regarding the countries publishing documents related to the subject. We presented detailed numerical and visual analyses on this topic in earlier sections of the study. It is not surprising that the USA dominates ecological research, given its significant funding and support for scientific research, as well as the presence of numerous world-renowned research institutions and universities. However, it is worth noting that other countries have also made substantial contributions to the field, including Germany, Spain, Brazil, and the United Kingdom, which collectively account for a significant proportion of the analyzed documents. Furthermore, developing countries such as China, India, and South Africa are increasing their research output in ecology and may play a more prominent role in the future.

REFERENCES

Atenstaedt, R. (2012). Word cloud analysis of the BJGP. British Journal of General Practice, 62(596), 148-148.

Baldock, C., Ma, R., & Orton, C. G. (2009). The index is the best measure of a scientist's research productivity. Medical Physics, 36(4), 1043-1045.

Black, P. E. (2004). Bradford's law, in dictionary of algorithms and data structures. Gathersburg: National Institute of Standards and Technology. (accessed February 2016).

Celik, E., Durmus, A., Adizel, O., & Nergiz Uyar, H. (2021b). A bibliometric analysis: what do we know about metals (loids) accumulation in wild birds?. Environmental Science and Pollution Research, 28, 10302-10334.

Chen, Z., Guo, Y., Yang, J., Ge, J., Li, L., & Chen, G. (2022). Frugivorous birds disperse seeds of Ligustrum lucidum, seed-feeding weevils, and parasitic wasps of weevils via endozoochory. Integrative Zoology, 17(5), 953-958.

Clark, C. J., Poulsen, J. R., Bolker, B. M., Connor, E. F., & Parker, V. T. (2005). Comparative seed shadows of bird-, monkey-, and wind-dispersed trees. Ecology, 86(10), 2684-2694.

Croll, D. A., Maron, J. L., Estes, J. A., Danner, E. M., & Byrd, G. V. (2005). Introduced predators transform subarctic islands from grassland to tundra. Science, 307(5717), 1959-1961.

Çelik, E., Durmuş, A., & Türkoğlu, M. (2021a). Iğdır İli ve Yakın Çevresinin Ornito-Turizm Perspektifinde Değerlendirilmesi. Journal of Academic Tourism Studies, 2(1), 32-44.

de Oliveira, O. J., da Silva, F. F., Juliani, F., Barbosa, L. C. F. M., & Nunhes, T. V. (2019). Bibliometric method for mapping the state-of-the-art and identifying research gaps and trends in literature: An essential instrument to support the development of scientific projects. In Scientometrics recent advances. IntechOpen.

DeVault, T. L., Rhodes, Jr, O. E., & Shivik, J. A. (2003). Scavenging by vertebrates: behavioral, ecological, and evolutionary perspectives on an important energy transfer pathway in terrestrial ecosystems. Oikos, 102(2), 225-234.

Engqvist, L., & Frommen, J. G. (2008). The h-index and self-citations. Trends in ecology & evolution, 23(5), 250-252.

Ford, H. A. (1985). Nectar-feeding birds and bird pollination: why are they so prevalent in Australia yet absent from Europe. In Proceedings of the Ecological Society of Australia (Vol. 14, pp. 153-158).

Garcia, D., Zamora, R., & Amico, G. C. (2010). Birds as suppliers of seed dispersal in temperate ecosystems: conservation guidelines from real-world landscapes. Conservation biology, 24(4), 1070-1079.

Hirsch, J. E. (2005). An index to quantify an individual's scientific research output. Proceedings of the National academy of Sciences, 102(46), 16569-16572.

Howe, H. F., & Smallwood, J. (1982). Ecology of seed dispersal. Annual review of ecology and systematics, 13(1), 201-228.

Kelly, D., Ladley, J. J., & Robertson, A. W. (2004). Is dispersal easier than pollination? Two tests in New Zealand Loranthaceae. New Zealand Journal of Botany, 42(1), 89-103.

Kulak, M. (2018). A bibliometric review of research trends in salicylic acid uses in agricultural and biological sciences: where have been studies directed. Agronomy, 61(1), 296-303.

Kulak, M., Ozkan, A., & Bindak, R. (2019). A bibliometric analysis of the essential oil-bearing plants exposed to the water stress: How long way we have come and how much further?. Scientia horticulturae, 246, 418-436.

Lotka, A. J. (1926). The frequency distribution of scientific productivity. Journal of the Washington academy of sciences, 16(12), 317-323.

Mols, C. M., & Visser, M. E. (2002). Great tits can reduce caterpillar damage in apple orchards. Journal of applied ecology, 39(6), 888-899.

Nathan, R., & Muller-Landau, H. C. (2000). Spatial patterns of seed dispersal, their determinants and consequences for recruitment. Trends in ecology & evolution, 15(7), 278-285.

Peña, R., Schleuning, M., Miñarro, M., & García, D. (2023). Variable relationships between trait diversity and avian ecological functions in agroecosystems. Functional Ecology, 37(1), 87-98.

Perfecto, I., Vandermeer, J. H., Bautista, G. L., Nunñez, G. I., Greenberg, R., Bichier, P., & Langridge, S. (2004). Greater predation in shaded coffee farms: the role of resident neotropical birds. Ecology, 85(10), 2677-2681.

Prakash, V., Pain, D. J., Cunningham, A. A., Donald, P. F., Prakash, N., Verma, A., & Rahmani, A. R. (2003). Catastrophic collapse of Indian white-backed Gyps bengalensis and long-billed Gyps indicus vulture populations. Biological conservation, 109(3), 381-390.

Rumeu, B., González-Varo, J. P., de Castro, C., López-Orta, A., Illera, J. C., Miñarro, M., & García, D. (2022). Increasing efficiency and reducing bias in the sampling of seed–dispersal interactions based on mist-netted birds. Oikos, e09261.

Sánchez-Piñero, F., & Polis, G. A. (2000). Bottom-up dynamics of allochthonous input: direct and indirect effects of seabirds on islands. Ecology, 81(11), 3117-3132.

Schreiber, M. (2008). An empirical investigation of the g-index for 26 physicists in comparison with the h-index, the A-index, and the R-index. Journal of the American Society for Information Science and Technology, 59(9), 1513-1522.

Scott, L., Anderson, H. M., Anderson, J. M., Cowling, R. M., Richardson, D. M., & Pierce, S. M. (1997). Vegetation history. Vegetation of southern Africa, 62-84.

Silva, L. B. (2022). Frugivory and primary seed dispersal of Elaeis guineensis by birds of prey. Brazilian Journal of Biology, 84.

Şekercioğlu, Ç. H., Daily, G. C., & Ehrlich, P. R. (2004). Ecosystem consequences of bird declines. Proceedings of the National Academy of Sciences, 101(52), 18042-18047.

Van Bael, S. A., Brawn, J. D., & Robinson, S. K. (2003). Birds defend trees from herbivores in a Neotropical forest canopy. Proceedings of the National Academy of Sciences, 100(14), 8304-8307.

Van Raan, A. F. (2006). Comparison of the Hirsch-index with standard bibliometric indicators and with peer judgment for 147 chemistry research groups. scientometrics, 67, 491-502.

Virú-Vásquez, P., Pardavé, R. H., Coral, M. F. C., Bravo-Toledo, L., & Curaqueo, G. (2022). Biochar and Compost in the Soil: A Bibliometric Analysis of Scientific Research. Environmental Research, Engineering and Management, 78(3), 73-95.

Whelan, C. J., Wenny, D. G., & Marquis, R. J. (2008). Ecosystem services provided by birds. Annals of the New York academy of sciences, 1134(1), 25-60.

Wolfe, K. M., Mills, H. R., Garkaklis, M. J., & Bencini, R. (2004). Post-mating survival in a small marsupial is associated with nutrient inputs from seabirds. Ecology, 85(6), 1740-1746.

CHAPTER IV

ANAEROBIC TREATMENT OF 2,4-DICLOROPHENOXY ACETIC ACID IN UP-FLOW ANAEROBIC PACKED BED REACTOR*

ÇAĞLA UYGUN [1] & CANSU FİLİK İŞÇEN [2] & ÜLKÜYE DUDU GÜL [3] & SEMRA İLHAN [4]

[1](Science Teacher) Eskişehir Osmangazi University, Graduate School of Sciences,Eskişehir/Türkiye e mail: caglauygun26@gmail.com
ORCID:0000-0002-3277-0531

[2] (Prof. Dr.) Eskişehir Osmangazi University, Faculty of Education, Department of Mathematics and Science Education, Eskisehir/Türkiye
e-mail:cfilik@gmail.com
ORCID: 0000-0001-5463-8825

[3] (Prof. Dr.) Bilecik Seyh Edebali University, Faculty of Engineering, Department of Bioengineering, Bilecik/Türkiye,
e-mail: ulkuyedudu.gul@bilecik.edu.tr
ORCID: 0000-0001-6443-1633

[4] (Prof. Dr.) Eskişehir Osmangazi University, Faculty of Sciences, Department of Biology, Eskişehir/Türkiye e-mail:silhan@ogu.edu.tr
ORCID:0000-0002-3787-2449

1. Introduction

Agriculture is the most important source of nutrition for the whole world, and the need for nutrition increases with the increasing population, so it was aimed to obtain more agricultural products. In line with

* This study is based in part on a master's thesis (Investigation of Anaerobic Digestibility of Different Pesticide Groups) completed at Eskisehir Osmangazi University in January 2021.

this purpose, it is tried to prevent all kinds of weeds, plants, and insects that can damage the agricultural product and affect its productivity of the product (Laetz,et al,2009) .

Uncontrolled and unconscious use of pesticides in order to provide high efficiency in agricultural areas is an important problem for human health and the environment. Studies on the treatment methods applied to eliminate the environmental effects of pesticides used in the fight against pests in agricultural areas have been increasing in recent years (Misra et al., 2013).

Anaerobic treatment systems are frequently used in the treatment of biological sludges and various wastewaters. Compared to aerobic processes, the need for less energy in the operation of the anaerobic system, the formation of methane gas as the final product, the economically valuable methane gas, and the low amount of sludge formed encourage the use of these systems (Akcal et al. 2011; Iscen and Ilhan, 2008).

In this study, the anaerobic treatment of the pesticide type 2,4-dichloro phenoxy acetic acid ($C_8H_6C_{l2}O_3$), which is widely used for the control of broadleaf weeds in agricultural areas, was investigated in a continuous reactor. The treatment conditions (hydraulic retention time (HRT), organic load, inlet pesticide concentration) of synthetic wastewater were optimized in the upflow anaerobic packed bed reactor (UAPBR). When the treated water obtained at the end of anaerobic treatment in continuous reactors is discharged, whether it has a toxic effect in the receiving environment or not has been determined using Microtox® (Vibrio fischeri) and Lepidium sativum tests.

2. Material and Method

2.1. Pesticide Solution

In this study, 2,4-diclorophenoxyacetic acid ($C_8H_6Cl_2O_3$), which appears to be a pesticide type that is widely used in agricultural fields, was used (Figure 2.1). Commercial pesticide solutions containing these active ingredients were obtained from Eskişehir Green Agricultural Products, Pesticides, and Tools Company to be economical in pesticide removal experiments in the batch reactor and to test the form widely used in agricultural activities in Eskişehir. The pesticide has been stored in a refrigerator at + 4 °C

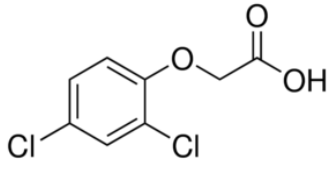

Fig. 2.1. 2,4-diclorophenoxyacetic acid

2.2. Inoculum

Anaerobic sludge (AS) used in the batch reactor was supplied from Eskişehir Sugar Factory Anaerobic Treatment Unit. Before use, the sludge was mixed thoroughly and homogenized, filtered through a filter with a pore diameter of 1 mm. Important properties of AS in terms of treatment were determined, such as pH, total suspended solids (TSS), and total solids (TS) (Table 3.1) (APHA-AWWA-WPCF., 1992).

2.3. Basal Medium

The composition of the basal medium used in the experiments is as follows (Concentrations of the components are given as mg. L^{-1}): NH_4Cl (1200), $MgSO_4$.7H2O (400), KCl (400), $Na_2S.9H_2O$ (300), $CaCl_2.2H_2O$ (50), $(NH_4)_2HPO_4$ (80), $FeCl_2.4H_2O$ (40), $CoCl_2.6H_2O$ (10), KI (10.0), $MnCl_2.4H_2O$ (0.5), $CuCl_2.2H_2O$ (0.5), $ZnCl_2$ (0.5), $AlCl_3.6H_2O$ (0.5), $NaMoO_4.2H_2O$ (0.5), H_3BO_3 (0.5), $NiCl_2.6H_2O$ (0.5), $NaWO_4.2H_2O$ (0.5), Na_2SeO_3 (0.5), ve cysteine (10.0). This basal medium contains all the micro and macronutrients necessary for optimum anaerobic microbial growth (Demirer and Speece,1998).

2.4. The HPLC Analysis of 2,4-Diclorophenoxyacetic Acid

Shimadzu UFLCXR model High-Pressure Liquid Chromatography System (HPLC) device was used for determining pesticide removal in a continuous reactor. Chromatographic instructions of HPLC device with DAD detector for the determination of 2,4-Diclorophenoxyacetic Acid (Smith, 1990).

Column: C18 (inner diameter: 250mm x 4.6mm, particle size: 5mm)

Mobile Phase: 0.05 M sodium phosphate buffer

Flow Rate: ml / min

Wavelength: 265 nm

The chromatogram obtained for the analysis of 2,4-Diclorophenoxyacetic Acid in HPLC is given in Figure 2.2. The calibration curves were created for all pesticides with the analysis made on the HPLC device. These curves include from 2.5 to 50 mg. L^{-1}. Standard solutions of 2,4 Diclorophenoxyacetic Acid (Sigma) are used and the obtained calibration chart is given in Figure 2.3.

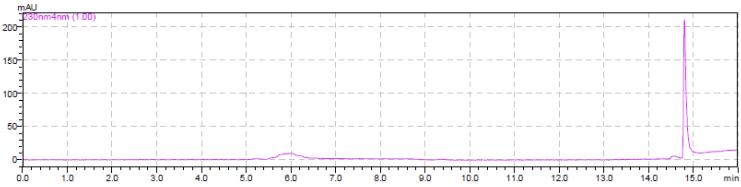

Fig. 2.2. Chromatogram obtained for 2,4D in HPLC

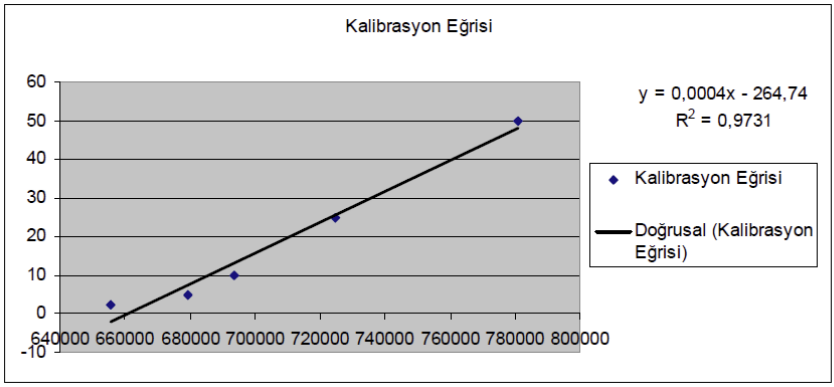

Fig. 2.3. Calibration graph for 2,4-D in HPLC

2.5. The Continuous Reactor

The continuous reactor process was performed using the Up-flow Anaerobic packed bed (UAPB**)** reactor (Iscen and Ilhan 2008). Both two reactors had a total liquid volume of 5.0 L and were filled up to 4.3 L of their volume with plastic balls. A jagged surface was achieved to maintain the bacterial biomass. The temperature of the reactors was maintained at mesophilic conditions through the use of electrical heating mats, and feeding reactors were provided by the peristaltic pufixedixed amount of sludge (inoculum) was added to the reactor.

Two and a half liters of non-granular anaerobic sludge were put into the reactor and fed with the feed solution. The biofilm formation in the reactor was achieved within the 53 day period. Varying concentrations of pesticide-containing (between 0.5 mg L^{-1} and 50 mg L^{-1}) were used in this continuous reactor. The organic loading rate (OLR) performed on the reactor ranged from 0.55-0.995 g COD $l^{-1}day^{-1}$, while the hydraulic retention time (HRT) was studied at 96 hours.

2.6. Analytical methods

COD, total solids (TS), suspended solids (SS), volatile suspended solids (VSS), alkalinity, and volatile fatty acids (VFA) were determined by standard methods (APHA-AWWA-WPCF., 1992). The volume of methane produced was measured daily by the liquid displacement method after first removing CO_2 by adsorption into the KOH solution. The toxicity level was also measured with a microtox analyzer (Microtox® Model 500 analyzer).

2.7. Toxicity Tests

2.7.1. Toxicity Test Using Vibrio fischeri

The effect of wastewater containing pesticides on prokaryotic organisms before and after treatment was determined by the *Vibrio fischeri* toxicity test. The experiment was performed on an SDI (United States) brand M500 Microtox® device. The determination of toxicity is based on the principle that the marine bacteria *Vibrio fischeri* culture decreases Luminescence properties in the presence of toxic substances. The experiments were carried out in 2% NaCl solution at 15 °C. Luminescence was measured at 490 nm. Results are expressed as the concentration at which 50% of the light emission (EC_{50}) is lost at 5 and 15 minutes (Gottlieb et al.,2003).

2.7.2. Toxicity Test Using Lepidium sativum

The toxic effect of pesticide-containing wastewater on eukaryotic vegetative cells before and after treatment was evaluated with its effect on the germination of *Lepidium sativum* seed. For the experiment, 2 Whatman No: 1 paper was sterilized in 10 cm Petri dishes, and 10 seeds were placed in each petri dish. All of Whatman No: 1 paper was wetted by adding 5 ml of samples before and after treatment into the petri dishes. Then the seeds were placed equidistantly between them. Measurements were made after 7 days of incubation. The germination number and root elongation for each concentration were used to determine the toxic effect (Tongur et al.,2017). The experiments were done in 2 replicates.

3. Results and Discussion

3.1 Determine the Properties of Anaerobic Sludge

Some properties of anaerobic sludge used in studies are given in Table 3.1.

Table 3.1. Properties of anaerobic sludge (AS)

Parameter	AS content
pH	7.4
TS (g. L^{-1})	36.4
TSS (g. L^{-1})	30.8

3.2. The Continuous Reactor

The UAPB reactor was used as the continuous reactor and was operated for 302 days. In the reactor, glucose was used as the co-substrate by the batch reactor

results. The reactor was fed with feed solution for anaerobic microorganisms for 53 days before the pesticide-containing wastewater was added to the reactor. After activation of the microorganisms, the reactor was put into operation with 0.5 mg L^{-1} pesticide-containing wastewater. The wastewater concentration was increased by each stage of operation as the experiment continued. The redox potential of wastewater was measured and resulted in observations between -310 and -411 mV.

All reactor operating conditions and the input-output values are shown in Tables 3.2.

During the continuous reactor process, the conditions with the highest treatment efficiency were tried to be reached by changing the input parameters COD and OLR. The anaerobic sludge in the continuous anaerobic reactor was fed with a glucose-containing feed solution to activate the anaerobic consortium. After activation of the consortium pesticide concentration increased gradually from 0.5 to 50 mg L^{-1}. HRT was kept constant at 96 hours during the study period. In the 302 study days, organic loading was between 0.55 – 0.99 g COD L^{-1} day^{-1} per day and COD removal ranged between 84.32% and 97.66%. When the literature is examined, studies on the anaerobic treatment of different pesticides are seen.

Puyol et al (2009) investigated the anaerobic degradation of 2,4-dichlorophenol (2,4-DCP) in upstream anaerobic sludge blanket (UASB) and expanded granular sludge bed (EGSB) reactors when glucose is used as the main carbon source. Loading rates of 1.9 g COD L^{-1} day^{-1} and 100 mg 2,4-DCP L^{-1} day^{-1} yielded 75% and 84% pesticide removal efficiencies, 61% and 80% COD removal efficiencies of this compound, respectively, with UASB and obtained in EGSB reactors (Puyol et al 2009). In a different study, a 97% pesticide removal efficiency of a herbicide mixture consisting of 2,4-D and ametrine was reported at an organic loading rate of 31.5 mg L^{-1} day^{-1} in a packed bed biofilm reactor (Sandoval-Carrasco et al.,2013).

The pH, alkalinity, and volatile fatty acid changes, which allow us to obtain information about the stability of the anaerobic treatment, were followed during the study period. When the pH values are examined, it is seen that the pH varies between 7.8 and 7.9 in all OYO changes applied in the reactor. A VFA/Alkalinity ratio of less than 0.4, used to monitor process stability, indicates that the reactor is stable, between 0.4-0.8 it is partially stable, and greater than 0.8 indicates that the reactor is unstable (Behling et al.1997). During the study, the VFA/Alkalinity ratio at the reactor outlet varied between 0.089 and 0.141. These values show that the reactor was stable during the whole

3.3. Toxicity Results

3.3.1. Toxicity Tests With Prokaryotic Cells

Vibrio fisheri toxicity test results of samples taken from different concentrations (12 mg L^{-1}, 20 mg L^{-1}, 35 mg L^{-1}) before and after treatment in the upstream anaerobic packed bed reactor are given in tables 3.3., 3.4, 3.5., 3.6, 3.7 and 3.8.

Table 3.3. *Vibrio fischeri* toxicity test results of 12 mg L^{-1} concentration before anaerobic treatment

			5 Mins Data			15 Mins Data		
Sample	**Concentration (mg. L^{-1})**	**I_0**	**I_t**	**Gamma**	**%effect**	**I_t**	**Gamma**	**%effect**
Control	0,000	118,95	167,34	1,000#		185,39	1,000#	
1	0,046	110,50	160,83	0,0000*	-3,000%	172,74	-3,000*	0,0000%
2	0,093	108,91	160,51	-4,000*	-4,000%	175,52	-3,000*	-3,000%
3	0,187	109,62	161,42	0,0000*	-4,000%	175,46	-2,000*	-2,000%
4	0,375	111,45	156,21	3,000*	0,0000%	162,75	0,0000#	6,000%
5	0,75	114,58	143,02	0,0000#	11,00%	13818	0,0000#	22,00%
6	1,5	112,07	135,17	0,0000#	14,00%	147,24	0,0000#	15,00%
7	3	105,16	115,90	0,0000#	21,000%	129,91	0,0000#	20,00%
8	6	109,00	107,73	0,0000#	29,00%	124,31	0,0000#	26,00%
9	12	105,02	89,38	0,0000#	39,00%	106,67	0,0000#	34,00%

Table 3.4. *Vibrio fischeri* toxicity test results of 12 mg L^{-1} concentration after anaerobic treatment

			5 Mins Data			15 Mins Data		
Sample	**Concentration (mg. L^{-1})**	**I_0**	**I_t**	**Gamma**	**%effect**	**I_t**	**Gamma**	**%effect**
Control	0,000	16,31	17,07	1,000#		18,06	1,000#	
1	0,046	15,53	16,40	-8,000*	0,0000%	17,45	-1,000*	-1,000%
2	0,093	14,87	16,57	-6,000*	-6,000%	17,78	-7,000*	-7,000%
3	0,187	14,60	16,88	-9,000*	-10,00%	17,38	-6,000*	-7,000%
4	0,375	14,30	16,63	0,0000*	-11,00%	17,03	0,0000*	-7,000%
5	0,75	15,03	17,38	-9,000*	-10,00%	18,37	-9,000*	-10,00%
6	1,5	14,53	16,28	-6,000*	-7,000%	17,18	-6,000*	-6,000%
7	3	14,36	15,83	-5,000*	-5,000%	16,54	-3,000*	-4,000%
8	6	14,32	15,62	-4,000*	-4,000%	16,44	-3,000*	-3,000%
9	12	14,23	15,11	-1,000*	-1,000%	15,60	1,000*	0,0000%

The input water had a toxic effect on the bacteria (34%) before anaerobic treatment at the concentration of 12 mgL^{-1}, while this rate decreased to 0% after treatment. This shows that the toxic value of wastewater containing pesticides has decreased after treatment.

Table 3.5. *Vibrio fischeri* toxicity test results of 20 mg L^{-1} concentration before anaerobic treatment

			5 Mins Data			15 Mins Data		
Sample	**Concentration (mg. L^{-1})**	**I_0**	**I_t**	**Gamma**	**%effect**	**I_t**	**Gamma**	**%effect**
Control	0,000	58,46	66,07	1,000#		56,97	0,0000#	
1	0,078	58,50	56,63	0,0000#	14,00%	45,10	0,0000#	20,00%
2	0,156	53,96	51,76	0,0000#	15,00%	41,73	0,0000#	20,00%
3	0,312	56,60	53,99	0,0000#	15,00%	44,09	0,0000#	20,00%
4	0,625	57,72	55,60	0,0000#	14,00%	48,49	0,0000#	13,00%
5	1,25	56,16	53,35	0,0000#	15,00%	47,64	0,0000#	12,00%
6	2,5	53,62	46,85	0,0000#	22,00%	43,98	0,0000#	15,00%
7	5	51,40	35,11	0,0000#	39,00%	33,52	0,0000#	33,00%
8	10	49,90	25,91	1,000#	54,00%	27,33	0,0000#	43,00%
9	20	54,77	16,10	2,000#	73,00%	17,68	0,0000#	66,00%

Table 3. 6. *Vibrio fischeri* toxicity test results of 20 mg L^{-1} concentration after anaerobic treatment

			5 Mins Data			15 Mins Data		
Sample	**Concentration (mg. L^{-1})**	**I_0**	**I_t**	**Gamma**	**%effect**	**I_t**	**Gamma**	**%effect**
Control	0,000	71,37	68,77	0,0000#		57,86	0,0000#	
1	0,078	72,12	66,88	3,000*	3,000%	53,83	8,000	7,000%
2	0,156	65,74	61,61	2,000*	2,000%	49,59	7,000	6,000%
3	0,312	67,84	64,34	1,000*	1,000%	53,79	2,000*	2,000%
4	0,625	67,97	64,31	1,000*	1,000%	53,47	3,000*	2,000%
5	1,25	67,18	62,76	3,000*	3,000%	51,70	5,000	5,000%
6	2,5	66,55	57,47	0,0000#	10,00%	46,98	0,0000	12,00%
7	5	67,51	53,38	0,0000#	17,00%	43,13	0,0000	21,00%
8	10	67,12	49,25	0,0000#	23,00%	39,90	0,0000	26,00%
9	20	66,52	45,53	0,0000#	28,00%	39,87	0,0000	26,00%

The concentration of 20 mg L^{-1} of inlet wastewater had a toxic effect on 66% of the bacteria before anaerobic treatment, while this rate decreased to 26% after treatment. This shows that the toxic value of wastewater containing pesticides has decreased after treatment.

Table 3.7. *Vibrio fischeri* toxicity test results of 35 mg L^{-1} concentration before anaerobic treatment

			5 Mins Data			15 Mins Data		
Sample	**Concentration (mg. L^{-1})**	**I_0**	**I_t**	**Gamma**	**%effect**	**I_t**	**Gamma**	**%effect**
Control	0,000	156,75	191,94	1,000#		197,02	1,000#	
1	0,136	157,67	196,63	-1,000*	-1,000%	106,44	0,0000	46,00%
2	0,273	151,52	185,72	-9,000*	-9,000%	185,79	2,000*	2,000%
3	0,546	158,25	187,01	3,000*	3,000%	191,13	4,000*	3,000%
4	1,093	157,15	188,35	2,000*	2,000%	198,88	-6,000*	0,0000%
5	2,187	156,86	187,63	2,000*	2,000%	194,84	1,000*	1,000%
6	4,375	148,25	175,87	3,000*	3,000%	199,28	-6,000*	-6,000%
7	8,75	144,29	159,37	0,0000#	9,000%	188,24	-3,000*	-3,000%
8	17,5	151,52	127,02	0,0000#	31,00%	168,13	0,0000	11,00%
9	35	153,61	92,41	1,000#	50,00%	134,37	0,0000	30,00%

Table 3.8. *Vibrio fischeri* toxicity test results of 35 mg L^{-1} concentration after anaerobic treatment

			5 Mins Data			15 Mins Data		
Sample	**Concentration (mg. L^{-1})**	**I_0**	**I_t**	**Gamma**	**%effect**	**I_t**	**Gamma**	**%effect**
Kontrol	0,000	23,15	30,64	1,000#		33,27	1,000#	
1	0,136	21,74	29,09	-1,000*	-1,000%	31,51	-8,000*	0,0000%
2	0,273	21,19	29,61	0,0000*	-5,000%	30,44	4,000*	4,000%
3	0,546	21,52	30,18	-5,000*	-5,000%	31,46	-1,000*	-1,000%
4	1,093	21,53	31,54	-9,000*	-10,00%	32,15	-3,000*	-3,000%
5	2,187	21,75	30,04	-4,000*	-4,000%	31,07	6,000*	0,0000%
6	4,375	23,14	29,71	3,000*	2,000%	32,39	2,000*	2,000%
7	8,75	21,54	25,79	0,0000	9,000%	28,40	9,000	8,000%
8	17,5	23,32	26,85	0,0000	13,00%	29,46	0,0000	12,00%
9	35	22,04	25,11	0,0000	13,00%	26,76	0,0000	15,00%

The concentration of 35 mg L^{-1} inlet water had a toxic effect on 30% of the bacteria before anaerobic treatment, while this rate decreased to 15% after treatment. This shows that the toxic value of wastewater containing pesticides has decreased after the treatmentprocess.

3.3.2. Toxicity Tests With Eukaryotic Cells

Toxicity test results on *Lepidium sativum* seed germination of samples taken from different concentrations (12 mg L^{-1}, 16 mg L^{-1}, 20 mg L^{-1}, 25 mg L^{-1},35 mg L^{-1}) before and after treatment in an upflow anaerobic packed bed reactor were given in Tables 3.9., 3.10., 3.11., 3.12. and 3.13.

Table 3.9. *Lepidium sativum* toxicity root and stem growths (12 mg L^{-1})

root (average)			stem (average)		
Control	**Before Treatment**	**After Treatment**	**Control**	**Before Treatment**	**After Treatment**
46,8 mm	0 mm	3 mm	34,9 mm	0 mm	6 mm

Table 3.10. *Lepidium sativum* toxicity root and stem growths (16 mg L^{-1})

root (average)			stem (average)		
Control	**Before Treatment**	**After Treatment**	**Control**	**Before Treatment**	**After Treatment**
46,8 mm	0 mm	8 mm	34,9 mm	0 mm	12 mm

Table 3.11. *Lepidium sativum* toxicity root and stem growths (20 mg L^{-1})

root (average)			stem (average)		
Control	**Before Treatment**	**After Treatment**	**Control**	**Before Treatment**	**After Treatment**
46,8 mm	2 mm	4 mm	34,9 mm	4 mm	10 mm

Table 3.12. *Lepidium sativum* toxicity root and stem growths (25 mg L^{-1})

root (average)			stem (average)		
Control	**Before Treatment**	**After Treatment**	**Control**	**Before Treatment**	**After Treatment**
46,8 mm	0 mm	4 mm	34,9 mm	0 mm	8 mm

Table 3.13. *Lepidium sativum* toxicity root and stem growths (35 mg L^{-1})

root (average)			stem (average)		
Control	**Before Treatment**	**After Treatment**	**Control**	**Before Treatment**	**After Treatment**
46,8 mm	0 mm	8 mm	34,9 mm	0 mm	5 mm

Tested pesticide concentrations showed toxic effects on Lepidium sativum root and stem growth before anaerobic treatment. After the anaerobic treatment studies carried out in the continuous reactor, root and stem germination increased to a certain extent (4mm-12mm). This shows that the toxic effect of wastewater after treatment is reduced. However, it is seen that the pressure on root and stem germination continues after treatment compared to control petri dishes.

After the biological treatment of pesticide-contaminated water, both the determination of the toxic effect and the removal of organic matter and pesticides are important parameters. The toxicity of samples before and after anaerobic treatment of 2,4-D with continuous reactor was investigated with both prokaryotic (*Vibrio fisheri*) and eukaryotic (*Lepidium sativum*) cells. Considering the results of the *Vibrio fisheri* toxicity test, it was determined that the toxic effect of the samples examined after treatment decreased compared to before treatment. When the toxicity test on *Lepidium sativum* seed germination is examined, it is seen that the toxic effects of the samples examined after treatment are reduced compared to the samples examined before treatment. Mierzejewska et al. (2020) examined the ecotoxicity of 2,4-D in their study. In

toxicity studies on plants, they reported that the herbicide had a strong inhibition of root germination (Mierzejewska et al.,2020).

As a result, in this study, anaerobic treatment of 2,4-dichloro phenoxy acetic acid, which is one of the pesticides used in agriculture, in a continuous reactor, by-product and toxic effects after treatment were revealed. First of all, it is essential to control the production and use of pesticides to prevent the pollution of the environment with pesticide residues. Awareness-raising training should be given to farmers about the use of pesticides. Thus, the number of pesticides released into the environment can be reduced. After these prevention applications are taken, wastewater treatment should also be improved and more advanced treatment systems should be used than the existing systems.

Acknowledgments

"This work has been supported by Eskisehir Osmangazi University Scientific Research Projects Coordination Unit under grant number 201821047"

Table 3.2. Continuous reactor anaerobic treatment results

Input Values							Output Values							
Day	**Pesticide Conc. (mg. L^{-1})**	**HRT (saat)**	**COD**	**pH**	**OLR**	**Alkalinity**	**COD**	**pH**	**Biogas**	**Alkalinity**	**VFA**	**COD Removal (%)**	**Pesticide Removal (%)**	**VFA/Alk.**
1-53	-	96	2200	8,0	0,550	3000	393	7,9	0,5	2188	265,65	%84,32	-	**0,121**
54-73	0,5	96	2300	8,0	0,575	3000	198	7,9	0,6	2069	270,70	%91,23	%59,07	**0,130**
74-100	1	96	2320	8,0	0,580	3000	166	7,9	0,5	2235	272,72	%93,54	%50,88	**0,122**
101-109	1,5	96	2230	7,9	0,557	3000	189	7,9	0,6	2156	272,72	%91,80	%60,65	**0,126**
110-124	2	96	2180	7,9	0,545	3000	187	7,8	0,8	2024	181,81	%91,40	%81,98	**0,089**
125-136	3	96	2245	8,0	0,561	3000	134	7,9	0,8	2086	192,92	%94,02	%85,52	**0,092**
137-154	4	96	2320	8,0	0,580	3000	187	7,8	0,8	2067	227,27	%91,91	%87,71	**0,109**
155-167	6	96	2410	8,0	0,602	3000	159	7,8	0,8	2125	220,20	%93,38	%87,15	**0,103**
168-181	8	96	2510	8,0	0,627	3000	106	7,9	0,8	2158	218,18	%95,77	%89,07	**0,101**
182-200	10	96	2730	8,0	0,682	3000	99	7,9	0,6	2135	242,42	%96,37	%84,55	**0,113**
201-212	12	96	2910	8,0	0,727	3000	142	7,9	0,4	2065	290,90	%95,11	%83,03	**0,141**
213-223	16	96	3150	8,0	0,787	3000	85	7,8	0,5	2143	280,80	%97,07	%84,87	**0,131**
224-249	20	96	3260	8,0	0,815	3000	106	7,8	0,4	2068	272,72	%97,30	%80,15	**0,131**
250-262	25	96	3520	8,0	0,880	3000	95	7,9	0,4	2136	250,50	%97,44	%90,57	**0,117**
263-279	35	96	3750	8,0	0,937	3000	84	7,9	0,6	2045	254,54	%97,60	%73,27	**0,124**
280-302	50	96	3980	8,0	0,995	3000	129	7,8	0,5	2185	218,18	%96,75	%72,66	**0,099**

COD(mg. L^{-1}); OLR (g KOİ L^{-1} $gün^{-1}$); alk : bicarbonate alkalinity (mg $CaCO_3$ L^{-1}); VFA (mg. L^{-1}); biyogas L^{-1} wastewater day^{-1}

References

Laetz, C. A., Baldwin, D. H., Collier, T. K., Hebert, V., Stark, J. D., Scholz, N. L., (2009). The synergistic toxicity of pesticide mixtures: implications for risk assessment and the conservation of endangered pacific salmon, Environ. Health Perspect, 117, 348-353.

Misra, R., Satyanarayan, S., & Potle, N. (2013). Treatment of agrochemical/ pesticide wastewater by coagulation/flocculation process. International Journal of Chemical and Physical Sciences, *2*, 39-51.

Akçal B., Iscen C.F., Ilhan S., Yavuz A.A. (2011). Statistical Optimisation for Decolour-isation of Burazol Blue ED, Using Anaerobic Consorsia. Fresen. Environ. Bull. 20, 2059- 2064.

Iscen C.F. and Ilhan, S. (2008). Sequential (anaerobic-aerobic) treatment of beet molasses alcoholic fermentation wastewater. Fresen. Environ. Bull. 17, 420-426

APHA-AWWA-WPCF., (1992). Standard methods for the examination of water and wastewater, 18th Ed., Washington DC., American Public Health Association, American Water Works Association and Water Pollution Control Federation, 10-137 p

Demirer, G. and R. Speece, (1998). Anaerobic biotransformation of four3-carbon compounds (acrolein, acrylic acid, allyl alcohol and n-propanol) in UASB reactors. Water research, 1998. 32(3): p. 747-759.

Smith SL A (1990) Simple HPLC method for the determination of 2,4-Dinitrophenyl derivates of Glyphosate and Aminomethylphosphonic ascid applicable to plant studies. Master Thesis, Simon Fraser University, Canada

Gottlieb, A., Shaw, C., Smith, A., Wheatley, A., Forsythe, S., 2003. The toxicity of textile reactive azo dyes after hydrolysis and decolourisation. Journal of biotechnology 101, 49-56.

Tongur, S., Yıldız, S., Ünal, A., Atalay, K., Yeniköşker, M (2017),. Toxıcıty Assessment of Beta-Blocker Drug By Lepıdıum Satıvum Toxıcıty Test Method.

Puyol, D., Mohedano, A. F., Sanz, J. L., & Rodriguez, J. J., (2009), Comparison of UASB and EGSB performance on the anaerobic biodegradation of 2, 4-dichlorophenol. Chemosphere, 76(9), 1192-1198.

Sandoval-Carrasco, C. A., Ahuatzi-Chacón, D., Galíndez-Mayer, J., Ruiz-Ordaz, N., Juárez-Ramírez, C., & Martínez-Jerónimo, F., (2013), Biodegradation of a mixture of the herbicides ametryn, and 2, 4-dichlorophenoxyacetic acid (2, 4-D) in a compartmentalized biofilm reactor. Bioresource technology, 145, 33-36

Behling, E., Diaz, A., Colina, G., Herrera, M., Gutierrez, E., Chacin, E., Fernandez, N., Forster, C., (1997). Domestic wastewater treatment using a UASB reactor. Bioresource Technology 61, 239-245

Mierzejewska, E., Baran, A., & Urbaniak, M., (2020), Biodegradation Potential and Ecotoxicity Assessment in Soil Extracts Amended with Phenoxy Acid Herbicide (2, 4-D) and a Structurally-Similar Plant Secondary Metabolite (Ferulic Acid). Bulletin of Environmental Contamination and Toxicology, 104(2), 200-205.

CHAPTER V

PERFORMANCE PREDICTION OF DTMB 4119 AND HIGHLY SKEWED MODEL PROPELLERS USING STAR-CCM+ CFD SOLVER

BURAK GÖKSU[1] & K. EMRAH ERGİNER[2]

[1] *(Res. Asst. Dr.) Zonguldak Bülent Ecevit* Üniversitesi*, Denizcilik Fakültesi,*
e-mail: burakgoksu@beun.edu.tr,
ORCID: 0000-0002-6152-0208

[2] *(Assist. Prof. Dr.), Dokuz Eylül* Üniversitesi*, Denizcilik Fakültesi,*
e-mail: emrah.erginer@deu.edu.tr,
ORCID: 0000-0002-2227-3486.

1. Introduction

The maritime sector is captivated by dependable propulsion technologies that function well. Increased propeller efficiency reduces shaft power requirements but involves a departure from conventional propeller geometry designs. Important is the planning of a model that minimizes energy consumption while producing the appropriate power within the desired speed range for a marine vehicle. As a propeller operates in the shear flow near the stern of a marine vessel, the propeller-induced velocity field and the rotational inflow are closely connected (D. H. Renick, 2001). In addition, a propeller that requires less maintenance and has a design that satisfies the thrust need will simplify the operational processes of the ship. This equipment, which is one of the most important components of the system, must be meticulously constructed for the mentioned reasons.

The performance attributes of conventional designs are also manufactured using conventional techniques. Although these approaches permit estimations with great precision, they do not provide trustworthy leads for non-traditional

designs (J. Gonzalez-Adalid et al., 2018). Using the ITTC'78 (International Towing Tank Conference) Performance Prediction Method, this case is commonly examined with studies to be undertaken for full-scale extrapolation of various designs. Hence, the ITTC comparison may be a substantial effort from this perspective and is also valuable for evaluating the accuracy of existing numerical methodologies supported by computer-based numerical calculations (ITTC, 2017). Recent interest in the topic of lowering propeller noise by various means has led to the introduction of numerous designs and enhanced the need for the development of performance estimation methods. It also includes a propeller design suitable for cavitation and the ship's underwater hydrodynamics. Consequently, to achieve effective propulsion performance, the optimal propeller and ship combination must be selected based on the optimal geometric design (A. Lungu, 2019). Geometry choices that are incompatible with one another will result in significant friction, noise, and instability. In order to accurately forecast performance and cavitation during the preliminary design phase, effective numerical solvers are required (S. H. Van et al., 2006).

One of the construction methods used today to meet the demands of modern ships is the design of a propeller with a highly skewed blade tip. The need for early and advanced study of designs with heavy loads, high efficiency, low noise, and low vibration levels in appropriate locations is becoming increasingly crucial (S. Gaggero et al., 2017). Flow around floating structures occurs in a nonlinear manner and is one of the problems that naval design must overcome. Special numerical models that can account for the transition region between laminar and turbulent flow provide a dependable and flexible alternate solution (S. Gaggero, 2020). Consequently, scale effect concerns in propeller analysis are eliminated. In fact, the recent development of autonomous underwater marine vehicles encourages lam propulsion systems' size and operating characteristics the size and operating characteristics of propulsion systems (S. Pawar and S. Brizzolara: 2019). Considering the limits of traditional experimental and analytical approaches in predicting complex viscous flows, the need for Computational Fluid Dynamics (CFD) simulations supported by high-performance numerical techniques keeps growing (J. Wang and D. Wan, 2020). The relevant literature is used to summarize several related investigations on this topic.

Several hydrofoil cross-sections have been used to build a new supercavitating propeller model that has optimal performance in both the super-cavitation and lower-cavitation zones (transition regime) (S. Brizzolara and L. Bonfiglio, 2015). Hence, lift, drag, and cavity forms are calculated and compared to conventional lower cavitation and super-cavitation profiles in

numerous cavitation numbers. The numerical computations are supported by a multiphase fully turbulent unstable Reynolds-Averaged Navier Stokes (RANS) equations solver with a dynamic bubble cavitation model to trace the generation and evaporation of the vapor phase.

To accurately predict the thrust properties of a fixed-pitch propeller in open water, the mesh and fluid field parameters for a RANS solver should be examined (M. Islam et al.,2015). Experiments are used to validate the outcomes of the various models when developing an optimization approach. The numerical analyses of scale impacts on Potsdam Propeller Test Case-II (PPTC-II) at model scale using fine prism grids to dissolve viscous sub-layer at low Reynolds number in Menter's Shear Stress Transport turbulence model (SST Menter k-ω model) (X. Q. Dong et al., 2018). The scale effect corrections offered by RANS simulations and those achieved by the ITTC approach are compared. To clarify the CFD results, cross-sectional forces were studied, and RANS and ITTC-based forecasts provided a reasonably consistent result for full-scale efficiency. The research demonstrates that the scale influence on propeller thrust may be much more significant than its effect on torque. In addition, the suitability of hexagonal cell grids for maritime propeller performance predictions has been studied (A. Sikirica et al.,2019). PPTC's hydrodynamic characteristics, thrust, and torque coefficients were calculated numerically using the STAR-CCM+ package program. The accuracy of the Realizable k-epsilon and SST k-omega turbulence models was then examined when examining the performance of maritime propellers. The results indicate that hexa and hybrid grids produce comparable results within a certain range of advance ratios; however, structured grids with the Realizable k-epsilon model can produce more precise results for both low and high advance ratios.

The CFD method is used to assess the cavitation generation and cavitation erosion for the reference states of the NACA 0015 hydrofoil and PPTC propeller (O. Usta and E. Korkut. 2019). The simulation was carried out using two distinct models: the SST (Menter) k-ω turbulence model and the Detached Eddy Simulation model (DES). The Schnerr-Sauer cavitation model estimates were modelled using the Euler Volume of Fluid (VOF) method to simulate cavitation, which may be a two-phase flow.

The computational fluid dynamics method predominates in the process of determining the hydrodynamic characteristics of propellers, as is evident from the studies mentioned above. The fact that engineering is growing swiftly under current conditions indicates that this method will continue to gain ground at an accelerating rate. Academia and industry have demonstrated their trust in

a CFD study based on RANS equations and with well-adjusted parameters by picking the suitable turbulence model. After introducing the propellers chosen for comparison analysis and having test results, the hydrodynamic properties of the propellers are detailed in the next section of this study. The technique for the calculations and the analysis results were then presented. These findings are examined and suggestions for future research are made in the final section.

2. The Properties of the Model Propellers

In this comparative analysis, computations were performed on two distinct propeller models. The first of these is the DTMB 4119 standard test propeller, the 3-bladed variable-pitch propeller, which is the most often used model in academic studies of the 5-propeller series constructed in the David Taylor Model Basin (S. Brizzolara and L. Bonfiglio, 2015). In the early 1970s, this propeller was designed to confirm the lifting line and lifting surface models (K. Koyama, 1993). Table 1 lists the technical characteristics of the DTMB 4119 standard test propeller.

Table 1. The technical features of the DTMB 4119

Particulars	Value	Unit
Diameter	0.3048	m
Sectional form	NACA 66 modified	-
Section meanline	NACA a=0.8	-
Advance ratio (J)	0.3 / 0.5 / 0.833 / 1.1	-
Advance velocity (Va)	0.914 / 1.524 / 2.54 / 3.353	m/s
Rotation direction	Right-handed	-
Rotational speed	600	rpm

Source: A. Sánchez-Caja, 1998.

Table 2. The geometric properties of the DTMB 4119

r/R	c/D	rk/D	sk(°)	P/D	t_{max}/c	f_{max}/c
0.20	0.3200	0.00	0.00	1.1050	0.2055	0.0143
0.30	0.3635	0.00	0.00	1.1022	0.1553	0.0232
0.40	0.4048	0.00	0.00	1.0983	0.1180	0.0230
0.50	0.4392	0.00	0.00	1.0932	0.0902	0.0218
0.60	0.4610	0.00	0.00	1.0879	0.0696	0.0207
0.70	0.4622	0.00	0.00	1.0839	0.0542	0.0200
0.80	0.4347	0.00	0.00	1.0811	0.0421	0.0197
0.90	0.3613	0.00	0.00	1.0785	0.332	0.0182
0.95	0.2775	0.00	0.00	1.0770	0.0323	0.0163
0.98	0.2045	0.00	0.00	1.0761	0.0321	0.0145
1.00	0.0800	0.00	0.00	1.0750	0.0316	0 .0118

Source: K. Boumediene and S. E. Belhenniche, 2016.

The geometric properties of the DTMB 4119 propeller are shown in Table 2, and where, **r** is the radius of the section, **R** is the radius of the propeller, **c** is the chord length along the blade, **D** is the diameter of the propeller, **rk** is the rake ordinate of the section, **sk(°)** is the angular skew value of the section, **P** is the pitch of blade section, $\mathbf{t}_{max}$ is the maximum thickness of each blade section and $\mathbf{f}_{max}$ is the maximum camber of each blade section. Also, the 3-D model of the DTMB 4119 propeller is shown in Figure 1.

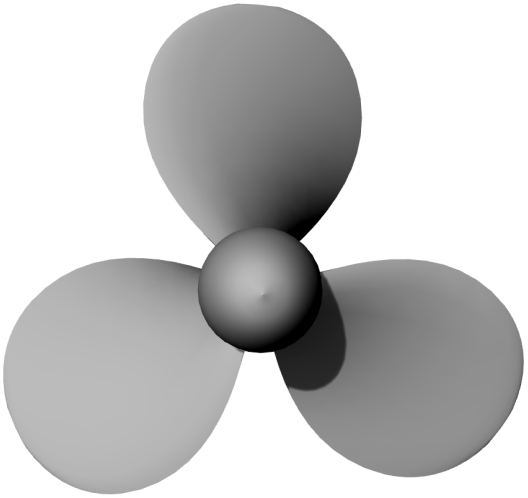

Figure 1. The 3-D model of the DTMB 4119 propeller.

The second propeller employed in this investigation is a highly skewed type with four blades and a 40-degree skew angle. Table 3 lists the model's technical specifications. The highly skewed propeller's geometric features are also displayed in Table 4, where **sk(m)** is the blade section skewback ordinate.

Table 3. The technical features of the highly skewed model propeller.

Particulars	Value	Unit
Diameter	0.30	m
Rake angle	0	degree
Skew angle	40	degree
Advance ratio (J)	0.8 / 0.7 / 0.6 / 0.5 / 0.4 / 0.3	-
Advance velocity (Va)	3	m/s
Rotation direction	Right-handed	-
Rotational speed	750 / 857.14 / 1000 / 1200 / 1500 / 2000	rpm

Source: M. Atlar et al., 2001.

Table 4. The geometric properties of the highly skewed model propeller.

r/R	c (m)	rk (m)	sk (m)	P/D	t_{max}	f_{max}
0.27619	0.04000	-0.00231	-0.00357	0.73370	0.01070	0.00084
0.30000	0.04714	-0.00310	-0.00500	0.74467	0.01023	0.00099
0.40000	0.07329	-0.00562	-0.01064	0.78227	0.00838	0.00157
0.50000	0.09329	-0.00672	-0.01464	0.81190	0.00674	0.00202
0.60000	0.10714	-0.00584	-0.01443	0.83470	0.00529	0.00234
0.70000	0.11357	-0.00254	-0.00707	0.84637	0.00403	0.00240
0.80000	0.11100	0.00303	0.00993	0.80603	0.00297	0.00215
0.90000	0.09400	0.00936	0.03871	0.70487	0.00210	0.00151
0.95000	0.07286	0.01193	0.05814	0.62587	0.00174	0.00104
1.00000	0.00000	0.01334	0.08100	0.52447	0.00142	0.00000

Source: M. Gorji et al., 2018.

The second model, a highly skewed model propeller is shown in Figure 2.

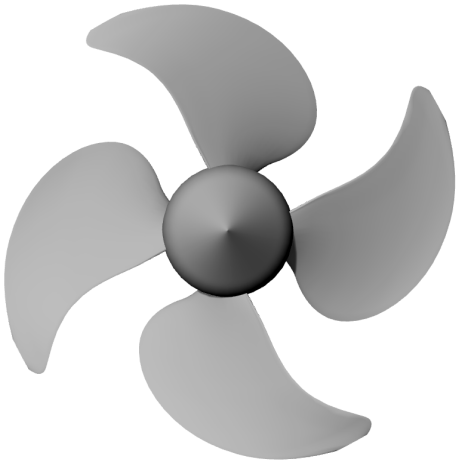

Figure 2. The 3-D model of the highly skewed model propeller.

3. Hydrodynamic Theory of a Propeller

The hydrodynamic characteristics of a propeller are a series of dimensionless coefficients that characterize its mechanical and fluid properties relative to performance. These coefficients are provided to facilitate comparisons between propeller types and sizes. The coefficients of thrust and torque are used to express thrust and torque values.

$$K_t = \frac{T}{\rho n^2 D^2} \tag{1}$$

$$K_q = \frac{Q}{\rho n^2 D^5} \tag{2}$$

where T is the thrust, ρ is the density of the fluid, n is the rotational speed of the propeller, D is the diameter of the propeller, and Q is the torque value. Furthermore, the advance ratio J is used to express the distance advanced by the propeller in one revolution, which is dimensionless with respect to propeller diameter.

$$J = \frac{V_a}{nD} \tag{3}$$

where V_a is the axial speed in relation to the undisturbed fluid.

Finally, the propeller's open water efficiency can be calculated as follows:

$$\eta = \frac{J}{2\pi}\frac{K_t}{K_q} \tag{4}$$

These coefficients are frequently introduced using open water diagrams, which correlate propeller speed with relative thrust, torque, and efficiency via the advance ratio.

4. Methodology

Both propellers are solved using the STAR-CCM+ CFD Solver, and Table 5 details the mesh structures used to generate the results.

Table 5. The properties of the generated mesh structures.

Features	Values
Base mesh surface size	0.01 m
Target mesh surface size for the static fluid domain	100% of the base size
Target mesh surface size for the rotate fluid domain	100% of the base size
Minimum mesh surface size for all surfaces	10% of the base size
Maximum mesh surface size for outer surfaces	400% of the base size
Surface growth rate	1.3
Prism layer quantity on the propeller surfaces	12
Prism layer stretching	1.3
Prism layer total thickness	20% of the base size
Mesher models	•Trimmed cell mesher •Surface remesher •Automatic surface repair
Reference frame	Moving reference frame

4.1. Computational Domains and Boundary Conditions

CFD solver was used to build computational domains with equal mesh sizes so that findings for the DTMB 4119 and highly skew propellers could be compared exactly. The computational domains have the smallest mesh element sizes in the computational area in the propeller section and grow from the blade to the boundary as the distribution of mesh element sizes increases. Around 4,500,000 components make up the computational domains provided for CFD solver. Figure 3 depicts the mesh architectures of DTMB 4119 and the highly skewed model propeller designs.

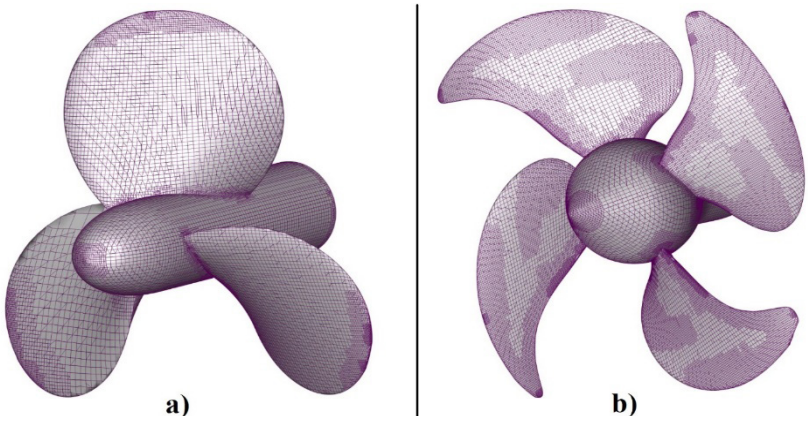

Figure 3. The mesh structure details of a) DTMB 4119, b) the highly skewed model propeller.

In numerical computations, boundary conditions were adopted to approximate open water conditions for both propellers evaluated. As seen in Figure 4, the selected boundary conditions are indicated on the computation domain via coloring. The velocity-inlet boundary condition (red) was applied to assure uniform velocity 5D from the front side of the propeller, while the pressure-outlet boundary condition (blue) was applied 13D behind the propeller (shaft-side). On the surfaces of the cylindrical outer flow volume (grey), which is concentric with the propeller, a symmetry boundary condition is applied with a 3D diameter value that is large enough to represent open water conditions without affecting the propeller. On shaft (green), propeller blades (yellow), and hub (black) surfaces, a no-slip wall condition boundary condition was imposed. In addition, the interface boundary condition was applied to the boundary surfaces of the propeller-covering inner volume (orange). Thus, the impact of

propeller rotation is achieved by defining merely the rotation speed of the inner volume.

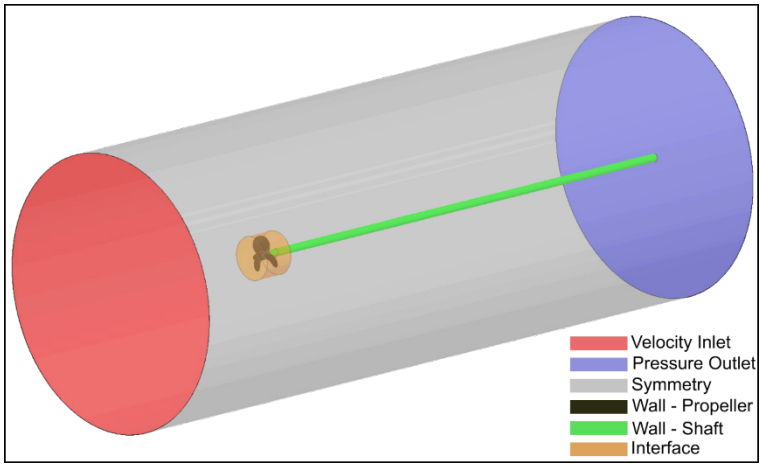

Figure 4. The boundary conditions of the computational domains.

4.2. Computational Modelling and Governing Equations

In addition to the meshing strategy used when creating the computational domains, the CFD solver approaches used in commercial programs were also kept similar. The governing equations are solved using the SIMPLE algorithm for coupling pressure-velocity under steady-state conditions. The advection and diffusion terms of the governing equations were discretized with the second-ordered upwind and second-ordered central difference scheme, respectively. The governing equations for continuity, momentum, and turbulence used in the computational fluid dynamics (CFD) analyses under the above-given assumptions are as follows in general form (C. Metin et al., 2019):

The continuity equation,

$$\frac{\partial \rho}{\partial t} + \nabla \cdot (\rho \vec{v}) = 0 \tag{5}$$

The momentum equation,

$$\frac{\partial}{\partial t}(\rho \vec{v}) + \nabla \cdot (\rho \vec{v} \vec{v}) = -\nabla p + \nabla \cdot (\bar{\bar{\tau}}) + \rho \vec{g} + \vec{F} \tag{6}$$

where "ρ" is the density of the fluid, "$\vec{v}$" is the velocity vector, "p" is the static pressure, and "$\bar{\bar{\tau}}$" is the stress tensor given by:

$$\bar{\bar{\tau}} = \mu \left[(\nabla \vec{v} + \nabla \vec{v}^T) - \frac{2}{3} \nabla \cdot \vec{v} I \right] \tag{7}$$

where "μ" is the viscosity, "I" is the unit tensor, and the second term on the right-hand side is the effect of volume dilation. The time expression "t" in the general form of the continuity and momentum equations is taken as zero under the steady-state conditions.

In addition to the continuity and momentum governing equations, the selected turbulence model also includes Reynolds-averaged Navier-Stokes (RANS) equations. In the first analyses of this work, the Spalart-Allmaras model, which is a one-equation turbulence model, and the k-ω and k-ω models, which are two-equation turbulence models, are utilized in CFD solver. Thus, the effect of these turbulence models on the results was originally studied by configuring the mesh structures in Table 5 in the commercial CFD solver to determine the correct approach. Following the selection of the optimal structure, additional analyses of the study were conducted.

5. Results

In this part, the CFD study results for the DTMB 4119 and highly skewed model propellers are shown. For CFD analysis to be effective, the settings must be specified properly, and the fluid field must be modelled by the problem. The water advances turbulently during the propeller's rotation in the fluid domain. This circumstance is readily apparent in the experimental environment, and as a result, experimental results based on actual operating conditions are collected. Yet, due to the nature of the CFD study, the flow motion caused by the propeller must be precisely predicted. Several turbulence models have been developed to model a variety of fluid characteristics. To calculate the open water hydrodynamic parameters of the model propellers, the appropriate turbulence model must be chosen from among them. Three commonly used models for J=0.833 are compared firstly to choose the suitable turbulence model. The values calculated in two different commercial CFD software and experimental results for the DTMB 4119 are indicated in Table 6 for V_a=2.54 m/s and n=600 rpm (J. Kulczyk et al., 2007).

Table 6. Open water hydrodynamic properties of the DTMB 4119 propeller at J=0.833.

Turbulence model	STAR-CCM+			Experiment
	k-ε	k-ω	Spalart-Allmaras	
T (N)	125.20	123.99	124.43	125.70
Q (Nm)	7.320	7.378	7.350	7.348
K_t	0.1454	0.1440	0.1445	0.1460
$10K_q$	0.2789	0.2811	0.2801	0.2800
η_0	0.6914	0.6794	0.6844	0.6916

T, Q, K_t, $10K_q$, and η_0 parameters were evaluated together because obtaining a single parameter value close to the experimental data would not be a meaningful comparison. As a result, as shown in Table 6, the k-ε turbulence model produced results that were more similar to the experimental data (J. Kulczyk et al., 2007). The results of calculating the hydrodynamic parameters of the DTMB 4119 propeller at a constant rotation speed of n=600 rpm with various dimensionless advancing coefficients (J=0.3, 0.5, 0.833, 1.1) are shown in Table 7. Also, the mesh structure was constructed by dimensionless wall distance range $30<y^+<300$ with k-ε turbulence model.

Table 7. Open water hydrodynamic properties of the DTMB 4119 propeller.

Advance coeff. (J)	STAR-CCM+				Experiment			
	0.3	0.5	0.833	1.1	0.3	0.5	0.833	1.1
T (N)	328.73	249.70	125.20	26.533	322.87	245.38	125.70	29.27
Q (Nm)	15.743	12.433	7.320	2.864	15.484	12.518	7.348	2.782
K_t	0.3818	0.2900	0.1454	0.0308	0.3750	0.2850	0.1460	0.0340
$10K_q$	0.5999	0.4738	0.2789	0.1091	0.5900	0.4770	0.2800	0.1060
η_0	0.3039	0.4871	0.6914	0.4944	0.3035	0.4755	0.6916	0.5616

In STAR-CCM+, K_t, $10K_q$, and η_0 values deviated from the experimental data by approximately 9.36%, 2.95%, and 11.96%. When this comparison is conducted with different advancing coefficients, the deviation values presented in Table 8 are derived. Using the k-ε turbulence model, the performance criteria of the DTMB 4119 propeller at four different advancing coefficients were computed with slightly less divergence from the test findings, especially at the 0.833 advance ratio.

Table 8. Performance comparison of the CFD solver for the DTMB 4119.

Advance coefficient (J)	**0.3**	**0.5**	**0.833**	**1.1**
Error at K_t (%)	1.814	1.758	0.402	9.362
Error at $10K_q$ (%)	1.677	0.678	0.382	2.956
Error at η_0 (%)	0.135	2.453	0.020	11.965

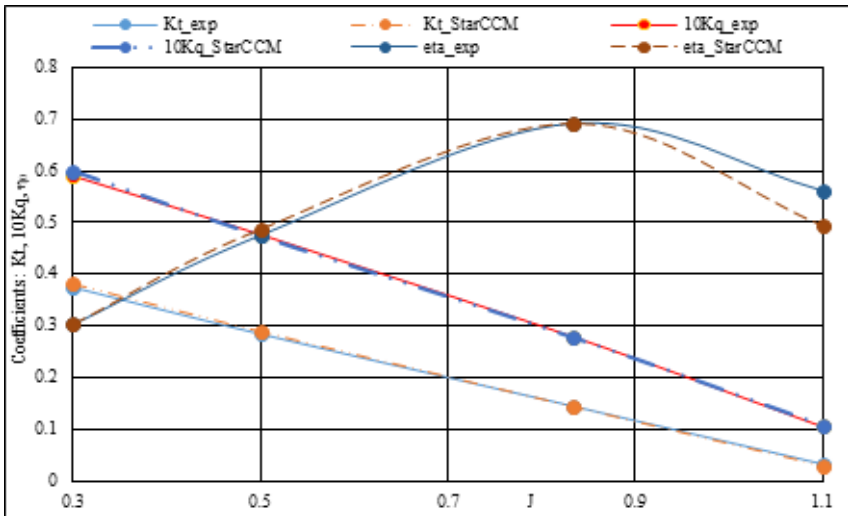

Figure 5. Hydrodynamic coefficients for the DTMB 4119 propeller.

The k-ε turbulence model is then selected based on Table 6's data, and the outcomes of the CFD analyses performed on the highly asymmetric model propeller at V_a=3 m/s are presented in Table 9. In this propeller model, the water flow velocity is fixed, and the propeller revolution speed has been modified to accommodate various advance coefficients.

Table 9. The comparison of the open water hydrodynamic properties of the highly skewed model propeller with experimental results and STAR-CCM+.

Advance coeff. (J)	STAR-CCM+						Experiment					
	0.3	**0.4**	**0.5**	**0.6**	**0.7**	**0.8**	**0.3**	**0.4**	**0.5**	**0.6**	**0.7**	**0.8**
n (rpm)	2000	1500	1200	1000	857.14	750	2000	1500	1200	1000	857.14	750
T (N)	2299. 0	1067.01	540.57	275.30	122.61	25.79	2244.51	1050.43	533.30	269.34	118.73	23.99
Q (Nm)	84.970	41.480	22.480	12.540	6.640	2.790	82.420	40.450	21.530	11.780	5.940	1.820
K_t	0.2561	0.2113	0.1672	0.1227	0.0744	0.0204	0.2500	0.2080	0.1650	0.1200	0.0720	0.0190
$10K_q$	0.3155	0.2738	0.2318	0.1862	0.1342	0.0736	0.3060	0.2670	0.2220	0.1750	0.1200	0.0480
η_0	0.3876	0.4913	0.5742	0.6289	0.6175	0.3533	0.3901	0.4959	0.5915	0.6548	0.6685	0.5040

Table 10. Performance comparison of the CFD solver for the highly skewed model propeller.

Advance coefficient (J)	**0.3**	**0.4**	**0.5**	**0.6**	**0.7**	**0.8**
Error at K_t (%)	2.44	1.59	1.33	2.25	3.33	7.37
Error at $10K_q$ (%)	3.10	2.55	4.41	6.40	11.83	53.33
Error at η_0 (%)	0.64	0.93	2.92	3.96	7.63	29.90

The error rates listed in Table 10 are absolute numbers indicating how far the CFD analysis deviates from the experimental data (M. Atlar et al., 2001). As with the DTMB 4119 propeller, the STAR-CCM+ software generated results that were comparable to experimental data while simulating highly skewed model propeller.

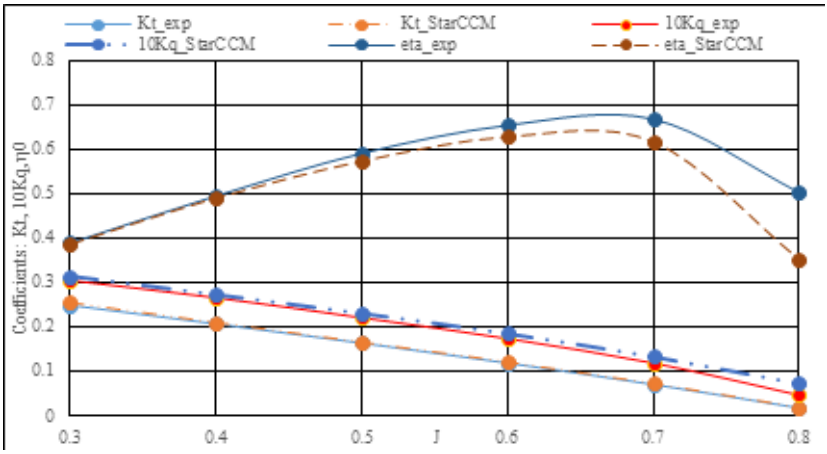

Figure 6. Hydrodynamic coefficients for the highly skewed propeller.

6. Conclusion and Discussion

The more comprehensive study of this book chapter was presented at GMO Shipmar 2021 by the authors and their friends (http://www.gmoshipmar.org/GMOSHIPMAR2021/Proceedings/Proceedings_GMO-SHIPMAR_2021.pdf). So only the parts that are been solved by using STAR-CCM+ solver have been examined in this study as: DTMB 4119 and highly skewed model propeller CFD solver calculation results have been carried out. Hydrodynamic performance predictions have been performed by STAR-CCM+. Thrust and torque values obtained as a result of our study, have been utilized to predict the performance characteristics of the propeller (K_t, K_q, and η_0) and finally compared with the results of the experimental data. Therefore, the overall performance of STAR-CCM+ when compared with the experimental results is evaluated as sufficient. In addition to the use of commercial programs, the comparison of turbulence models that have a direct effect on the results in CFD programs has also been studied. The results obtained in the selection of the appropriate turbulence model were compared with the experimental data and the suitability of the k-**ε** turbulence model was decided due to the non-cavitation condition. In this study, the evaluation was made without including the cavitation effect since all the computations were conducted on open-water cases.

In future studies, the number of CFD solvers will be increased by adding similar CFD solvers as NUMECA, Comsol Multiphysics, and OpenFOAM (Ansys Fluent was used in the study, which is presented at Shipmar 2021, https://www.gmoshipmar.org/GMOSHIPMAR2021/). Besides noise analyses can be performed in future studies. Alternative turbulence models should be re-evaluated in studies that include the cavitation effect which is the most used model as the k-omega turbulence model. Hence, a suitable boundary layer meshing could be determined by comparative studies. In addition, the effect of the cavitation model on the results will be examined. As the advance ratio increases, the deviation rates in the results of both software increase. This may be due to the need for a more precise mesh structure for modelling velocity gradients due to the increase in the advance coefficient. This may require a computer with high computational power. If the results obtained with the existing computer infrastructure are examined, results similar to the curve characteristic of the experimental data have been produced, although it is not possible to estimate the efficiency (η_0) value precisely.

References

A. Lungu, "DES-based Computation of the Flow Around the DARPA Suboff," in *IOP Conference Series: Materials Science and Engineering*, 2019, vol. 591, no. 1.

A. Sánchez-Caja, "DTRC Propeller 4119 Calculations at VTT," in *22nd ITTC Propulsion Committee Propeller RANS/Panel Method Workshop*, 1998, no. April 1998.

A. Sikirica, Z. Carija, L. Kranjcevic, and I. Lucin, "Grid Type and Turbulence Model Influence on Propeller Characteristics Prediction," *J. Mar. Sci. Eng.*, vol. 7, no. 10, 2019.

C. Metin, O. Gök, A. U. Atmaca, and A. Erek, "Numerical investigation of the flow structures inside mixing section of the ejector," *Energy*, vol. 166, pp. 1216–1228, 2019.

D. H. Renick, "An Improved Analysis Methodology for the Prediction of Steady Propulsor Performance," *Mar. Technol. SNAME News*, vol. 38, no. 2, pp. 95–101, 2001.

Http://www.gmoshipmar.org/GMOSHIPMAR2021/Proceedings/Proceedings_GMO-SHIPMAR_2021.pdf: 01.03.2023.

ITTC, "1978 ITTC Performance Prediction Method," *ITTC - Recommended Procedures and Guidelines, 7.5-02-03-01.4*. 2017.

J. Gonzalez-Adalid, M. Perez-Sobrino, S. Gaggero, G. Gennaro, and A. Moran Guerrero, "The Use of Modern Computational Tools in the Design Process of Unconventional Propellers for Performance Prediction and Full-scale Extrapolation," in *Technology and Science for the Ships of the Future - Proceedings of NAV 2018: 19th International Conference on Ship and Maritime Research*, 2018, no. June, pp. 264–274.

J. Kulczyk, Ł. Skraburski, and M. Zawiślak, "Analysis of Screw Propeller 4119 Using the Fluent System," *Arch. Civ. Mech. Eng.*, vol. 7, no. 4, pp. 129–137, 2007.

J. Wang and D. Wan, "Application Progress of Computational Fluid Dynamic Techniques for Complex Viscous Flows in Ship and Ocean Engineering," *J. Mar. Sci. Appl.*, vol. 19, no. 1, pp. 1–16, 2020.

K. Boumediene and S. E. Belhenniche, "Numerical analysis of the turbulent flow around DTMB 4119 marine propeller," *Int. J. Mech. Aerospace, Ind. Mechatron. Manuf. Eng.*, vol. 10, no. 2, pp. 347–351, 2016.

K. Koyama, "Comparative Calculations of Propellers By Surface Panel Method," *Pap. Sh. Res. Inst.*, no. 15, 1993.

M. Atlar, A. Takinaci, E. Korkut, N. Sasaki, and T. Aono, "Cavitation tunnel tests for propeller noise of a FRV and comparisons with full-scale measurements," in *International Symposium on Cavitation*, 2001, p. 13.

M. Gorji, H. Ghassemi, and J. Mohamadi, "Calculation of sound pressure level of marine propeller in low frequency," *J. Low Freq. Noise Vib. Act. Control*, vol. 37, no. 1, pp. 60–73, 2018.

M. Islam, F. Jahra, and M. Doucet, "Optimization of RANS Solver Simulation Setup for Propeller Open Water Performance Prediction," in *Proceedings of the ASME 2015 34th International Conference on Ocean, Offshore and Arctic Engineering*, 2015, pp. 1–11.

O. Usta and E. Korkut, "Prediction of Cavitation Development and Cavitation Erosion on Hydrofoils and Propellers by Detached Eddy Simulation," *Ocean Eng.*, vol. 191, no. March, p. 106512, 2019.

S. Brizzolara and L. Bonfiglio, "Comparative CFD Investigation on the Performance of a New Family of Super-Cavitating Hydrofoils," in *9th International Symposium on Cavitation (CAV2015)*, 2015, vol. 656, no. 1, pp. 2–6.

S. Gaggero and D. Villa, "Steady Cavitating Propeller Performance by Using OpenFOAM, StarCCM+ and a Boundary Element Method," in

Proceedings of the Institution of Mechanical Engineers Part M: Journal of Engineering for the Maritime Environment, 2017, vol. 231, no. 2, pp. 411–440.

S. Gaggero, "Influence of Laminar-to-Turbulent Transition on Model Scale Propeller Performances. Part I: Fully Wetted Conditions," *Ships Offshore Struct.*, pp. 1–13, 2020.

S. H. Van, W. J. Kim, H. S. Yoon, Y. Y. Lee, and I. R. Park, "Flow Measurement Around a Model Ship with Propeller and Rudder," *Exp. Fluids*, vol. 40, no. 4, pp. 533–545, 2006.

S. Pawar and S. Brizzolara, "Relevance of transition turbulent model for hydrodynamic characteristics of low Reynolds number propeller," *Appl. Ocean Res.*, vol. 87, no. April, pp. 165–178, 2019.

X. Q. Dong, W. Li, C.-J. Yang, and F. Noblesse, "RANSE-based Simulation and Analysis of Scale Effects on Open-Water Performance of the PPTC-II Benchmark Propeller," *J. Ocean Eng. Sci.*, vol. 3, no. 3, pp. 186–204, 2018.

CHAPTER VI

CFD (HAD) APPLICATIONS AND APPROACHES IN INDOOR AND OUTDOOR DESIGN

MUHAMMET FATIH AYHAN[1] & *ÖZLEM* AYDIN[2]

[1] (Mimar)Karadeniz Technical University
e-mail: mfayhan@gmail.com
ORCID: 0000-0002-7343-5019

[2] (Öğr. Gör. Dr.) Karadeniz Technical University
e-mail: ozlem.aydin@ktu.edu.tr
ORCID: 0000-0002-3666-3557

1. Introduction

CFD is a joint field of study of fluid mechanics, mathematics, computer science, and aeronautics. This field, which gained rapid momentum with the computer revolution in the 1960s, primarily aimed to analyze fluids in engineering fields, but today it has become the field of study of many disciplines, including construction and building. CFD has become a powerful alternative to time-consuming and costly experimental studies such as wind tunneling, and although it stands out with its advantages, it also brings many limiting factors and disadvantages. Despite all these, it still does a good job in terms of cost and benefit. In addition, many software alternatives that have emerged in this process show that this field will be on the agenda more in the coming years. With all these efforts to establish a semantic relationship, CFD will become indispensable for both designers and manufacturers in the process from the design phase to the final optimization of many design products in the coming years. In this context, the effect of CFD applications on indoor and outdoor physical comfort conditions during the design phase of buildings was evaluated through sample projects.

Computational Fluid Dynamics (CFD), a sub-branch of fluid mechanics, is a branch of science that studies the behavior of the fluid in motion using mathematical approaches with the help of computer-aided computing power. CFD method is based on the numerical modeling and analysis of complex fluid dynamics problems using methods such as finite differences, finite elements, or finite volumes. Although the foundations of computational fluid dynamics were laid on the axis of aerospace and heat transfer problems, it was later adapted and developed for many engineering problems where fluid mechanics is effective (Kiriççi, 2016).

The process, which started with the developments in numerical methods in the 1950s, gained momentum in the 2000s and reached the point of creating general and special-purpose CFD algorithms and software that enable the modeling of complex problems as we know them today. Today, the method, which is widely used in many engineering disciplines such as aerospace, machinery, chemistry, biomechanics, environment, and construction, provides effective results in both industrial and academic design and analysis processes. In particular, in parallel with the development of computer technology, significant progress has been made in the software used in CFD and many commercial and open-source software have been developed (Kiriççi, 2016). (Figure 1).

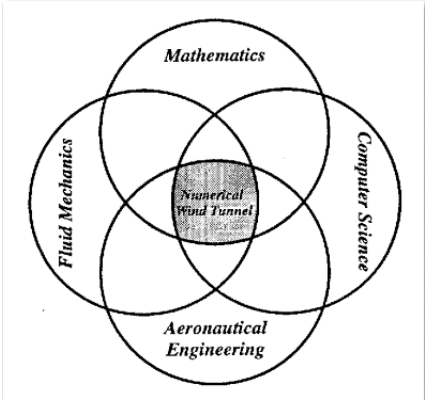

Figure 1. Co-working fields of CFD (Jameson,2012)

The main CFD software used today with commercial licenses and open source codes are Autodesk CFD, ANSYS CFD-CFX, ANSYS Fluent, OpenFOAM, CFD Module, Flowsquare, Paraview, and Altair CFD. With the CFD software that is still being developed, it is possible to solve complex flow problems in three dimensions by using the desired turbulence model, and

modeling the real conditions in a time-dependent way to simulate. It is also known that CAD/CAM/BIM software such as Revit and Solidworks have add-ons for CFD.

Although various calculation methods have been developed since the 1960s during the development of CFD, most of them are based on the Navier-Stokes equation. The basic equations describing the motion of fluids are the Navier-Stokes equations, which are derived from the principle of conservation of mass, momentum, and energy. The Navier-Stokes equations are very difficult to solve directly because they contain complex and nonlinear (elliptic, hyperbolic) differential expressions. However, these equations can be solved by transforming them into algebraic expressions, discretizing them in space and time by numerical methods, and then determining the initial and boundary conditions.

The process that started with "linear potential" in the 1960s continues with "nonlinear potential" in the 1970s, "Euler" in the 1980s, RANS method in the 1990s, and more hybrid methods such as LES, VLES, DES, URANS in the 2000s.

Numerical and physical modeling methods have their own advantages and disadvantages. For this reason, it would be more accurate to see the two methods as complementary tools rather than alternatives to each other.

The main areas where computational fluid dynamics is used are as follows:

- Aerospace (aerodynamic and aeroacoustic analysis)
- Automotive industry and motorsports (aerodynamic analysis)
- Ship and boat construction and engineering (pressure behavior and analysis)
- Environmental, mechanical, and energy systems engineering (HVAC) thermal designs, aerodynamic analysis)
- ***Architecture and Structural Engineering***
- Geophysical and mining engineering
- Chemical industry and engineering
- Industrial product design, medical product design, etc.

2. CFD Applications and Approaches in Architecture

The effects of airflow in architectural designs have been showing themselves in architectural discourses recently. However, there are also structures in which the effect of airflow on the design is foreseen with the unrealistic intuitions of

the architects most of the time. Among these buildings, the Tjibaou Cultural Center in New Caledonia is known for its ecological design, but researchers have proven that the airflow in and around the building is different from the way it was designed. (Wu, et al., 2011). In the study, the simulation results of the building were compared with the diagrams drawn by the architect during the design phase (Figure 2). As a result, the intuition of the designer was insufficient to perceive the turbulence caused by the interaction of the wind with the obstacles. Wind tunnel tests, in which the effects of airflow on the structure are evaluated, are the best experimental studies that can be a solution. However, very few architectural projects with critical airflow issues in terms of cost and implementation time include these tests. In this context, CFD applications can produce excellent results for the designer.

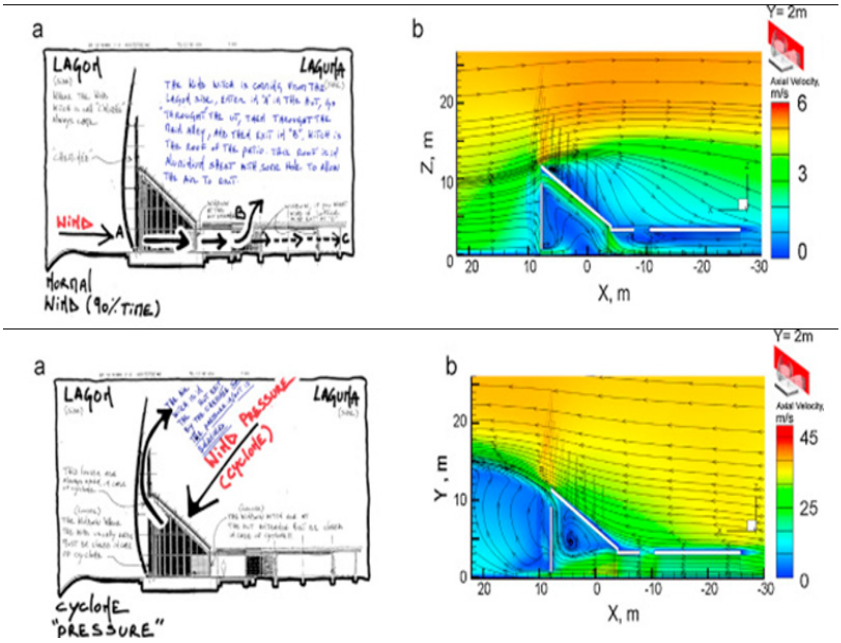

Figure 2. Comparison of airflow schemes presented by architects in the design of Tjibaou Cultural Center with CFD analysis (Wu, et al., 2011)

In architectural designs, CFD applications provide meaningful data visualization to help designers make better decisions (Roudsari and Pak, 2014). CFD applications found a place in the architectural field in the 1990s due to their useful contributions in the design phase. Initially, numerical methods and mechanical systems were studied in research on CFD applications in the

architectural field. With many studies and research, its versatile use in the field of architecture has increased. In this context, studies on the use of CFD in architecture have gained momentum since 1997 (Zhai, 2006). However, the lack of case-based studies that will enable architects to connect with HAD is the biggest problem in front of this situation (Den Hartog, et al, 2000). Lack of knowledge about the principles of fluid mechanics was another obstacle (Jo, 2018).

Jo's literature study on the emergence of CFD applications and approaches in architecture revealed that this field has attracted attention in recent years in terms of both practice and research. These research trends demonstrate the potential of CFD as a tool for early design phases. Unlike traditional methods, the results of these applications show that CFD can be actively included in the design decision-making process. The inclusion of CFD in architectural design can also change the development process of the design. (Jo, 2018). Figure 3 summarizes the general trends in research on CFD in the architectural field (Figure 3). The study reveals that the interest of designers in HAD has increased over time as its use in architecture.

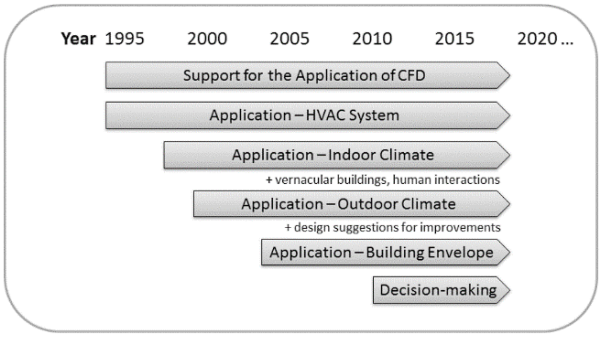

Figure 3. Expansion of research areas related to CFD in architecture (Jo, 2018)

2.1. CFD Applications in Indoor Design

At the final stage of the design process, experts try to predict the indoor climate through CFD applications to evaluate indoor comfort conditions. Experts may encounter problems arising from the design decisions made by the architects. At this stage, the final form of the design becomes permanent with the collaborative work, and the building is prepared in a simulation environment with the assumptions of indoor climate conditions. Optimum comfort of the environment achieved with re-propositions. In this context, the advantages of

CFD applications are remarkable. Such applications can be advantageous when designs in the final stages do not have enough time and budget to adopt new concepts for indoor air conditioning. The inclusion of applications in the early stages of design is important for design optimization. One way to achieve this is to systematically analyze design performance at an early stage. Using digital visualization designers can easily access the benefits of advanced simulations and formal analysis. That will allow designers to make balanced and motivating decisions in areas such as indoor climate (Den Hartog, et al, 2000).

In order to determine the building's performance, it is necessary to conduct experiments in the substance environment. These experimental environments include building scale models and observing behavior under realistic conditions. Especially when it comes to indoor airflow, these experiments take a lot of time, practice, and budget. It is very difficult to carry out experiments in which the forms can change, and each variant requires separate testing at the early design stage. In this context, it is more feasible to use CFD simulations to test the predictions of variants. In CFD applications, given the right amount of correct input, most of the climate parameters can occur at any time or anywhere in the building (Table 1). As a result, climate experts can simulate dynamic phenomena such as temperature swings and turbulence that can be used to validate design performance.

Table 1. Indoor climate parameters and CFD (Den Hartog, et al, 2000)

INDOOR CLIMATE PARAMETER	PROVIDED BY CFD?
Air Temperature (AT)	Yes
Radiant Temperature (RT)	Yes
Air Velocity (Av)	Yes
Relative Humidity (RV)	No
Ventilation Rate (Nv)	Yes
Pollution concentrations (Cp)	When modeled

The indoor climate of the buildings consists of thermal, auditory, olfactory, and visual comfort areas. Airflow and ventilation-related issues affect both thermal and olfactory comfort. Thermal comfort is affected by air temperature, radiant temperature, air velocity, and air humidity. Human-related factors, such as metabolism and clothing, also have an impact on the physical properties of the indoor environment. Maintaining healthy air quality refers to the ventilation (NV) of the space to reduce the pollution concentration (CP). In the act of ventilation, airflow has an effect on factors related to thermal comfort. Weather-related factors should be kept at limited values to create a healthy indoor climate.

2.2. CFD Applications in Outdoor Design

In the literature, 4 topics are generally addressed for CFD in outdoor building performance simulations:

- Pedestrian wind around buildings,
- Rain directed by the wind on the building facades (WDR),
- Convective heat transfer coefficients on building exteriors and Convective heat transfer
- Air pollutant distribution around buildings (Blocken et al., 2011).

Apart from these topics, wind loads and natural ventilation in buildings have also been addressed. However, while the use of CFD in research is quite prominent for indoor applications, outdoor applications are significantly less prominent (Figure 4).

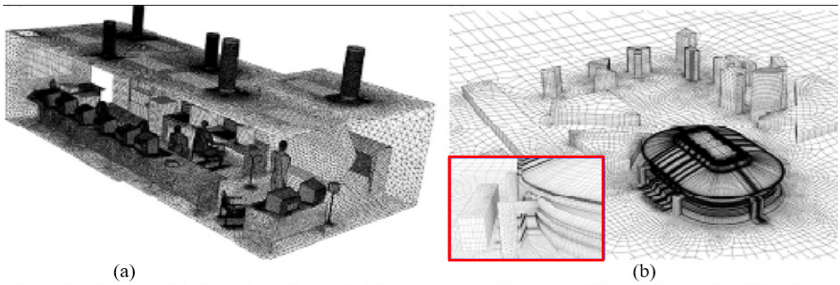

(a) (b)

(a) Unstructured grille for simulation of airflow in computer room (3.7 million cells) (Abanto et al.,2004). (b) Hybrid body grille for urban wind flow and indoor natural ventilation of a multifunctional stadium (5.6 million cells) (Van Hooff and Blocken, 2010).

Figure 4. CFD applications for complex indoor and outdoor environments

Investigation of complex environmental problems such as pedestrian wind disturbance and dispersion of wind-induced air pollutants is done in wind tunnels. In addition, WDR effect and convective heat transfer coefficients on building exteriors are calculated with simplified empirical or semi-empirical formulas. CFD can be a powerful alternative to applications that require physical modelings such as wind tunnels and calculations with empirical/semi-empirical formulas (Blocken et al., 2011).

2.2.1. Pedestrian Wind Environment Around Buildings

Tall buildings can cause high wind speeds at the pedestrian level. This can lead to uncomfortable and even dangerous situations. The negative effects of wind should be taken into account in terms of the comfort of the use of new

buildings. Today, many city administrations require wind comfort studies to be carried out together with the construction permit for tall buildings to be built. It is essential to determine the data showing that the negative results for the pedestrian-wind environment are limited in terms of building use.

In the wind comfort study, a combination of three types of data is usually performed. These are statistical meteorological information; aerodynamic information, and comfort criteria. CFD or wind tunnel data can be used to provide some aerodynamic information. In wind comfort studies, calculations are made taking into account the pedestrian height (z = 1.75 or 2 m). In wind tunnel tests, laser or point measurements are usually made. Sand erosion and infrared thermography methods have also been used in the past. (Blocken et al., 2011).

One of the advantages of CFD in pedestrian-level wind comfort studies is the time saving by providing all flow field data. Basically, there are many CFD studies of pedestrian wind conditions in complex urban environments, as well as studies to examine the pedestrian wind environment around individual buildings or general building configurations (Figure 5). Almost all of these studies have been performed with the stable RANS method and a version of the k-ε model. Only He and Song (1999) used the LES in their study. One of the general approaches in CFD studies for the pedestrian wind environment is verification studies. CFD applications in this area can easily affect the results due to numerical and physical modeling errors. Many validation studies have taken this approach in verifying CFD with wind tunnel measurements and field measurements. There are few studies in the literature on CFD simulation validation of multiple building configurations.

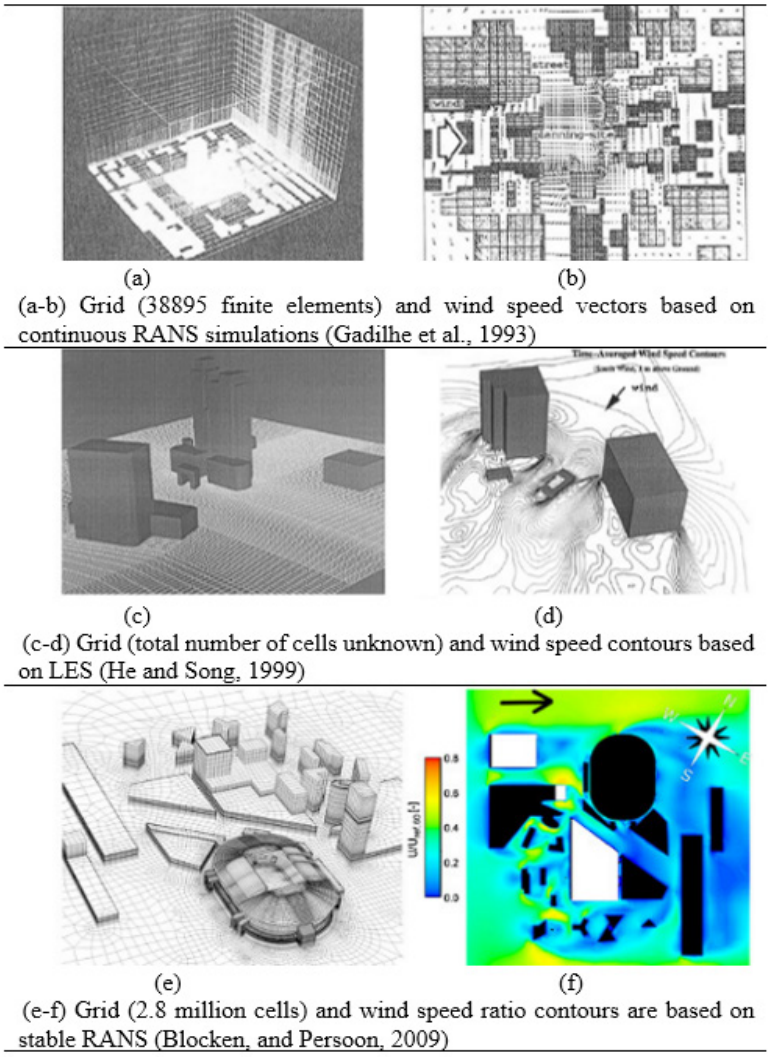

(a) (b)

(a-b) Grid (38895 finite elements) and wind speed vectors based on continuous RANS simulations (Gadilhe et al., 1993)

(c) (d)

(c-d) Grid (total number of cells unknown) and wind speed contours based on LES (He and Song, 1999)

(e) (f)

(e-f) Grid (2.8 million cells) and wind speed ratio contours are based on stable RANS (Blocken, and Persoon, 2009)

Figure 5. Examples of CFD studies of the wind environment at the pedestrian level in urban areas

Blocken and Carmeliet (2008) performed stable RANS CFD simulations with the k-ε model for three parallel building configurations and compared the results with sand erosion wind tunnel experiments performed by Blocken and Carmeliet (2008). Two of these comparisons are shown in Figure 6.

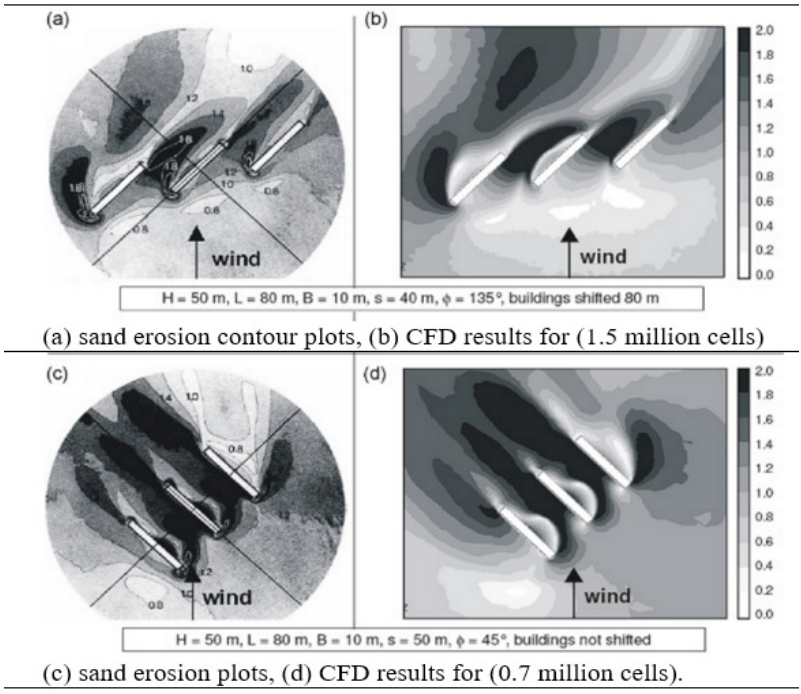

Figure 6. Validation study by Blocken and Carmeliet (2008) for parallel building configurations

2.2.2. Wind-Driven Rain (WDR) on Building Facades

One of the most important moisture sources affecting the hygrothermal performance and durability of building façades is rain directed by the wind on the façades. Rain on the façade can have many negative effects. Moisture accumulation in porous materials can lead to rainwater penetration and structural cracking due to thermal and moisture gradients. There are many parameter effects in the evaluation of WDR density on building facades. These are building geometry, ambient topography, location on the façade, wind speed, wind direction, turbulence density, precipitation density, and raindrop size distribution. CFD can be the most suitable solution to save time, eliminate experimentation and obtain more detailed and accurate information from calculations made with formulas. In this context, techniques have been developed to evaluate the effects of wind and rain on the building. These analyzes are; it provides the determination of the surface distribution of WDR on building facades for constant values of wind speed, wind direction, and horizontal precipitation intensity (Abanto, 2004). So far, CFD validation studies for WDR have been rather limited in the

literature (Figure 7). For verification studies, in situ measurement method was applied instead of the wind tunnel. On the other hand, some researchers found significant discrepancies between simulations and measurements, while others reported good accuracy. In addition, verification studies have generally focused on low-rise buildings.

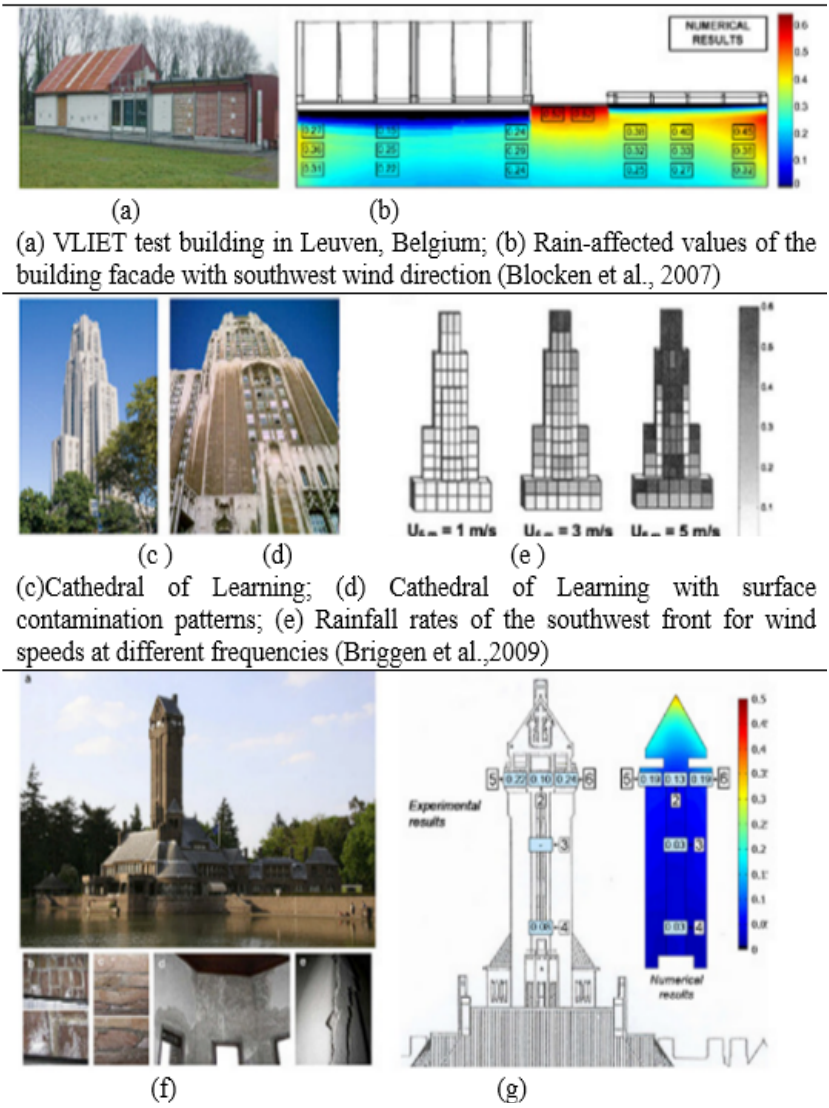

Figure 7. CFD verification of wind-driven rain on building facades

Another one of the recent CFD studies on WDR in the literature is the study conducted by Llarena et al. (2018). In the study, the San Mames Stadium,

a WAS (World Architecture Festival) award-winning stadium (best sports structure completed in 2015) in Spain, was examined. Different alternative structures were derived for the WDR problem on the roof of the stadium using CFD method. The study is also an example where CFD simulation results are supported by an in-situ measurement method (Figure 8).

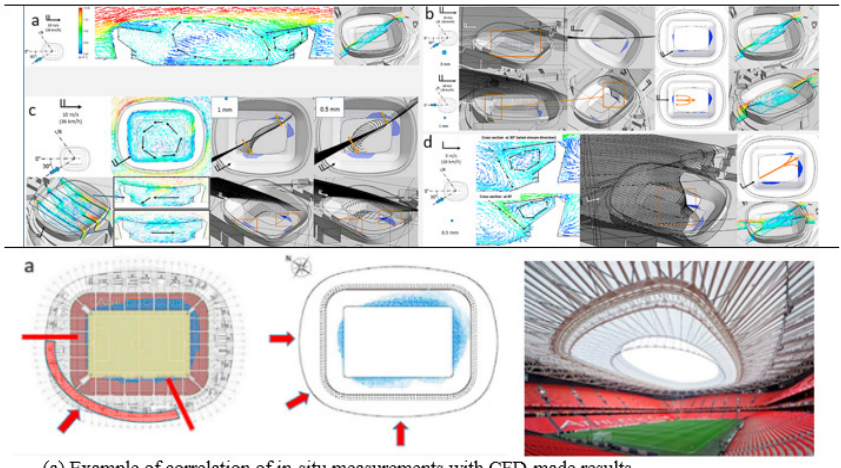

(a) Example of correlation of in-situ measurements with CFD-made results.

(b) (c)

(b) Example of wetting model comparison between different alternatives. (c) View and cross-section of the roof extension selected for the new San Mames stadium (Llarena et al., 2018)

Figure 8. Wind flow model and raindrop trajectory effect for the original stadium configuration

2.2.3. Convective Heat Transfer Coefficients (CHTC) on Building Facades

Determining external CHTC values along building facades is a difficult task. It includes a wide variety of parameters including building geometry, environmental topography, wind speed, wind direction, turbulence intensity, surface roughness, texture, and moisture content. Although many experimental studies have been done on this subject, the number of CFD analyses for outdoor CHTC for buildings is very few. In addition, the number of studies in which

the accuracy of these CFD models is checked with wind tunnel studies is also very few. Due to the limitations of the RANS model, studies in this field can only analyze the wind-facing facades of simple cubic structures (Figure 9). Improved flow modeling achievable with hybrid URANS/LES or LES should be used to obtain accurate results on differently shaped facades (Blocken et al., 2011). Such high-resolution CFD simulations are not very useful for real building simulations. Therefore, it is not easy to verify building exterior heat transfer simulations with CFD. It may fall outside the scope of many practical building simulation studies.

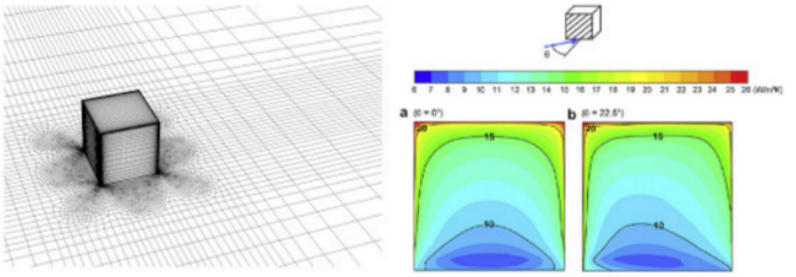

(a) (b)

(a) high-resolution grid for CFD simulation of convective heat transfer coefficients around a cubic building model; (b) forced convective heat transfer coefficients at the wind front for a reference wind (Blocken et al., 2011)

Figure 9. Building exterior heat transfer simulations with CFD

2.2.4. Air Pollutant Distribution Around Buildings

Outdoor air pollution is one of the most important environmental problems today. In the built environment, both the outdoor exposure of pedestrians and the indoor exposure of occupants are of concern. Outdoor and indoor air pollution is the most important problem for building and air conditioning engineers who design ventilation inlets and outlets on building facades or roofs (Figure 10). Indoor air pollution from outdoor air pollutants can result from the re-ingestion of polluted air by the same building or from other sources such as nearby buildings, traffic, and parking lots. The same applies to concentrations in streets and squares.

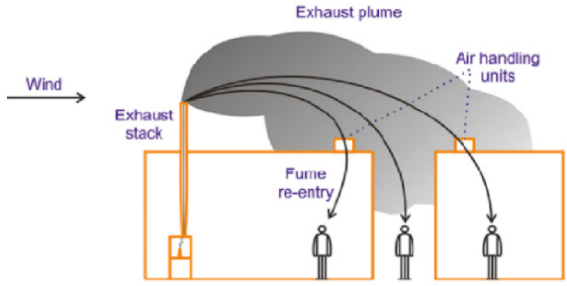

Figure 10. Re-absorption of polluted air by the same building or other buildings and accumulation in the streets (Blocken et al., 2011)

On-site measurements, wind tunnel measurements, semi-empirical formulas, and CFD can be used for polluted air density. Some wind tunnel studies have also been conducted in the past to better understand the behavior of wind-borne pollutants. However, there have been cases where wind tunnel tests were not preferred due to their disadvantages, such as being time-consuming and costly, inapplicability for light wind conditions, and scaling and similarity issues. Instead, Gaussian and ASHRAE models are preferred (Blocken et al., 2011).

One of the case-based studies in the literature on pollutant dispersion around buildings in urban areas is the study by Gousseau et al. in an urban area in Montreal, Canada. In the study, 2 different CFD methods, RANS (Standard k-ε model) and LES, were applied to analyze the pollutant dispersion in the urban area and validated with wind tunnel tests. The aim here is to determine the differences between RANS and LES methods in determining the pollutant distribution and to create the right model in terms of applicability (Figure 11), (Gousseau, et al., 2011).

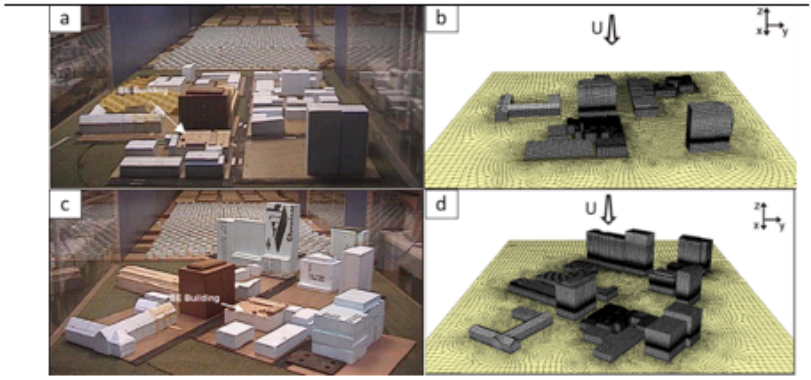

Figure 11. Wind tunnel and simulation analysis of air circulation depending on wind direction in the urban area

2.2.5. Wind Loads on Buildings

In the literature, one of the CFD study areas oriented external to the environment in buildings is the wind loads formed on the surfaces of buildings. Studies in this area are generally aimed at wind loads occurring in high-rise

buildings. The study by Shireen and James is an example of the determination of wind loads in high-rise buildings. Within the scope of the study, the wind loads generated by the wind flow on two different facades of the HHHR Tower (Blue Tower) in Dubai, which is one of the high-rise buildings selected as an example, were determined by the RANS (RNG k-ε turbulence model) CFD method with the help of ANSYS CFX 14.0 software (Figure 12). The reason why the RNG k-ε turbulence model is preferred instead of the Standard k-ε in the RANS method preferred here is that RNG k-ε gives more consistent results in the analysis of wind flow and wind loads in high-rise buildings as stated by the authors (Saadullah, Haido, 2017).

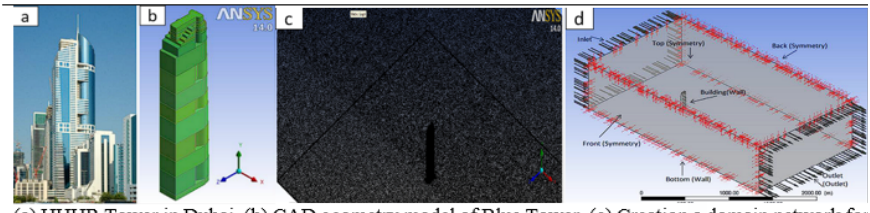

(a) HHHR Tower in Dubai, (b) CAD geometry model of Blue Tower, (c) Creation a domain network for Blue Tower, (d) Boundary conditions in the domain of the HHHR Tower model (Saadullah, Haido, 2017)

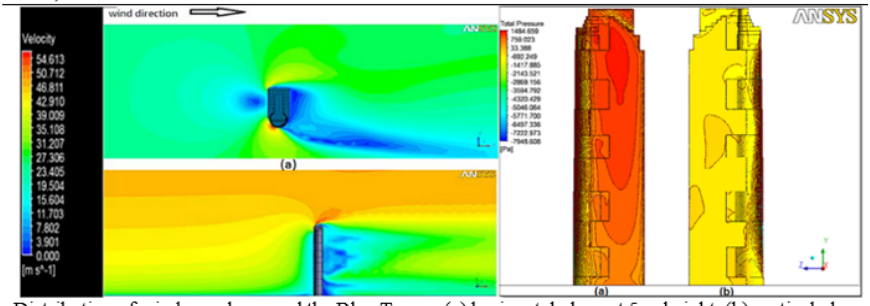

Distribution of wind speeds around the Blue Tower: (a) horizontal plane at 5 m height, (b) vertical plane. Pressure contour lines on building faces with wind direction at 0° angle: (a) windward facing facade, (b) non-windward facing facade (Saadullah, Haido, 2017)

Figure 12. Studies for the determination of wind loads in high-rise buildings

In the study of Shireen and James, wind flow analysis and wind load determination from 2 different facades with the CFD model of the building and comparison with wind tunnel experiments were performed. (Figure 13).

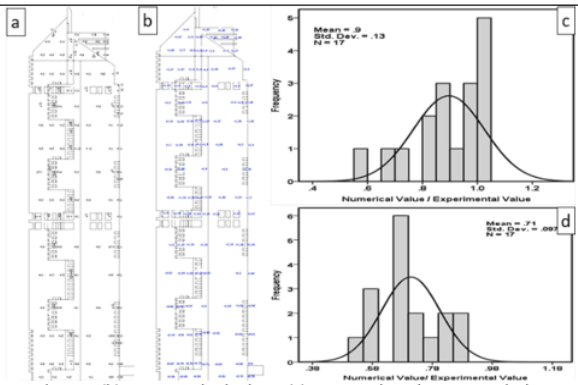

(a) With wind tunnel test ; (b) CFD analysis data, (c) Comparison between wind pressures of the wind tunnel test and CFD analysis of the Blue Tower at 0° wind direction, (d) Comparison between wind pressures of the wind tunnel test and CFD analysis of the Blue Tower at 90° wind direction (Saadullah, Haido, 2017)

Figure 13. Wind pressures in kN/m² on the windward face of the Blue Tower at 0° wind direction

3. Conclusions

This study provides an overview of CFD applications for building performance simulations, focusing on the indoor and outdoor environment (Table 2). In the first part of the study, CFD is defined, followed by the development of CFD, the sectors in which it is used, and its advantages and disadvantages compared to experimental applications. As mentioned in this section, studies on CFD have gained rapid momentum since the 1960s and evolved into RANS studies in the 1990s and methods such as DES/LES/DNS today. While many sectors benefit from these applications in this process, their use in architecture has only started in recent years due to limiting problems.

In architecture, studies on the application of CFD in the design of indoor and outdoor environments are mostly case-based and are aimed at the optimization of the structure. In indoor environment studies, CFD can be used to analyze ambient temperature, radiant temperature, air humidity, and airflow velocities for thermal comfort. In outdoor environments, CFD is still limited for urban-scale studies but is applicable for smaller-scale studies. With the exception of a few urban-scale studies, the majority of studies in the literature are on the performance determination of isolated structures. Studies on the outdoor environment are generally focused on pedestrian-level wind, WDR (wind-driven-rain), convective heat transfer, pollutant dispersion, wind loads, and natural ventilation. In many of these studies, CFD analyses have been

supported by experimental studies in wind tunnels, while testing the accuracy of CFD. Of these study topics, convective heat transfer has been the least studied, mainly due to the fact that CFD analyses are still not adequate for such studies in outdoor environments and some limiting factors such as scale.

Table 2. Evaluation of CFD applications in architecture

	CFD Advantages	CFD Disadvantages	Validation Studies
CFD Applications in Indoor Design	• It can be an alternative to time-consuming and costly experimental studies and semi-empirical formulas. • It can simulate most of the indoor climate parameters (air temperature, radiant temperature, air velocity, ventilation degree, and pollutant concentration) with high accuracy.	• Environmental humidity, which is an indoor parameter, is usually not simulated. • Requires validation work for the accuracy of the results.	• Wind Tunnel and Field Measurements (usually field measurements are used)
Pedestrian Wind Environment Around Buildings	• It can be an alternative to wind tunnel studies. • Many good practice guides and working examples are available. • Can simulate pedestrian wind environment around buildings with high accuracy. • The ability to apply LES models as well as RANS models for different application scenarios.	• Problems experienced at the point of selection of suitable models (cases where stable RANS model is insufficient for multiple building configurations, etc.) • Requires validation work for the accuracy of the results	• Wind Tunnel and Field Measurements
Wind-Driven Rain (WDR) on Building Facades	• It can be an alternative to time-consuming and costly experimental studies and semi-empirical formulas. • It can simulate WDR distribution on building facades.	• The effects of many parameters such as building geometry, ambient topography, location on the building facade, wind speed, wind direction, turbulence density, precipitation density, and raindrop size distribution. • Requires validation work for the accuracy of the results.	• Wind Tunnel and Field Measurements
Convective Heat Transfer Coefficients (CHTC) on Building Facades	• It can be an alternative to experimental studies.	• Sample study is very few. • Influence of results by a wide variety of parameters, including building geometry, environmental topography, wind speed, wind direction, turbulence intensity, surface roughness, texture, and moisture content. • Often use semi-empirical formulas instead of CFDs.	• Wind Tunnel (usually not applicable), Field Measurements, Semi-Empirical Formulas
Air Pollutant Distribution Around Buildings	• It can be an alternative to wind tunnel studies • It can simulate the pollutant dispersion created by the buildings with high accuracy. • LES can be preferred in scenarios such as urban areas.	• The results are affected by parameters such as building geometry, wind speed, wind direction, turbulence density, pollutant particle size, and concentration. • Confirmation work is required for the accuracy of the results.	• Wind Tunnel and Field Measurements
Wind Loads on Buildings	• It can be an alternative to wind tunnel studies.	•It can simulate wind loads in buildings with high accuracy. •Generally applicable for single structures. •Requires validation work for the accuracy of the results.	• Wind Tunnel and Field Measurements

Another controversial issue in indoor and outdoor structural applications of CFD is the method and model. While most of the studies in the literature use the stable RANS method, there are a few studies that use the LES method as an exception. Although the capabilities of LES in solving the flow cannot be

ignored, when evaluated in terms of cost/benefit for large-scale analyses such as buildings and urban areas, it is a fact that such applications will be very costly and verification will take a very long time. When evaluated in this sense, it is seen that the RANS method is applicable and can provide more benefits with less cost in the preliminary stage or optimization of the design. Another method, URANS, is generally preferred over LES as it assumes unsteady flows and requires high-resolution studies for the solution.

4. REFERENCES

Abanto, J, Barrero, D, Reggio, M. and Ozell, B., (2004). Airflow modelling in a computer room. Building and Environment, 39 (12), 1393-1402.

Blocken, B., Carmeliet, J. and Stathopoulos, T., (2007). CFD evaluation of wind speed conditions in passages between parallel buildings-effect of wall-function roughness modifications for the atmospheric boundary layer flow. Journal of Wind Engineering and Industrial Aerodynamics, 95 (9-11), 941-962.

Blocken, B, Carmeliet, J.,(2008). Pedestrian wind conditions at outdoor platforms in a high-rise apartment building: generic sub-configuration validation, wind comfort assessment and uncertainty issues. Wind and Structures, 11 (1), 51-70

Blocken, B., Persoon, J., (2009). Pedestrian wind comfort around a large football stadium in an urban environment: CFD simulation, validation and application of the new Dutch wind nuisance standard. Journal of Wind Engineering and Industrial Aerodynamics, 97 (5-6), 255-270.

Blocken B., Stathopoulos T., Carmeliet J., Hensen J., (2011). Application of CFD in building performance simulation for the outdoor environment: an overview, Journal of Building Performance Simulation, Vol. 4, No. 2, June 2011, 157–184

Briggen, P.M., Blocken, B., Schellen, H.L., (2009). Wind-driven rain on the facade of a monumental tower: numerical simulation, full-scale validation and sensitivity analysis. Building and Environment, 44 (8), 1675-1690.

Den Hartog, JP, A Koutamanis, and PG Luscuere, (2000). “Possibilities and limitations of CFD simulation for indoor climate analysis”

Gadilhe, A., Janvier, L., Barnaud, G., (1993). Numerical and experimental modelling of the three-dimensional turbulent wind flow through an urban square. Journal of Wind Engineering and Industrial Aerodynamics, 46-47: 755-763.

Gousseau P, Blocken B, Stathopoulos, T, van Heijst GJF., (2011). CFD simulation of near-field pollutant dispersion on a high-resolution grid: a

case study by LES and RANS for a building group in downtown Montreal. Atmospheric Environment 45: 428-438

He, J., Song, C.C.S., (1999). Evaluation of pedestrian winds in urban area by numerical approach. Journal of Wind Engineering and Industrial Aerodynamics, 81, 295–309.

Jameson, T.A., (2012). Computational Fluid Dynamics: Past, Present and Future, Future Directions in CFD Research National Institute for Aerospace August 6–8, 2012, Hampton, VA.

Jo, S., (2018). Trends in the application of CFD for architectural design. ARCC – EAAE 2018.

Kiriççi, V., (2016). Osman Gazi Köprüsüne Etkiyen Rüzgâr Yüklerinin HAD Metodu ile İncelenmesi, (Yüksek Lisans Tezi), Fen Bilimleri Enstitüsü, Anadolu Üniversitesi, Eskişehir.

Llarena J., Cabezuelo L., Bilbao A., (2018). Application of CFD simulations of wind-driven rain (WDR) on the new roof extension for San Mames new football stadium, Journal of Wind Engineering & Industrial Aerodynamics 178 (2018) 105–111.

Roudsari, M, and Pak, M., (2014). "Ladybug: A Parametric Environmental Plugin for Grasshopper to Help Designers Create an Environmentally-Conscious Design." 13th International Conference of the International Building Performance Simulation Association (BS2013), Chambery, France.

Saadullah S., T. & James H. Haido, (2017). Wind Analysis of Tall Building in Duhok City Using Computational Fluid Dynamic (CFD), Journal of University of Duhok, Vol. 20, No.1 (Pure and Eng. Sciences), Pp 520-536.

Tang, W, Davidson, CI., (2004). Erosion of limestone building surfaces caused by wind-driven rain. 2. Numerical modelling. Atmospheric Environment, 38 (33), 5601-5609.

Van Hooff, T, Blocken, B.,(2010). Coupled urban wind flow and indoor natural ventilation modelling on a high-resolution grid: A case study for the Amsterdam ArenA stadium. Environmental Modelling & Software, 25 (1), 51-65.

Zhai, Zhiqiang (2006). "Application of computational fluid dynamics in building design: aspects and trends." Indoor and built environment 15 (4):305-313.

Wu, Yu-Chou, An-Shik Yang, Li-Yu Tseng and Chin-Lung Liu, (2011). "Myth of ecological architecture designs: Comparison between design concept and computational analysis results of natural-ventilation for Tjibaou Cultural Center in New Caledonia." Energy and buildings 43 (10):2788-2797.

CHAPTER VII

MODELING FUNCTIONALLY GRADED MATERIALS IN ANSYS APDL

AHMED HASSAN AHMED HASSAN[1] & NACI KURGAN[2]

[1] Ondokuz Mayis University, Mechanical Engineering Department, Engineering Faculty, Samsun, Turkey, e-mail: 15210457@stu.omu.edu.tr
ORCID: 0000-0002-4880-0184

[2] Ondokuz Mayis University, Mechanical Engineering Department, Engineering Faculty, Samsun, Turkey, e-mail: naci.kurgan@omu.edu.tr
ORCID: 0000-0001-7297-7249

1. Introduction

Functionally graded materials (FGM) are relatively new kind of composites in which the interface between different materials where sudden change of properties occurs (see Figure 1) is replaced by a wider interface which has a gradual change in material, as shown in Figure 2. The aim of this replacement is to get rid of the stress concentration that occur due to the response difference of the two adjacent different materials at the interface.

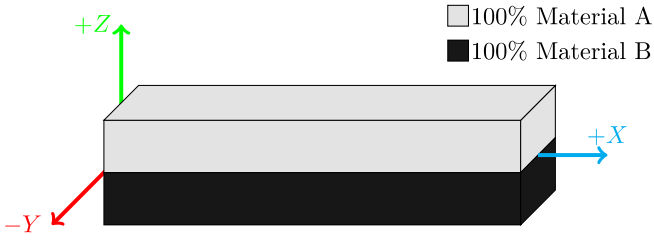

Figure 1. Bi-material composite part

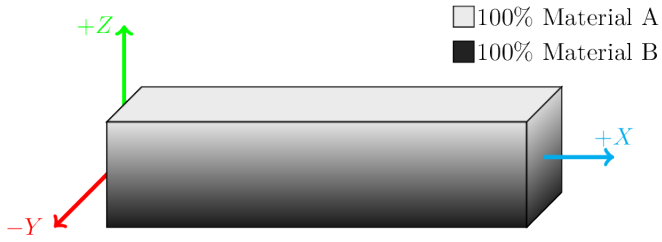

Figure 2. FGM-Z-C

The gradation of properties normally results from the change in material, phase, or porosity. FGM have been used in many applications, such as thermal barriers and cutting tools. For recent reviews on the applications of FGM see (Akshaya et al., 2021; Li & Han, 2018; Saleh et al., 2020). Due to limitations of some certain manufacturing processes, the gradation of material through the FGM part might not be continuous but stepped, as the one shown in Figure 3. Skim the recent reviews (Li et al., 2020; Loh et al., 2018; Parihar et al., 2018; Zhang et al., 2019) to get enlightened on the advances in manufacturing FGMs.

Hereinafter, FGM with continuous variation of properties through the Z direction, as the one shown in Figure 2, will be referred to as FGM-Z-C, where C and Z denote the continuity and direction of the properties variation, respectively. Following the same pattern, FGM with discrete properties variation, as the one shown in Figure 3, is referred to as FGM-Z-S, where S denotes the stepped variation of the properties.

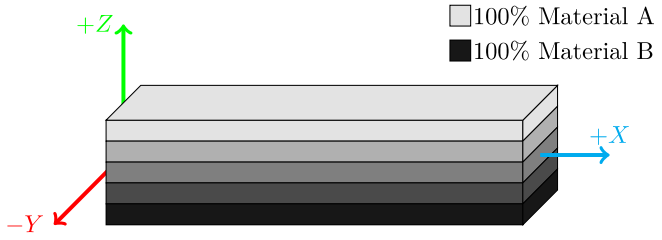

Figure 3. FGM-Z-S

Properties variation may take place in any direction. For example, Figure 4 and Figure 5 show two FGMs having respectively continuous and stepped properties variation through their lengths, i.e., the X direction. These two FGMs are referred to as FGM-X-C and FGM-X-S, following the same coding convention as in the above cases. Material variation could be in more than one

dimension. An example for three-dimensional (3D) material variation is shown in Figure 6.

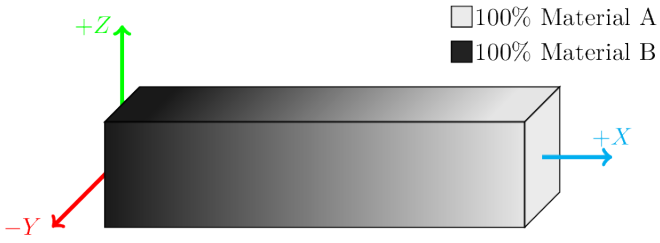

Figure 4- FGM-X-C

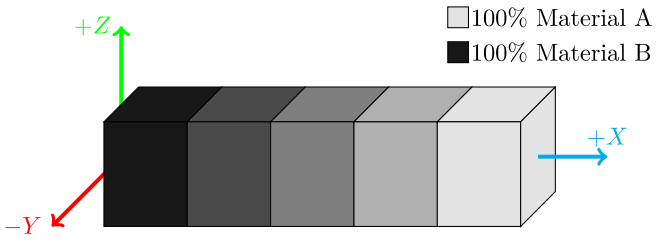

Figure 5- FGM-X-S

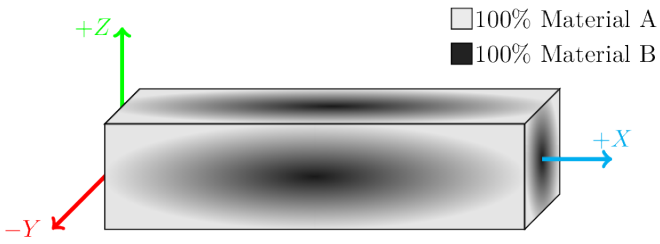

Figure 6- FGM-XYZ-C

In FEM, continuous variation of properties through an FGM part can be modeled at the level of integration points within the elements/layers/cells. While the stepped variation is modeled at the higher level of whole elements/ layers/cells. Note that in ANSYS, layers and cells are the divisions of sections of sectional elements, namely, shells and beams. Due to its more simplicity, many researchers implement the element-wise variation model, i.e., stepped variation, even in modeling the continuous one. That is done by increasing the number of elements/layers/cells in the variation direction to the point that the continuous

variation is approximated. Depending on the geometry of the FGM part, it can BE modeled as 3D solid elements, 2D plane elements, or by using the simplified structural elements, such as shell, plate, beam, etc. Using such elements is far more efficient than using 3D solid elements. Structures with significant slenderness, i.e. two dimensions are both small compared to the third, would be modeled using beam elements. Beam element is a line element describes the length of direction. In case of wide thin structures those have thickness significantly small compared to the other two dimensions, are typically modeled using shell elements. Shell element is an area element describes the geometry of the structure. Thickness is divided into layers which each can have different material properties. Properties variation through the sections of such elements is treated differently from the variation through the other model dimensions.

Through the years, many methods are proposed to model and analysis FGM parts. By far the most implemented one is the finite element method (FEM), that is due to many reasons including the availability of trusted powerful packages of FEM, such as ABACUS, and ANSYS (Barbero, 2007). (Martínez-Pañeda, 2019) illustrated and compared two methods of modeling FGM in ABACUS. The illustrated techniques were the fictive thermal load and the element-wise material assignment. Similar illustration of modeling techniques of FGM in ANSYS is missed in the literature. Only one article, (Hassan & Keleş, 2017), illustrated the fictive thermal load method to model FGM in ANSYS. All other publications mention with no illustration the implemented techniques. This article illustrates techniques for modeling FGM parts implemented in APDL.

2. Problem De inition

Considering the coordinate system and part geometry shown in Figure 2, dimensions of the considered FGM part is taken as follows. The length (L is along the X direction; the thickness (H is along the Z direction; lastly, the width (B) is along the Y direction. According to the coordinate system shown in Figure 2, The considered FGM part lays within $X \in \{0,L\}$, $Y \in \{-B/2, +B/2\}$ and $Z \in \{-H/2, +H/2\}$

The considered FGM can be modeled in various ways as shown in Figure 7. The first model is the intuitive one of modeling the part as it is, i.e. a 3D solid part using 3D solid elements. However, due to the uniform width of the considered FGM, a simplification can be implemented by modeling it as a 2D plane with a predefined width. Further simplification can be done by modeling it as a beam line element with predefined cross-section properties, assuming that its cross-section dimensions are both small enough compared to its length.

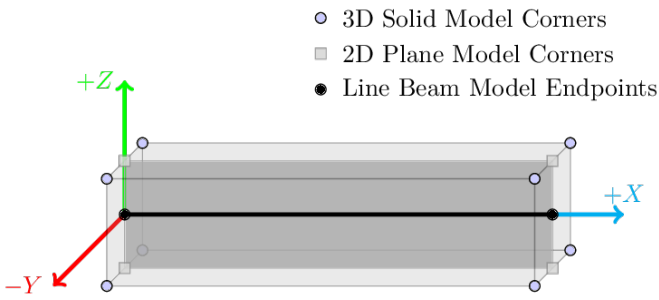

Figure 7. Geometry models

Both continuous and stepped properties variations are considered in this study. Considered directions of variation are the Z and X axes, i.e. through the thickness or length of the FGM. The resulting considered cases are FGM-Z-C, FGM-Z-S, FGM-X-C, and FGM-X-S.

Following the material labeling stated above, the constitutive two materials are considered as follows. The elasticity constants of Materials A and B are to be referred to as E_C and E_M, respectively. Poisson's ratio of both materials is assumed constant and referred to as . The properties variation through the thickness is assumed to follow a simple power rule that is shown in Eq.(1).

$$E_{(Z)} = E_M + (E_C - E_M)\left(\frac{2Z+H}{2H}\right)^N \tag{1}$$

N is a power index that controls the the variation equation. If $N = 0$ then the part is homogeneous with a constant elasticity equals to E_C . If $N = \infty$ then the part is also homogeneous but with a constant elasticity equals to E_M. Otherwise, the elasticity constant is E_M at $Z = +H/2$, and E_C at $Z = -H/2$. Properties variation is assumed exponential for the cases in which it occurs in the length direction. The assumed exponential function is shown in Eq.(2).

$$E_{(X)} = E_M e^{\beta\frac{X}{L}} \tag{2}$$

β is an exponential index controls the properties variation. The elasticity constant at the $x = 0$ is E_M. If $\beta = 0$ then the part is homogeneous with elasticity equals E_M. Else, the elasticity through the length of the FGM part gets increasing or decreasing following the sign of β. A uniformly distributed load of QN/mm^2 is applied on the whole length pushing the part down in the $-Z$ direction. Clamped, cantilever, and simply supported boundary conditions are to be examined.

In many cases it might be desirable to consider certain plane as reference one. For homogeneous beams and shells under bending, the reference plane is

typically at the middle where coupling between extension and lateral deflections vanishes, i.e., physical neutral plane. Thus, at such plane bending and buckling problems get much simpler with less variables to solve for. In the case of FGM, the neutral plane does not necessarily coincide on the middle plane. Assuming that the bending occurs in the XZ plane, FGM parts with properties variation through its thickness do have offset *(C)* between the neutral and middle (Wang et al., 2017). Note that for the considered FGM part, the middle plane lays on the YZ plane. ANSYS has no problem in considering any reference plane and solves the coupled equations. However, taking the neutral plane as reference allows the results to be comparable with those in literature. The offset *C* can be easily derived for beams and plates from their coupled governing equations by equating the coupling integral to zero (Hassan et al., 2022; Wang et al., 2017), as shown in Eq.(3).

$$\int (Z - C) \frac{E_{(Z)}}{1 - v_{(Z)}^2} dZ = 0 \tag{3}$$

$v_{(Z)}$ is the Poisson's ratio given as a function of Z. The difference in v is normally negligible, so it is often considered constant through the FGM part, then Eq.(4) can be written as follows.

$$C = \frac{\int Z E_{(Z)} dZ}{\int E_{(Z)} dZ} \tag{4}$$

For the special case considered in this work of $E_{(Z)}$ varies continuously according to the simple power rule of Eq.(1), C is obtained here analytically using the Python library for symbolic mathematics SymPy (Meurer et al., 2017). The Python code is provided in Program 1. The analytical solution of C results as shown in Eq.(5).

$$C = \frac{HN(E_C - E_M)}{2(N+2)(E_C + E_M N)} \tag{5}$$

Program 1- Symbolic Integrations and C calculation (python3 code)

```
from sympy import symbols, solve, simplify
from sympy import integrate as ii
' ' '
PRODUCES THE SYMBOLIC ANALYTICAL SOLUTIONS FOR C AND
INTEGRALS OF THE PRE-INTEGRATED SECTION PROPERTIES
      C: OFFSET BETWEEN NEUTRAL AND MIDDLE PLANES
     IE: INTEGRATION OF E(Z)
  IZN2E: INTEGRATION OF (Z-C)**2*E(Z)
' ' '
EM, EC, H, N, Z, C = symbols('EM EC H N Z C')
II = lambda F:ii(F,(Z,-H/2,H/2),conds='none').simplify()
# ================================================
# E(Z) DEFINITION: MODIFY THIS FUNCTION AS DESIRED
E = EM + (EC-EM)*((2*Z+H)/(2*H))**N
# ================================================
C = solve(II((Z-C)*E),C)[0];  print(f'C     = {C}')
IE = II(E);                   print(f'IE    = {IE}')
IZN2E = II((Z-C)**2*E);       print(f'IZN2E = {IZN2E}')
```

Note that if $E_{(Z)}$ is constant or symmetric about $Z = 0$, then C vanishes and the neutral plane coincides with the middle plane. Alternatively, to the analytical solution, C can be found numerically using any integration scheme. 5-points Gauss-Legendre quadrature rule is considered for this task. n-points Gauss-Legendre quadrature rule provides the exact integration for polynomials of degree up-to $(2n - 1)$. Therefore, the considered integration scheme provides exact solutions for $N \leq 9$. For the other case of stepped variation, the integrals that are needed to calculate C are obtained using the trapezoidal quadrature rule. The intervals of the integration are set to match the steps of the material variation so that an exact integration is obtained.

3. Arrangement of Common Tasks

The modeling techniques described here are illustrated by examples. Each example is given as separate macro file. A macro file is a set of APDL commands run sequentially once called. However, there are many blocks of APDL code repeatedly appear in many examples. To help making the presented code shorter

and manageable, these repetitive common tasks are gathered as macros. In order to ease the management of the common-tasks macros, they are all gathered in one macro library, presented in Program 13. Macro library is a group of macros listed in one text file. Once the macro library is set identifiable, each contained macro can be called using its given name. Note that the sequence of macros within a macro library has no importance. Worth mentioning is that macros readily read, modify, and create global variables. In addition, macros can have their own local variables. An important note to point at is that APDL is not case-sensitive. To summarize, the general map of the presented code is that each example is an APDL macro which may call one or more common-task macros from the macro library Program 13. Following is a presentation of the common-tasks macros that appear in all later-on examples of FGM modeling techniques. Other less appearing common-tasks macros will be presented once needed. For the sake of clarity, only main macros are listed below. Those main macros may call other smaller ones also contained in the macro library Program 13.

The macro "INITIATION" mainly clears the previous model, if found, and gives title to the new run. This macro is needed at the beginning of each program. "INPUTDATA" macro sets the main input data of the beam geometry *(L, B, H)*, material properties *(E_M, E_C, NU)*,variation indices *(N, BETA)*, load *(LOAD)*, and mesh size *(NL, NH, NB)*. Note that *NU* is the Poisson's ratio *v*; while *BETA* is the exponential index *β*. *NL*, *NB*, and *NH* are the number of elements of the meshed part in the X, Y, and Z directions, respectively. In beam elements, *NB* and *NH* are the number of section cells in the Y and Z directions, respectively.

"EZ-FUNCTION" macro takes the Z coordinate as an argument and calculates the elasticity constant *EZ* according to the given function, which is the simple power law that is presented in Eq.(1). "EX-FUNCTION" calculates *EX* for X coordinate input according to exponential function of Eq.(2).

The macros "GEOM-MESH" creates both geometries and meshes of the 3D solid, 2D plane, and line beam models. Elements selected for the 3D solid model are the brick **SOLID186** elements. For the 2D plane model, **PLANE183** elements are considered. Lastly, the **BEAM189** elements are selected to build the line beam model. Detailed documentation on those elements can be found in (*ANSYS Mechanical APDL Element Reference*, 2016). Mapped mesh having regular pattern is considered in both the 3D solid and 2D plane models. The reference plane is considered at the physical neutral plane that has offset *C* from middle plane.

"BC-LOADS" is the macros in which the boundary conditions and loads are applied to the corresponding models. "SOLVE-PLOT" macro runs the analysis

and plots the resulted lateral displacement. "SYMBOLIC-INTEGRATION" macro calculates the offset *C* between the neutral and middle planes, along with other integrals. The formulae used in this macro are obtained from the analytical symbolic solution resulted from the Python code in Program 1.

"GAUSSIAN-QUADRATURE" macro calculates the same quantities but numerically using 5-points Gaussian integration scheme. As discussed above, this integration scheme is as accurate as the analytical solution for $N \leq 9$. Both the analytical and Gaussian quadrature are to be used in the case of continuous variation of properties. For the stepped variation, "TRAPEZOID-QUADRATURE" is used to obtain the exact integration given that the intervals of the integration are set to match the steps of properties variation.

4. Modeling Techniques of FGM in ANSYS APDL

4.1. User-Defined Field Variables (UF)

ANSYS provides the ability to define various material properties dependent on field variables, such as temperature, time, frequency, and pressure. In addition to those field variables, ANSYS allows user to define custom field variables, typically named as UF01, UF02, ..., UF09. These user-defined field variables (UF)'s can depend on the initial state of the model which includes the initial coordinates of the nodes. FGM can be modeled by relating its varying properties to such a coordinates clone UF. The UF technique can model the continuous properties variation through the geometry nodes. So, for the considered FGM part and notations, the variation of properties through the length can be modeled by implementing this technique to the 3D solid, 2D plane, and line beam models. However, with this technique the properties variation through the depth can be modeled only on the 3D solid and 2D plane models, but not on the line beam model.

There are two main steps in this technique. First is to relate the varying properties to an UF over the model dimension through which the properties variation takes place. The first user-defined field variable typically takes the name (**UF01**) which then increments for additional ones. Second step is to relate that UF to the initial coordinates. This relation is typically a direct mapping, i.e. cloning. This is done by declaring UF01 as an initial state field variable using the APDL command **INISTATE**, then iterating through geometry nodes defining the value of UF01 at each node as its initial coordinate that of interest. Since this mapping of coordinates to UF is linear, value of UF at each integration point between nodes would be exactly its coordinate as well. As a result, continuous

variation can be modeled using UF. Following are two examples of APDL code for implementing UF technique in modeling the continuous variation of properties through the length, and depth of the FGM part.

The first example models the bending of an FGM beam having continuous variation of properties through its length using the UF technique. The APDL code for this example is given in Program 2. In this example, UF01 is defined as the X coordinate at each model node. At each geometry integration point, UF01 would have an interpolated value of the surrounding nodes. While UF01 values over the nodes are nothing but the linearly varying X coordinates, so UF01 at each integration point would be its X coordinate. Therefore, using the node-based UF technique one can model the continuous variation of properties. Note that the variation in the length direction using this node-based technique is valid for the 3D solid, 2D plane models, and the line beam model, since all of these models have geometry nodes in that direction.

Program 2- Modeling 3D-, 2D-, and Beam- FGM-X-C using UF

```
*ULIB,'MAIN_LIB','MACLIB',' ' ! IDENTIFIES MACRO LIBRARY
*USE,INITIATION
*USE,INPUTDATA
MODEL = 2  ! 1:LINE BEAM, 2:2D PLANE, 3:3D SOLID MODELS
BC = 1     ! 1:CLAMPED, 2:CANTILEVER, 3:SIMPLY SUPPORTED
*USE,GEOM_MESH
*USE,BC_LOAD
!================================================     ||
! USER-DEFINED FIELD VARIABLE (UF) TECHNIQUE           ||
!    IMPLEMENTATION IN MODELING FGM-X-C                ||
!-------------- (STEP 1) ----  RELATES UF01, E, & X    ||
TB,ELASTIC,1                 !                         ||
*DO,XI,0,L,L/100             !                         ||
TBFIELD,UF01,XI              !                         ||
*USE,EX_FUNCTION, XI         !                         ||
TBDATA,1,EX,NU               !                         ||
*ENDDO                       !                         ||
!-----------------------------                         ||
!---------------- (STEP 2) ---  ASSIGNS UF01= Xi       ||
INISTATE,SET,NODE,1          !   TO EACH NODE i        ||
INISTATE,SET,DTYP,UF01       !                         ||
*GET,NUMNODES,NODE,,NUM,MAX  !                         ||
*DO,II,1,NUMNODES            !                         ||
IEXIS=NSEL(II)               !                         ||
*IF,IEXIS,EQ,1,THEN          !                         ||
UFVAL=NX(II)                 !                         ||
INISTATE,DEFINE,II,,,,UFVAL  !                         ||
*ENDIF                       !                         ||
*ENDDO                       !                         ||
!-----------------------------                         ||
!=====================================================  ||
*USE,SOLVE_PLOT
*ULIB                      ! UN-DECLARE MACRO LIBRARY
```

The second example is similar to the first one, but the variation of properties is set to be in the depth direction. The APDL code for this example is given in Program 3. Since the properties vary in the thickness direction, then the neutral and middle planes are at offset *C*. In this example, the neutral plane is taken as reference.

In this example, UF01 is defined as the Z coordinate of each node. Following the same reasoning in the previous section, UF01 at each geometry integration point takes the value its Z coordinate. Note that the variation in the depth direction using this node-based technique is valid only for 3D solid and 2D plane models, since the line beam model has no geometry nodes in the depth direction.

Program 3- Modeling 3D- and 2D- FGM-Z-C using UF

```
*ULIB,'MAIN_LIB','MACLIB',' ' ! IDENTIFIES MACRO LIBRARY
USE,INITIATION
*USE,INPUTDATA
*USE,SYMBOLIC_INTEGRATION  ! ONLY C IS NEEDED
MODEL = 2  ! 2:2D PLANE, 3:3D SOLID MODELS
BC = ARG2  ! 1:CLAMPED, 2:CANTILEVER, 3:SIMPLY SUPPORTED
*USE,GEOM_MESH
*USE,BC_LOAD
!=======================================================
! USER-DEFINED FIELD VARIABLE (UF) TECHNIQUE             ||
!   IMPLEMENTATION IN MODELING FGM-Z-C                   ||
!-------------- (STEP 1) ----  RELATES UF01, E, & Z      ||
TB,ELASTIC,1                 !                           ||
*DO,ZI,-H/2,H/2,H/100        !                           ||
TBFIELD,UF01,ZI              !                           ||
*USE,EZ_FUNCTION, ZI         !                           ||
TBDATA,1,EZ,NU               !                           ||
*ENDDO                       !                           ||
!-----------------------------                           ||
!---------------- (STEP 2) ---  ASSIGNS UF01= Zi         ||
INISTATE,SET,NODE,1          !   TO EACH NODE i     ||
INISTATE,SET,DTYP,UF01       !                           ||
*GET,NUMNODES,NODE,,NUM,MAX  !                           ||
*DO,II,1,NUMNODES            !                           ||
IEXIS=NSEL(II)               !                           ||
*IF,IEXIS,EQ,1,THEN          !                           ||
UFVAL=NZ(II)                 !                           ||
INISTATE,DEFINE,II,,,,UFVAL  !                           ||
*ENDIF                       !                           ||
*ENDDO                       !                           ||
!-----------------------------                           ||
!=======================================================
*USE,SOLVE_PLOT
*ULIB                  ! UN-DECLARE MACRO LIBRARY
```

4.2. Fictive Thermal Load (FT)

This is claimed to be the most used method in modeling FGM using finite element packages (Martínez-Pañeda, 2019). Fictive thermal load (FT) technique may also be referred to as dummy temperature method (Ashirbekob et al., 2020; Hassan & Keleş, 2017), auxiliary non-physical temperature method (Martínez-Pañeda, 2019), and pseudo-temperature method (Prashant Singh et al., 2022). The idea is to make temperature represent the location through the model, then relate the varying material properties to it. This should result in location-dependent properties through the model, which is the sought goal.

Implementing the fictive thermal load technique (FT) requires two capabilities to be available on the finite element package. The first is the ability to define temperature-dependent material properties. The second is the ability to vary temperature through the model. Both capabilities are available on ANSYS since it provides temperature as a predefined field variable. One issue that has to be taken care of is the stress/strain effects of the thermal load. This is typically overcome by setting the thermal expansion coefficient to zero. In ANSYS, defining temperature-dependent material properties is provided out of the box. This relation can be expressed as a table of ascending values of temperature versus the corresponding values of the varying properties. Note that ANSYS allows only up to 100 points in such a table. Temperature variation through the model can be obtained using a simple thermal study that results in the temperature at each node/element/layer through the model, as in (Ashirbekob et al., 2020; Hassan & Keleş, 2017; Prashant Singh et al., 2022). Another simpler way is to directly assign temperature at each node/element/layer as an additional load together with the other loads and boundary conditions of the original targeted analysis. Assigning temperature to each node/element/layer can be achieved using a simple iteration or as a function. Despite its simplicity, FT technique complicates some types of analysis, such as the eigenvalue analyses. Another drawback of this method is the inability to include other thermal loads which probably exist in the FGM applications.

FT technique allows both continuous and stepped variation of properties to be modeled through one or more of the model's dimensions as well as through sections of sectional elements, e.g., beams, shells. Continuous properties variation through the model is modeled by node wise temperature assignment, that is loading each node by a temperature rise equals to its coordinate value in the direction of variation. So, temperature will represent the location. Since this is linear mapping of coordinates on temperature, each integration point within

an element would have exactly temperature rise equals to its coordinate value as well. Modeling continuous properties variation through the section of sectional element follows the same logic. For layered shell elements, the temperature is assigned at the interfaces between the layers, so that the sectional integration points will have their exact coordinates value as temperature load on them. For beam elements with properties variation taking place through the section, a section-wise FT is used. ANSYS provides a specific way to express linear temperature variation through the beam section.

Stepped variation of properties through the model can be modeled using element-wise temperature assignment, i.e. loading each element, or group of elements, by temperature having value equals to some reference coordinate of those elements, which is typically their center. The integration points will have the same temperature assigned to the element they lay within. Again, the stepped variation through sections follows the same logic. Each layer is loaded by temperature rise equals to the center coordinate value of that layer/group of layers. Note that continuous variation can be approximated using element/layer-wise temperature assignment but with numerous enough elements/layers in the direction of variation.

The first step in the FT technique is to create the temperature-properties curves. Temperature in this curve must represent the coordinates in the variation direction.

To disable the fictive thermal load from introducing strains and stresses to the part, reference temperature, thermal expansion coefficient, and thermal conductivity are all set to zero. The second step is to assign temperature rise through the model in a way that each node/element gets a temperature rise equals to its coordinate in the direction of properties variation. This is achieved by a simple loop through all nodes/elements. Five example cases are presented here. The first two examples are for FGM beam with stepped and continuous properties variation through the length direction. The second and third are FGM beams with stepped and continuous variation through the depth direction, modeled using 3D solid and 2D plane elements. The same latter case but modeled using line beam element is lastly presented.

Program 4 shows the APDL code that implements the element wise FT technique in modeling the first example case of stepped variation through the length of an FGM beam. The properties variation follows the function defined in the macro EX-FUNCTION provided in the macro library Program 13. Note that the same code is applicable to 3D solid, 2D plane, line beam elements.

Program 4- Modeling 3D-, 2D-, and Beam- FGM-X-S using FT

```
*ULIB,'MAIN_LIB','MACLIB',' ' ! IDENTIFIES MACRO LIBRARY
*USE,INITIATION
*USE,INPUTDATA
MODEL = 2  ! 1:LINE BEAM, 2:2D PLANE, 3:3D SOLID MODELS
BC = 1     ! 1:CLAMPED, 2:CANTILEVER, 3:SIMPLY SUPPORTED
*USE,GEOM_MESH
*USE,BC_LOAD
!=================================================   ||
!     FICTIVE THERMAL LOAD (FT) TECHNIQUE             ||
!    IMPLEMENTATION IN MODELING FGM-X-S               ||
!-------------- (STEP 1) ---  RELATES TEMP., E, & X    ||
*DO,XI,0,L,L/99              !                         ||
*USE,EX_FUNCTION, XI         !                         ||
MPTEMP,,XI                   !                         ||
MPDATA,EX,1,,EX              !                         ||
MPDATA,PRXY,1,,NU            !                         ||
*ENDDO                       !                         ||
!-----------------------------                         ||
!------------------- DISABLES THERMAL STRAINS          ||
TREF, 0                      !                         ||
MP, ALPX, 1, 0               !                         ||
MP, KXX, 1, 0                !                         ||
!-------------------                                   ||
!---------------- (STEP 2) ---ASSIGNS TEMP.= XC TO     ||
*GET,LASTE,ELEM,,NUM,MAX     ! EACH WHOLE ELEMENT II   ||
*DO,II,1,LASTE               !                         ||
IEXIS = ESEL(II)             !                         ||
*IF,IEXIS,EQ,1,THEN          !                         ||
XC = CENTRX(II)              !                         ||
BFE,II,TEMP,1,XC             !                         ||
*ENDIF                       !                         ||
*ENDDO                       !                         ||
!-----------------------------                         ||
!=================================================   ||
*USE,SOLVE_PLOT
*ULIB       !UN-DECLARE MACRO LIBRARY
```

Modeling the continuous variation through the length using FT is achievable by implementing the same code in Program 4 except that the fictive temperature is assigned on nodes not elements. In particular, the difference between the two cases is in Step 2, which is shown below in Program 5 for the case of node wise FT that models FGM-X-C. Note that the rest of the program is identical to that in Program 4.

Program 5- Step 2 In Modeling 3D-, 2D-, and Beam- FGM-X-C using FT

```
!----------------     (STEP 2) ---  ASSIGNS TEMP.= XN   ||
*GET,LASTN,NODE,,NUM,MAX        !    TO EACH NODE II    ||
*DO,II,1,LASTN                  !                       ||
IEXIS = NSEL(II)                !                       ||
*IF,IEXIS,EQ,1,THEN             !                       ||
XN = NX(II)                     !                       ||
BF,II,TEMP,XN                   !                       ||
*ENDIF                          !                       ||
*ENDDO                          !                       ||
!-----------------------------                          ||
```

Next case to consider is modeling of continuous variation through the depth of an FGM beam using node wise FT technique. An APDL program for this case is shown in Program 6. Properties variation follows the function defined in the macro EZ-FUNCTION provided in the macro library Program 13. This code is applicable only to models of 3D solid and 2D plane elements since line beam element have no geometry nodes in its depth direction. In the second step, fictive temperature could be applied on each node through a simple iteration similar to Program 5 but in the Z direction, however, an alternative way is to use tables. Here, a table is defined, using *DIM command, in a way that the Z coordinate of a given node is returned. In that sense, this table is basically a cloning function to be used in the assignment of fictive temperature to all nodes in one step. Each node will have its Z coordinate value assigned as temperature body load. Using such table make it possible to use an alternate way in node wise assignment of the fictive temperature. In addition to the direct way of node assignment using BF command, the element wise command BFE when used with table can provide the same result of continuous variation.

Program 6- Modeling 3D- and 2D- FGM-Z-C using FT

```
*ULIB,'MAIN_LIB','MACLIB',' ' ! IDENTIFIES MACRO LIBRARY
*USE,INITIATION
*USE,INPUTDATA
*USE,SYMBOLIC_INTEGRATION  ! ONLY C IS NEEDED
MODEL = 2  ! 2:2D PLANE, 3:3D SOLID MODELS
BC = 1     ! 1:CLAMPED, 2:CANTILEVER, 3:SIMPLY SUPPORTED
*USE,GEOM_MESH
*USE,BC_LOAD
!=====================================================||
!       FICTIVE THERMAL LOAD (FT) TECHNIQUE           ||
!        IMPLEMENTATION IN MODELING FGM-Z-C           ||
!-------------- (STEP 1) ---   RELATES TEMP., E, & Z ||
*DO,ZI,-H/2,H/2,H/99          !                       ||
*USE,EZ_FUNCTION, ZI          !                       ||
MPTEMP,,ZI                    !                       ||
MPDATA,EX,1,,EZ               !                       ||
MPDATA,PRXY,1,,NU             !                       ||
*ENDDO                        !                       ||
!------------------------------                       ||
!------------------- DISABLES THERMAL STRAINS         ||
TREF, 0                       !                       ||
MP, ALPX, 1, 0                !                       ||
MP, KXX, 1, 0                 !                       ||
!-------------------                                  ||
!---------------- (STEP 2) ---   ASSIGNS TEMP.= ZI    ||
*DIM,ZTEMP,TABLE,2,,,Z,,,11   !    TO EACH NODE I     ||
ZTEMP(1) = -H/2, H/2          !                       ||
ZTEMP(1,0) = -H/2, H/2        !                       ||
!-------------------------    !                       ||
BF,ALL,TEMP,%ZTEMP%       !    !                       ||
!! OR ALTERNATIVELY:      !    !                       ||
! BFE,ALL,TEMP,1,%ZTEMP%  !    !                       ||
!-------------------------    !                       ||
!------------------------------                       ||
!=====================================================||
*USE,SOLVE_PLOT
*ULIB       !UN-DECLARE MACRO LIBRARY
```

Modeling of the stepped properties variation through the depth can be achieved by element wise fictive temperature assignment, just as in Program 4. However, it would be wiser not to iterate over each element one-by-one, instead, all elements in the same layer could be selected and then get fictive temperature assigned to the whole group at once. ANSYS APDL does not provide the capability of selecting elements by location, therefore nodes in the targeted layer are selected by location then elements attached to those nodes are selected. This layer wise temperature assignment is shown in Step 2 in Program 7, which presents the modeling 3D- and 2D- FGM-Z-S. Note that this program and the one in Program 6 are also different in the quadrature rule. In FGM-Z-C modeling shown in Program 6, the symbolic integration is implemented, while in FGM-Z-S modeling, shown in Program 7, the trapezoidal quadrature rule is implemented.

Program 7- Modeling 3D- and 2D- FGM-Z-S using FT

```
*ULIB,'MAIN_LIB','MACLIB',' ' ! IDENTIFIES MACRO LIBRARY
*USE,INITIATION
*USE,INPUTDATA
*USE,TRAPEZOID_QUADRATURE  ! ONLY C IS NEEDED
MODEL = 2  ! 2:2D PLANE, 3:3D SOLID MODELS
BC = 1     ! 1:CLAMPED, 2:CANTILEVER, 3:SIMPLY SUPPORTED
*USE,GEOM_MESH
*USE,BC_LOAD
!=====================================================||
!       FICTIVE THERMAL LOAD (FT) TECHNIQUE           ||
!        IMPLEMENTATION IN MODELING FGM-Z-C            ||
!-------------- (STEP 1) ---   RELATES TEMP., E, & Z  ||
*DO,ZI,-H/2,H/2,H/99           !                       ||
*USE,EZ_FUNCTION, ZI           !                       ||
MPTEMP,,ZI                     !                       ||
MPDATA,EX,1,,EZ                !                       ||
MPDATA,PRXY,1,,NU              !                       ||
*ENDDO                         !                       ||
!-----------------------------                         ||
!------------------- DISABLES THERMAL STRAINS          ||
TREF, 0                        !                       ||
MP, ALPX, 1, 0                 !                       ||
MP, KXX, 1, 0                  !                       ||
!-------------------                                   ||
!---------------- (STEP 2) ---------- ASSIGNS TEMP     ||
*DO,LAYERi,1,NH                      !  =ZCENTER  i  TO  ||
BOTTOMNODES = -H/2 +(LAYERi-1)*H/NH  !    ALL ELELEMNTS ||
TOPNODES = BOTTOMNODES + H/NH        !   IN LAYER i     ||
ZCENTERi = (BOTTOMNODES+TOPNODES)/2  !                  ||
NSEL,S,LOC,Z,BOTTOMNODES,TOPNODES    !                  ||
ESLN,S,1                             !                  ||
BFE,ALL,TEMP,1,ZCENTERi              !                  ||
ALLSEL,ALL                           !                  ||
*ENDDO                               !                  ||
!-----------------------------------                   ||
!=====================================================||
*USE,SOLVE_PLOT
*ULIB       !UN-DECLARE MACRO LIBRARY
```

The last case here is the modeling of continuous variation of properties through the depth of line beam element. This case has a special treatment that is shown in Program 8. APDL offers special option in **BFE** command to directly express temperature variation through the cross-section (*ANSYS Mechanical Apdl Element Reference*, 2016 Chapter I. Element Library/Beam189). BFE command needs three values. The first, named as TI00, is the temperature on at the X axis of the section, i.e., at Y=0 and Z=0. The second needed value, named as TI10, is the temperature at a unit distance from the X axis in the Y direction. The last one, named as TI01, is the temperature at a unit distance from the X axis in the Z direction. Setting TI00 = TI10 = 0 and TI01 = 1 makes temperature clone the Z coordinate through the depth. Note that there is no need to iterate through elements in this particular case since all of the elements share the same properties variation through section.

Program 8- Modeling Beam- FGM-Z-C using FT

```
*ULIB,'MAIN_LIB','MACLIB',' ' ! IDENTIFIES MACRO LIBRARY
*USE,INITIATION
*USE,INPUTDATA
*USE,SYMBOLIC_INTEGRATION  ! ONLY C IS NEEDED
MODEL = 1  ! 1:LINE BEAM
BC = 1     ! 1:CLAMPED, 2:CANTILEVER, 3:SIMPLY SUPPORTED
*USE,GEOM_MESH
*USE,BC_LOAD
!=====================================================||
!      FICTIVE THERMAL LOAD (FT) TECHNIQUE            ||
!       IMPLEMENTATION IN MODELING FGM-Z-C BEAM       ||
!-------------- (STEP 1) ---  RELATES TEMP., E, & Z   ||
*DO,ZI,-H/2,H/2,H/99          !                       ||
*USE,EZ_FUNCTION, ZI          !                       ||
MPTEMP,,ZI                    !                       ||
MPDATA,EX,1,,EZ               !                       ||
MPDATA,PRXY,1,,NU             !                       ||
*ENDDO                        !                       ||
!-----------------------------                        ||
!------------------- DISABLES THERMAL STRAINS         ||
TREF, 0             !                                 ||
MP, ALPX, 1, 0      !                                 ||
MP, KXX, 1, 0       !                                 ||
!-------------------                                  ||
!---------- (STEP 2) -------- DEFINES TEMP.=Z         ||
TI00 = 0                    ! TEMP. AT (Y = 0, Z = 0) ||
TI10 = 0                    ! TEMP. AT (Y = 1, Z = 0) ||
TI01 = 1                    ! TEMP. AT (Y = 0, Z = 1) ||
BFE,ALL,TEMP,1,TI00,TI10,TI01 !                       ||
!------------------------------                       ||
!=====================================================||
*USE,SOLVE_PLOT
*ULIB       !UN-DECLARE MACRO LIBRARY
```

4.3. Element/Layer-Wise Material Assignment (EW)

This technique models stepped variation of properties through FGM part by assigning a new material-model to each element or group of elements. Properties

of each material-model are dependent on location of the targeted elements. EW technique is also applicable through sections of the sectional elements, e.g., layers of shell, and cells of beam elements. Continuous variation of properties can be approximated using EW technique by increasing the number of elements/layers/cells in the direction of variation (Hassan & Kurgan, 2020; Hassan Ahmed Hassan & Kurgan, 2020). EW technique consists of iterating through elements, layers, or cells, creating a new material-model based on location of the current element/layer/cell and assigned to it. An example APDL code is given below for an FGM beam having stepped varying elasticity through its length. It is wiser to create new model for groups of elements instead of individual ones. Each group of elements, named "elements component" in ANSYS, would contain all elements that share the same coordinate of interest. This would considerably reduce the number of iterations, size of the material-model files, and computation time. However, for the sake of clarity, the herein given Program 9 iterates over each single element and creates a new material-model for each element.

Program 9- Modeling 3D-, 2D-, and Beam- FGM-X-S using EW

```
*ULIB,'MAIN_LIB','MACLIB',' ' ! IDENTIFIES MACRO LIBRARY
USE,INITIATION
*USE,INPUTDATA
MODEL = 2  ! 1:LINE BEAM, 2:2D PLANE, 3:3D SOLID MODELS
BC = 1     ! 1:CLAMPED, 2:CANTILEVER, 3:SIMPLY SUPPORTED
*USE,GEOM_MESH
*USE,BC_LOAD
!=====================================================||
!  ELEMENT WISE MATERIAL ASSIGNMENT (EW) TECHNIQUE    ||
!        IMPLEMENTATION IN MODELING FGM-X-S            ||
*GET,FIRSTE,ELEM,,NUM,MIN                            !||
*GET,LASTE,ELEM,,NUM,MAX                             !||
*DO,II,FIRSTE,LASTE                                  !||
!------------------ LOOPS THROUGH ALL ELEMENTS ---!   ||
IEXIS = ESEL(II)          !                        !   ||
*IF,IEXIS,EQ,1,THEN       !                        !   ||
XI = CENTRX(II)           !                        !   ||
*USE,EX_FUNCTION, XI      !                        !   ||
!------------------                                 !   ||
MP,EX,II,EX       ! CREATES NEW MATERIAL MODEL i   !   ||
MP,PRXY,II,NU     !   BASED ON LOCATION Xi         !   ||
MPCHG,II,II,      ! ASSIGNS IT TO ELEMENT i        !   ||
!------------------                                 !   ||
*ENDIF                                             !   ||
!-------------------------------------------------!    ||
*ENDDO                                                !||
!=====================================================
*USE,SOLVE_PLOT
*ULIB       !UN-DECLARE MACRO LIBRARY
```

4.4. Pre-Integrated Cross-Sections

The hereinabove discussed FGM modeling techniques so far share the main theme of controlling the material properties through the model based on a given function. Then when the analysis runs, the system inquires these properties at each integration point in order to calculate the stiffness matrices. For elements with sections, i.e., sectional elements such as beams and shells, modeling and computation efforts can be considerably reduced by having the stiffness matrix

or inertia properties of the section pre-calculated. However, one downside of using pre-integrated sections is the inability to examine the through-section and inter-lamina resulting stresses and strains. The stiffness matrix as well as the inertia properties are both integrals through the section. Analytical formulae of the required integrals as well as the implementation of the numerical 5-point Gaussian-Legendre and trapezoidal quadrature rules are given in the macro library Program 13 as macros named SYMBOLIC-INTEGRATION, GAUSSIAN-QUADRATURE, and TRAPEZOID-QUADRATURE respectively. The analytical formulae are obtained using the Python program in Program 1.

This section presents the implementation of the two approaches on the bending problem of FGM beam having elasticity varying through its thickness by a simple power rule. The first way is to provide the system with pre-integrated cross-section stiffness matrix, by defining the section as composite (COMB). The second is to provide the system with modified pre-integrated cross-section inertia properties and modified material properties, by defining the section as arbitrary (ASEC).

4.4.1. Pre-Integrated Cross-Section Stiffness Matrix

Here, FGM beam is modeled as composite beam with pre-integrated cross-section stiffness matrix. The behavior of beam elements is governed by the generalized stress / generalized strain relationship of the form:

$$\begin{bmatrix} N_0 \\ M_1 \\ M_2 \\ \tau \\ S_1 \\ S_2 \end{bmatrix} = \boldsymbol{S} \begin{bmatrix} \varepsilon \\ \boldsymbol{\kappa_1} \\ \boldsymbol{\kappa_2} \\ \chi \\ \boldsymbol{\gamma_1} \\ \boldsymbol{\gamma_2} \end{bmatrix} \tag{6}$$

S is the cross-section stiffness matrix; (N_o, ε) are the axial force and strain, respectively; $(M_1, S_1, \boldsymbol{\kappa_1}, \boldsymbol{\gamma_1})$ are the bending moment, transverse shear force, curvature, and transverse shear strain, respectively, all in XZ plane. $(M_2, S_2, \boldsymbol{\kappa_2}, \boldsymbol{\gamma_2})$ are the corresponding terms in XY plane; τ is the sectional twisting torque; and χ is the twist of the cross section. The general stiffness matrix of beam element considering offsets in both width and thickness directions is given in Eq.(7) (*ANSYS Mechanical Apdl Structural Analysis Guide*, 2016 Chapter 12.5.3).

$$S = B \int_{-H/2}^{H/2} E_{(Y,Z)} \hat{S} dZ \tag{7}$$

$\hat{S}$ is a symmetrical matrix given as follows.

$$\hat{S} = \begin{bmatrix} 1 & Z_c & Y_c & 0 & 0 & 0 \\ & {Z_c}^2 & Z_c Y_c & 0 & 0 & 0 \\ & & {Y_c}^2 & 0 & 0 & 0 \\ & & & \kappa^*({Y_s}^2 + {Z_s}^2) & -Y_s\kappa^* & -Z_s\kappa^* \\ & & & & \kappa^* & 0 \\ & & & & & \kappa^* \end{bmatrix} \quad (8)$$

$\boldsymbol{\kappa^* = \frac{\kappa}{2(1+\nu)}}$, *and* $\boldsymbol{\kappa}$ is the shear correction factor. Z_C and Y_C are the offsets in the thickness and width directions between the centroid and the reference planes, respectively. Note that Z_C is a shorthand for $(Z - C)$. Z_S and Y_S are the distances between the centroid and the shear center. Since the considered beam has rectangular section, then Z_S and Y_S are both zeros. In the case of the example in hand of FGM beam having properties variation through its thickness and under lateral load in the Z direction, there is no offset between the centroid and the reference plane in the Y direction, i.e., $Y_c = 0$, and there is no bending in the XY plane, and no torsion. Therefore $(M_2, \tau, S_2, \kappa_2, \chi, \gamma_2)$ are all zeros. Since the neutral plane is considered as the reference, the lateral and axial deformations are totally uncoupled. Therefore, for the problem in hand, N_0 and ε are also irrelevant to this analysis.

The remaining relevant quantities are $(M_1, S_1, \kappa_1, \gamma_1)$, which are on the second and fifth rows of the matrix *S*. Only the corresponding rows of the stiffness matrix need to be accurate, others can have any arbitrary values and will not affect the results. Typically, all irrelevant elements of the stiffness matrix are set to zero. The resulting simplified stiffness matrix is shown in Eq.(9). Note that if the beam was under axial load through its neutral plane, i.e., no moment generated, then the only relevant value in the stiffness matrix is the first one. The point is that, for different loading configurations, different simplifications should be implemented.

$$S = B \int_{\frac{-H}{2}}^{\frac{H}{2}} \begin{bmatrix} 0 & 0 & 0 & 0 & 0 & 0 \\ 0 & (Z-C)^2 E_{(Z)} & 0 & 0 & 0 & 0 \\ 0 & 0 & 0 & 0 & 0 & 0 \\ 0 & 0 & 0 & 0 & 0 & 0 \\ 0 & 0 & 0 & 0 & \frac{\kappa E_{(Z)}}{2(1+\nu)} & 0 \\ 0 & 0 & 0 & 0 & 0 & 0 \end{bmatrix} dZ \quad (9)$$

In APDL, a beam element declared as composite with pre-integrated stiffness matrix by using the **COMB** option in defining the beam section type, then filling the stiffness matrix through the command **CBMX**. By using CBMX one can model both the continuous and discrete variation through the beam section. The only difference between modeling those two cases is the integration scheme. For the continuous variation exact analytical integration or 5-points Gaussian-Legendre quadrature rule can be implemented, while for the discrete variation case a simple trapezoidal quadrature rule reveals the exact integration. The following APDL program shown in Program 10 presents an example of using CMBX in modeling the continuous properties variation through the depth of an FGM part, i.e., Beam- FGM-Z-C.

Program 10- Modeling Beam- FGM-Z-C using CMBX

```
*ULIB,'MAIN_LIB','MACLIB',' ' ! IDENTIFIES MACRO LIBRARY
*USE,INITIATION
*USE,INPUTDATA
MODEL = 1  ! 1:LINE BEAM
BC = 1     ! 1:CLAMPED, 2:CANTILEVER, 3:SIMPLY SUPPORTED
*USE,GEOM_MESH
*USE,BC_LOAD
!--- CALCULATES THE REQUIRED INTEGRATIONS: IE, IZN2E---
*USE,SYMBOLIC_INTEGRATION !  OR TRAPEZOID_QUADRATURE  |
!-----------------------------------------------------
!=====================================================
! PRE-INTEGRATED CROSS-SECTION STIFFNESS MATRIX      ! ||
!  TECHNIQUE IMPLEMENTATION IN MODELING FGM-Z-C BEAM ! ||
K = 5/6 ! SHEAR CORRECTION FACTOR                    ! ||
SECTYPE,1,COMB,MATRIX                                ! ||
CBMX,1,  0,      0,  0,  0,                0,  0     ! ||
CBMX,2,     B*IZN2E, 0,  0,                0,  0     ! ||
CBMX,3,              0,  0,                0,  0     ! ||
CBMX,4,                  0,                0,  0     ! ||
CBMX,5,                    K*B*IE/(2*(1+NU)),  0     ! ||
CBMX,6,                                      0        ! ||
! =====================================================
*USE,SOLVE_PLOT
*ULIB       !UN-DECLARE MACRO LIBRARY
```

4.4.2. Modified Pre-Integrated Cross-Section Inertia Properties

The cross-section inertia properties (e.g., area, moments of inertia, centroid, etc.) of a beam's section are typically calculated from the user provided basic sectional geometry data, i.e. shape and dimensions. However, ANSYS provides an additional option to directly input the inertia properties as an arbitrary beam section (**ASEC**), instead of the basic geometry data. Properties to be provided by the user in order to define an arbitrary beam section are the area *(A)*, moment of inertia about the Y and Z axes *(I_{yy}, I_{zz})*, product of inertia (*I_{yz})*, warping constant *(lw)*, torsional constant *(J)*, Y and Z coordinates of centroid *(CG_y, CG_z)*, Y and Z coordinates of shear center *(SH_y, SH_z)*, and maximum thickness along Z and Y axes, *(TK_Z, TK_y)*.

The trick to modeling FGM beam using ASEC is to transfer the varying stiffness terms from the material definition to the geometry properties matrix. For the example in hand of FGM beam having rectangular cross-section and under lateral loading in Z direction, i.e., bending is only in the plane XZ, the only relevant terms are *A*, I_{yy}, TK_Z, and TK_y. The latter two are the depth and width, i.e., $TK_z = H$, $TK_y = B$. I_{zz} and *J* can have any arbitrary non-zero positive values and will not affect the results. Wrapping is neglected; so is assumed zero. For the rectangular cross-section, the centroid and shear center both lay on the geometric center of the section, i.e., *(CG_y, CG_z, SH_y, SH_z)* are all zeros. As mentioned above, the geometry terms *A* and I_{yy} are replaced by modified versions, A^S and I_{zz}^{s}, which include the stiffness terms and are given as follows.

$$A^S = kB\int_{\frac{-H}{2}}^{\frac{H}{2}} E_{(Z)}dZ, \qquad I_{yy}^{s} = B\int_{\frac{-H}{2}}^{\frac{H}{2}} (Z-C)^2 E_{(Z)}dZ \tag{10}$$

The material definition must then exclude the varying stiffness properties, which in this case is the elasticity, i.e., set elasticity constant to unity in the material model. Similar to CBMX, according to the implemented quadrature rule ASEC can model both the continuous and discrete variation through the beam section. The following APDL program shown in Program 11 presents an example of using ASEC in modeling the discrete properties variation through the depth of an FGM part, i.e., Beam- FGM-Z-S.

Program 11- Modeling Beam- FGM-Z-S using ASEC

```
*ULIB,'MAIN_LIB','MACLIB',' ' ! IDENTIFIES MACRO LIBRARY
*USE,INITIATION
*USE,INPUTDATA
MODEL = 1  ! 1:LINE BEAM
BC = 1     ! 1:CLAMPED, 2:CANTILEVER, 3:SIMPLY SUPPORTED
*USE,GEOM_MESH
*USE,BC_LOAD
!--- CALCULATES THE REQUIRED INTEGRATIONS: IE, IZN2E---
*USE,TRAPEZOID_QUADRATURE !  OR SYMBOLIC_INTEGRATION  |
!-----------------------------------------------------
!=====================================================
! PRE-INTEGRATED CROSS-SECTION INERTIA PROPERTIES    ! ||
!  TECHNIQUE IMPLEMENTATION IN MODELING FGM-Z-S BEAM ! ||
K    = 5/6  ! SHEAR CORRECTION FACTOR                ! ||
IR   = 1 ! ARBITRARY NON-ZERO VALUE FOR IRRELEVANTS  ! ||
AREA = K*IE*B                                        ! ||
IYY  = IZN2E*B                                       ! ||
IYZ  = 0                                             ! ||
IZZ  = IR                                            ! ||
IW   = 0                                             ! ||
J    = IR                                            ! ||
CGY  = 0                                             ! ||
CGZ  = 0                                             ! ||
SHY  = 0                                             ! ||
SHZ  = 0                                             ! ||
TKZ  = H                                             ! ||
TKY  = B                                             ! ||
SECTYPE,1, BEAM, ASEC                                ! ||
SECDATA,AREA,IYY,IYZ,IZZ,IW,J,CGY,CGZ,SHY,SHZ,TKZ,TKY!||
! ====================================================
!============= MODIFIED MATERIAL PROPERTIES =====
MP,EX,1,1 ! MODIFIED YOUNG'S MODULUS          !||
MP,PRXY,1,NU                                  !||
!=================================================
*USE,SOLVE_PLOT
*ULIB       !UN-DECLARE MACRO LIBRARY
```

4.5. Advanced Techniques: User Programmable Features (UPF)

Under this category fall the techniques that require recompiling the ANSYS executable and/or linking custom libraries to it. ANSYS provides such capabilities through User-Programmable Features (UPF) by which users can tailor their own material behavior, element definition, load types, and optimization algorithms (*ANSYS Documentation*, 2016). Detailed illustration of the advanced techniques in ANSYS APDL is available in (Barbero, 2007).

Implementation of these advanced techniques requires strong programming skills such as linking libraries and compiling a new version of the ANSYS executable. Steps to do so are different for different operating systems. UPS normally written in FORTRAN; however other programming languages can be used but then FORTRAN interface has to be provided. Benefiting from UPF is only available for certain license class of ANSYS, namely the ANSYS Mechanical Enterprise family of products (*ANSYS Documentation*, 2016). Due to the mentioned difficulties, only a brief on those techniques is presented below.

The first advanced method proposed to model FGM is to craft a new element that obeys the desired governing equations and kinetics. This approach is very demanding in terms of programming skills and detailed knowledge of element's formulation. User-defined elements are created using **UserElem.F** subroutine provided by ANSYS. Another advanced method is to use standard elements but with modified material constitutive model using the subroutine **usermat.F** in which user can fully control the material definition. By using this ANSYS provided routine, user can define how material properties change among elements and through the section of each element.

The simplest alternative among the advanced techniques is to use **user_tbelastic.F** subroutine, which specifically controls the elasticity properties, i.e. the stiffness Matrix, at each integration point of the model. user_tbelastic.F subroutine, provided by ANSYS, grants an access to coordinates and temperature of each integration point. The stiffness constants can be formulated as functions of these inputs and directly returned as an output of the subroutine. So, it is easy to express the temperature dependency of properties coupled with the spatial variation. A modified version of the user_tbelastic.F imposes the elasticity variation through the length of line model is provided in Program 12. As mentioned above, a new ANSYS executable has to be compiled linked to this subroutine in order to use it. If not this difficulty, this method would be an easy and direct way to impose the properties variation through an FGM in ANSYS.

Program 12- Modified user_tbelastic.F

```
*DECK,USER_TBELASTIC   USERDISTRIB   PARALLEL        GAL
    SUBROUTINE USER_TBELASTIC(EN, MI, XYZ, TI, NP, PROP)
C   ---------------
C - INPUTS: EN: ELEMENT NUMBER
C           MI: MATERIAL ID
C           TI: TEMPERATURE AT THE INTEGRATION POINT
C          XYZ: X,Y,Z COORDS OF THE INTEGRATION POINT
C -OUTPUTS: NP: NUMBER OF CONSTANTS
C               NP = 2 FOR ISOTROPIC ELASTICITY
C         PROP: VALUES OF MATERIAL ELASTIC CONSTANTS
C               PROP(1):  E: ELASTICITY (YOUNG) CONST.
C               PROP(2): NU: POISSON'S RATIO
C -CONSTS:   L: BEAM LENGTH
C           EM: ELASTICITY CONSTANT AT X=0
C         BETA: EXPONENTIAL INDEX (BETA)
C   ----------------------
C   THIS SUBROUTINE ACHIEVES THE FOLLOWING ELASTICITY
C   VARIATION THROUGH THE LENGTH:E(X) = EM*EXP(BETA*X/L)
C   WHERE (BETA, L, EM, NU) ARE ALL GIVEN
#INCLUDE "IMPCOM.INC"
#INCLUDE "FILEUSR.INC"
      INTEGER          MI, EN, NP
      DOUBLE PRECISION TI, NU, EM, L, BETA
      DOUBLE PRECISION PROP(NP), XYZ(5)
      EM      = 70000.0D0
      L       =   300.0D0
      BETA    =     2.0D0
      NU      =     0.3D0
C XYZ(1) IS THE X COORDS OF THE CURRENT INTEG. POINT
      PROP(2) = NU
      PROP(1) = EM*EXP(BETA*XYZ(1)/L)
      RETURN
      END
C=======================================================
```

5. Implementation

This section shows a set of comparisons between the presented modeling techniques of FGM. Various boundary conditions are considered, namely, fully clamped, cantilever, and simply supported FGM beam under uniformly distributed load. The dimensions considered in these analyses are shown in Table 1.

Table 1. Dimensions and Material Properties

L (mm)	*H (mm)*	*B (mm)*	*v*	$E_c (N/mm^2)$	$E_m (N/mm^2)$
600	30	15	0.3	$380 \cdot 10^3$	$70 \cdot 10^3$

The first case is the FGM having its properties smoothly varying through its depth, i.e. FGM-Z-C, following the simple power law of Eq.(1) with a power index $N = 2$. Figure 8 compares the various techniques-models by comparing results of each to those of FT technique implemented on 3D model, i.e. FT-3D results. The compared result is the lateral deflection *UZ* over the length as recorded at the neutral plane.

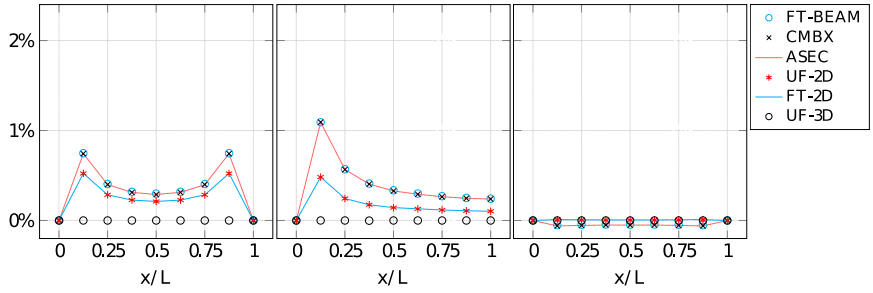

(a) Clamped (b) Cantilever (c) Simply supported

Figure 8- Percentage difference in deflection (as compared to FT-3D solution) of various modeling techniques of FGM-Z-C with N= 2 under various boundary conditions

It is obvious the perfect agreement between results of the various modeling techniques of FGM implemented on the 3D models, namely, the FT-3D and the UF-3D. Complete agreement is also observable between UF-2D and FT-2D, and also between the three techniques applied on section of the beam element, namely, FT-BEAM, ASEC, and CMBX. This simply tells the equivalence of the modeling techniques applied on each different model. The 2D models are found

closer to the 3D ones compared to the beam models. It is also clear that the 3D model is the stiffest, then the 2D model, while the beam model comes last. In other words, the 2D and beam models overestimate the deflection, compared to the 3D model. The difference between various models depends on the boundary conditions. For the clamped and cantilever cases, it is observable that the percentage difference is highest near the clamped edges. Overall, various models show higher percentage differences in the cases of clamped and cantilever cases, compared to the almost vanishing difference in the simply supported case.

The differences in the presented results come from the models rather than the techniques of modeling the properties variation. Figure 9 shows the same comparison but for homogeneous part of the same dimensions, load, and boundary conditions. Same level of differences between the various models is observable when compared to the results of the FGM part shown in Figure 8.

It is also worth pointing out that if the Poisson's ratio v is set to zero and the shear correction factor k is set to one, then the 3D-, 2D-, and Beam- models must give the same exact results. Setting v and k as so makes the mechanics of the beam obey the classical Euler–Bernoulli beam theory.

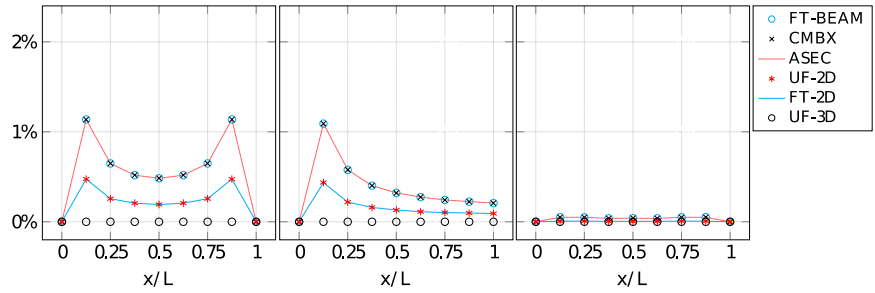

(a) Clamped (b) Cantilever (c) Simply supported

Figure 9. Percentage difference in deflection (as compared to FT-3D solution) of various modeling techniques of homogeneous beam having N= 0 and β= 0 under various boundary conditions

The level of differences between the various models is expected to decrease as the slenderness increases. Slenderness is the ratio between length and thickness of a part. As the slenderness ratio increases, better agreement in results should be obtained. To validate this expectation, clamped FGM beams with different slenderness ratios are examined. Three different beams having L

= 300, 600, 900mm but the same cross-section, load, and boundary conditions. Results are shown in Figure 10.

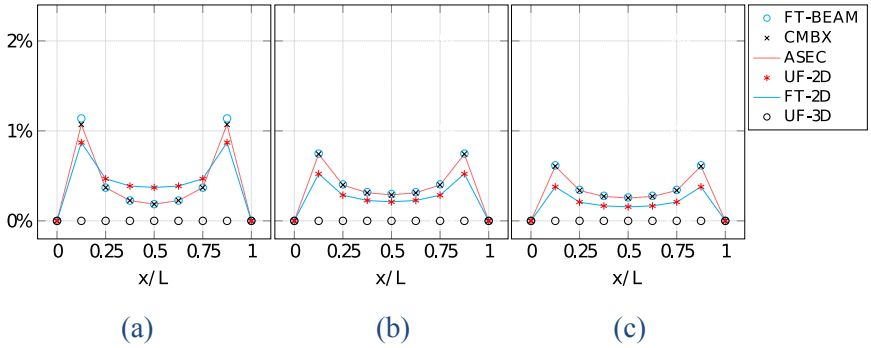

(a) *L/H = 300/30* (b) *L/H = 600/30* (c) *L/H = 900/30*

Figure 10. Comparison between differences in deflection of clamped FGM-Z-C with N = 2 with different slenderness ratios

Next, the variation of properties is set to be continuous in the length direction following the exponential function that is shown in Eq.(2). The exponent index is set to be $\beta = 2$. The same comparisons as the previous case are conducted and shown in Figure 11. EW and FT techniques are implemented on both 2D and 3D models. Again, results show the equivalence of various methods applied on each different model. The various boundary conditions present the same pattern as in the previous case. That is, high difference occurs near the clamped edges, and the low difference between various methods is observed in the simply supported case, compared to the clamped and cantilever ones. The levels of percentage difference between the 3D and 2D models are comparable to those in Figure 11 of the previous case of FGM having properties variation in the thickness direction.

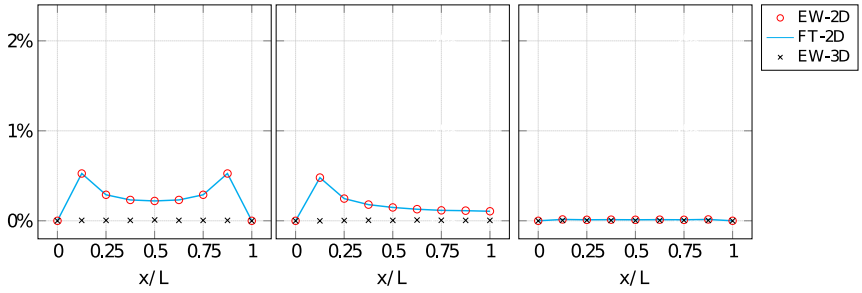

(a) Clamped (b) Cantilever (c) Simply supported

Figure 11. Percentage difference in deflection (as compared to FT-3D solution) of various modeling techniques of FGM-X-C with $\beta = 2$ u under various boundary conditions

The third case is similar to the second one but with stepped instead of the continuous properties' variation through its length. Here FT and EW techniques are implemented. 3D, 2D, and beam models are considered. Percentage difference between the various techniques-models is shown in Figure 12. One thing to be observed is that the higher level of difference in results between the beam models and the 2D- and 3D- models compared to the previous cases.

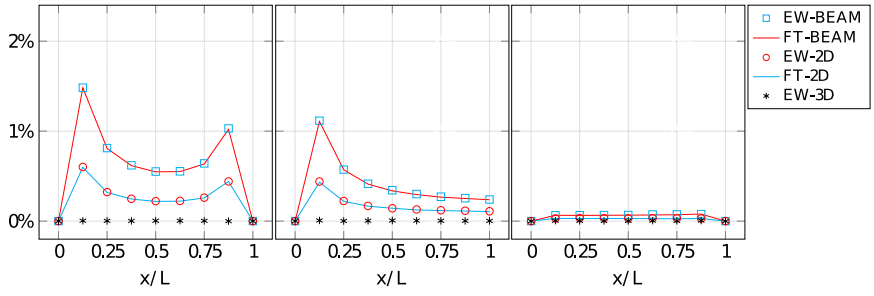

(a) Clamped (b) Cantilever (c) Simply supported

Figure 12. Percentage difference in deflection (as compared to FT-3D solution) of various modeling techniques of FGM-X-S with $\beta = 2$ u under various boundary conditions

6. Conclusion

This work explores and compares the various techniques to model the variation of properties through a functionally graded material (FGM) in ANSYS APDL. However, the techniques presented here should be applicable in any other FEM package. APDL codes are provided for the various considered cases.

Four methods are presented, namely, the user-defined field variable (UF), the fictive thermal load (FT), the element/layer-wise material modeling (EW), the pre-integrated cross-section properties, and lastly, some advanced methods are briefly mentioned. As to give a practical example, a slender FGM part is selected to apply those methods on. Part geometry, loading and boundary conditions are set in a way that allows three different models to be used, namely, 3D solid, 2D plane, and beam model.

Using a user-defined field variable (UF) facilitates the modeling of continuous variation of properties though FGM part. Simpler than UF is to use an already defined field variable, namely, temperature. In such case, temperature is made fictive by limiting its effects only on the material properties by suppressing the resulting thermal strain. Presented UF method can model the properties variation through geometry nodes of the FGM part. Downside of using such fictive temperature (FT) in modeling properties variation is that it complicates the simulation if there was other temperature load in the problem. Using FT allows modeling of both continuous and discrete properties variation through the FGM part. FT can model the properties variation though geometry nodes/elements and/or section cells/layers. Another method to model the discrete variation is by assigning different material model to elements/layers according to their location. This method is referred as EW. In this method, a new material model is defined according to location of the targeted element/layer. EW models the properties variation through elements and layers of the FGM part. For the special case of using beam elements, pre-integrated section properties can be imposed with the variation of material properties. Two distinct cross-section properties can be modified in order to model the FGM. First is the stiffness of the cross-section. Alternatively, one can modify the inertia properties of the cross-section. Note that in this case material properties have to be modified as well. Using pre-integrated cross-section properties allows modeling of both continuous and discrete properties variation through the section of an FGM beam part. Lastly, a brief on other advanced methods is presented. Advanced methods include those require re-compiling of the ANSYS.exe executable. Those methods require extended programming skills as well as extended technical knowledge of finite element formulations and algorithms.

The implemented methods are found equivalent. In other words, it is found that the various methods express correctly the properties variation through the FGM part.

References

Akshaya, S. L., Prakash, A., & Bharati Raj, J. (2021). Applications of functionally graded materials in structural engineering—a review. In K. Dasgupta, T. K. Sudheesh, K. I. Praseeda, G. Unni Kartha, P. E. Kavitha, & S. Jawahar Saud (Eds.), *Proceedings of secon 2020* (pp. 553–566). Springer International Publishing. https://doi.org/10.1007/978-3-030-55115-5_51

ANSYS documentation. (2016). SAS IP, Inc.

ANSYS Mechanical APDL element reference. (2016). SAS IP, Inc.

ANSYS Mechanical APDL structural analysis guide. (2016). SAS IP, Inc.

Ashirbekob, A., Abilgaziyev, A., Kurokawa, S., & Ali, M. H. (2020). Modelling of functionally graded materials using thermal loads. *Journal of Engineering Science and Technology*, *15*(3), 1719–1730.

Barbero, E. J. (2007). *Finite element analysis of composite materials*. CRC press.

Hassan, A. H. A., & Keleş, İ. (2017). FGM modelling using dummy thermal loads. *Journal of Selcuk International Science and Technology*, *1*(10-16).

Hassan, A. H. A., & Kurgan, N. (2020). The relations between the various critical temperatures of thin fgm plates. *Journal of Applied and Computational Mechanics*, *6*(Special Issue), 1404–1419. https://doi.org/10.22055/jacm.2020.34697.2459

Hassan, A. H. A., Kurgan, N., & Can, N. (2022). The correct derivation of the buckling equations of the shear-deformable fgm plates for the extended antorovich method. *Meccanica*, 1–16. https://doi.org/10.1007/s11012-021-01441-0

Hassan Ahmed Hassan, A., & Kurgan, N. (2020). Bending analysis of thin fgm skew plate resting on winkler elastic foundation using multi-term extended kantorovich method. *Engineering Science and Technology, an International Journal*, *23*(4), 788–800. https://doi.org/10.1016/j.jestch.2020.03.009

Li, W., & Han, B. (2018). Research and application of functionally gradient materials. *IOP Conference Series: Materials Science and Engineering*, *394*, 022065. https://doi.org/0.1088/1757-899X/394/2/022065

Li, Y., Feng, Z., Hao, L., Huang, L., Xin, C., Wang, Y., Bilotti, E., Essa, K., Zhang, H., Li, Z., & others. (2020). A review on functionally graded materials and structures via additive manufacturing: From multi-scale design to versatile

functional properties. *Advanced Materials Technologies*, *5*(6), 1900981. https://doi.org/10.1002/admt.201900981

Loh, G. H., Pei, E., Harrison, D., & Monzón, M. D. (2018). An overview of functionally graded additive manufacturing. *Additive Manufacturing*, *23*, 34–44.

Martínez-Pañeda, E. (2019). On the finite element implementation of functionally graded materials. *Materials*, *12*(2), 287. http://dx.doi.org/10.3390/ma12020287

Meurer, A., Smith, C. P., Paprocki, M., Čertík, O., Kirpichev, S. B., Rocklin, M., Kumar, A., Ivanov, S., Moore, J. K., Singh, S., Rathnayake, T., Vig, S., Granger, B. E., Muller, R. P., Bonazzi, F., Gupta, H., Vats, S., Johansson, F., Pedregosa, F., … Scopatz, A. (2017). SymPy: Symbolic computing in python. *PeerJ Computer Science*, *3*, e103. https://doi.org/10.7717/peerj-cs.103

Parihar, R. S., Setti, S. G., & Sahu, R. K. (2018). Recent advances in the manufacturing processes of functionally graded materials: A review. *Science and Engineering of Composite Materials*, *25*(2), 309–336. https://doi.org/10.1515/secm-2015-0395

Prashant Singh, A., Tailor, A., Singh Tumarte, C., & Mishra, D. (2022). Crack growth simulation in a functionally graded material plate with uniformly distributed pores using extended finite element method. *Materials Today: Proceedings*. https://doi.org/10.1016/j.matpr.2022.02.123

Saleh, B., Jiang, J., Fathi, R., Al-hababi, T., Xu, Q., Wang, L., Song, D., & Ma, A. (2020). 30 years of functionally graded materials: An overview of manufacturing methods, applications and future challenges. *Composites Part B: Engineering*, *201*, 108376. https://doi.org/10.1016/j.compositesb.2020.108376

Wang, C., Ke, L., Roy Chowdhury, A., Yang, J., Kitipornchai, S., & Fernando, D. (2017). Critical examination of midplane and neutral plane formulations for vibration analysis of fgm beams. *Engineering Structures*, *130*, 275–281. https://doi.org/10.1016/j.engstruct.2016.10.051

Zhang, C., Chen, F., Huang, Z., Jia, M., Chen, G., Ye, Y., Lin, Y., Liu, W., Chen, B., Shen, Q., Zhang, L., & Lavernia, E. J. (2019). Additive manufacturing of functionally graded materials: A review. *Materials Science and Engineering: A*, *764*, 138209. https://doi.org/10.1016/j.msea.2019.138209

Appendix

Program 13- MAIN_LIB.MACLIB (Mac Library)

```
INITIATION!=============================================
/NOPR   ! SUPPRESS PRINTING OF UNDO PROCESS          !||
/PMACRO ! ECHO FOLLOWING COMMANDS TO LOG             !||
FINISH  ! MAKE SURE WE ARE AT BEGIN LEVEL            !||
/CLEAR,NOSTART  ! CLEAR MODEL SINCE NO SAVE FOUND    !||
/TITLE, DISTRIBUTED LOADING OF A BEAM NEW            !||
/PREP7                                               !||
/EOF!===================================================
INPUTDATA!==============================================
L  =  300            ! BEAM LENGTH- X DIRECTION (MM) !||
B  =   15            ! BEAM WIDTH- Y DIRECTION  (MM) !||
H  =   30            ! BEAM THICKNESS- Z DIR.   (MM) !||
EM =   70E+3         ! E METALLIC CONSISTANT(N/MM^2) !||
EC =  380E+3         ! E CERAMIC CONSISTANT(N/MM^2)  !||
NU =    3E-1         ! POISSONS RATIO                !||
N  =    2         ! ELASTICITY VARIATION POWER INDEX !||
BETA =  2   ! ELASTICITY VARIATION EXPONENTIAL INDEX !||
LOAD =  1 ! UNIFORM DISTRIBUTED LATERAL LOAD (N/MM^2)!||
BC =    0 ! BOUNDARY CONDITIONS,                     !||
     ! 0: CLAMPED, 1: CANTILEVER, 2:SIMPLY SUPPORTED !||
NL = 8 ! NUMBER OF ELEMENTS IN THE LENGTH DIRECTION  !||
NB = 2 ! NUMBER OF ELEMENTS IN THE WIDTH DIRECTION   !||
NH = 2 ! NUMBER OF ELEMENTS IN THE THICKN. DIRECTION !||
PI =    4*ATAN(1)    ! THE CONSTANT PI               !||
C = 0  ! OFFSET BETWEEN NEUTRAL AND MIDDLE PLANES    !||
Q1 =    0                                            !||
Q2 =    0                                            !||
Q3 =    0                                            !||
/EOF!===================================================
EZ_FUNCTION!================= E(Z) =========
ZQ = ARG1                                  !||
*IF,N,EQ,0,THEN                           !||
EZ = EC                                    !||
*ELSE                                      !||
```

```
EZ = EM + (EC-EM)*((2*ZQ+H)/(2*H))**N    !||
*ENDIF                                    !||
/EOF!=========================================
EX_FUNCTION!============ E(X) =======
XQ = ARG1                            !||
EX= EM*EXP(BETA*XQ/L)                !||
/EOF!================================
GEOM_MESH!==================
*IF,MODEL,EQ,1,THEN          !||
*USE,LINE_MESH               !||
*ELSEIF,MODEL,EQ,2,THEN      !||
*USE,AREA_MESH               !||
*ELSE                        !||
*USE,VOLUME_MESH             !||
*ENDIF                       !||
/EOF!=======================
BC_LOAD!=================================
*IF,MODEL,EQ,1,THEN                  !||
*USE,BC_LOADS_LINE                   !||
*ELSEIF,MODEL,EQ,2,THEN              !||
*USE,BC_LOADS_AREA                   !||
*ELSE                                !||
*USE,BC_LOADS_VOLUME                 !||
*ENDIF                               !||
/EOF !==================================
SOLVE_PLOT!==================
FINISH                      !||
/SOLU                       !||
ANTYPE,0                    !||
OUTRES,ALL,ALL              !||
SOLVE                       !||
FINISH                      !||
/POST1                      !||
/EFACET,1                   !||
PATH,RESULTSC,2,30,NL*2,    !||
*IF,Q1,EQ,1,THEN            !||
```

```
PPATH,1,0,0,0,0             !||
PPATH,2,0,L,0,0             !||
*USE,SOLVE_PLOT_BEAM        !||
*ENDIF                      !||
*IF,Q2,EQ,1,THEN            !||
PPATH,1,0,0,C,0             !||
PPATH,2,0,L,C,0             !||
*USE,SOLVE_PLOT_2D          !||
*ENDIF                      !||
*IF,Q3,EQ,1,THEN            !||
PPATH,1,0,0,0,C             !||
PPATH,2,0,L,0,C             !||
*USE,SOLVE_PLOT_3D          !||
*ENDIF                      !||
/VIEW,1,,-1+Q2              !||
/ANG,1                      !||
/REP,FAST                   !||
/EOF!=========================
SYMBOLIC_INTEGRATION!================================
! NOTE: - ONLY VALID FOR THE SIMPLE POWER RULE:    !||
!     E(Z)=  EM + (EC-EM)*((2*Z+H)/(2*H))**N       !||
! CALCULATES: IE: INTEGRATION OF E(Z)              !||
!   IZN2E: INTEGRATION OF (Z-C)**2*E(Z)            !||
C = H*(EC-EM)*N/(2*(EC*N+2*EC+EM*N**2+2*EM*N))     !||
IE = H*(EC+EM*N)/(N+1)                             !||
IZN2E_1 = 12*EC**2+EM*N*(4*EC+EM*N)*(7+N*(4+N))    !||
IZN2E_2 = 12*(2+N)**2*(3+N)*(EC+EM*N)              !||
IZN2E = H**3*IZN2E_1/IZN2E_2                       !||
/EOF!=============================================
GAUSSIAN_QUADRATURE!=================================
! VALID FOR z FUNCTION DECLARED IN EZ_FUNCTION    !||
! CALCULATES: IE: INTEGRATION OF E(Z)               !||
!          IZN2E: INTEGRATION OF (Z-C)**2*E(Z)      !||
INTPNTSQTY = 5                                     !||
P0 = 0                          ! 0                !||
P1 = (1/3)*SQRT(5-2*SQRT(10/7)) ! 0.538469310105683 !||
```

```
P2 = (1/3)*SQRT(5+2*SQRT(10/7)) ! 0.906179845938664 !||
W0 = 128/225                    ! 0.568888888888889 !||
W1 = (322+13*SQRT(70))/900      ! 0.478628670499367 !||
W2 = (322-13*SQRT(70))/900      ! 0.236926885056189 !||
*DIM,INTPNTS,ARRAY,INTPNTSQTY,1,1, , ,              !||
*VFILL,INTPNTS,DATA,-P2,-P1,P0,P1,P2                !||
*DIM,INTWTS,ARRAY,INTPNTSQTY,1,1, , ,              !||
*VFILL,INTWTS,DATA,W2,W1,W0,W1,W2                   !||
*USE,RUNINTEGRATIONS                               !||
/EOF!================================================
TRAPEZOID_QUADRATURE!=============================
! VALID FOR z FUNCTION DECLARED IN EZ_FUNCTION  !||
! CALCULATES: IE: INTEGRATION OF E(Z)           !||
!          IZN2E: INTEGRATION OF (Z-C)**2*E(Z)  !||
INTPNTSQTY = NH+1   STEP = 2/NH                 !||
*DIM,INTPNTS,ARRAY,INTPNTSQTY,1,1, , ,          !||
*VFILL,INTPNTS,RAMP,-1,STEP                     !||
*DIM,INTWTS,ARRAY,INTPNTSQTY,1,1, , ,           !||
*VFILL,INTWTS,RAMP,2/NH,0INTWTS(1) = 1/NH       !||
INTWTS(NH+1) = 1/NH                             !||
*USE,RUNINTEGRATIONS                           !||
/EOF!============================================
RUNINTEGRATIONS!=====================================
IE = 0.0                                          !||
IZE = 0.0                                         !||
*DIM,ZS,ARRAY,INTPNTSQTY,1,1, , ,                 !||
*DIM,ES,ARRAY,INTPNTSQTY,1,1, , ,                 !||
*DO,II,1,INTPNTSQTY                               !||
ZS(II) = INTPNTS(II)*H/2                          !||
*USE,EZ_FUNCTION, ZS(II)                          !||
ES(II) = EZIE = IE + ES(II)*INTWTS(II)*H/2        !||
IZE = IZE + ZS(II)*ES(II)*INTWTS(II)*H/2          !||
*ENDDO                                            !||
C = IZE/IE                                        !||
IZN2E = 0.0                                       !||
*DO,II,1,INTPNTSQTY                               !||
```

```
IZN2E =IZN2E+((ZS(II)-C)**2)*ES(II)*INTWTS(II)*H/2 !||
*ENDDO                                             !||
/EOF!=============================================
LINE_MESH!=======================
Q1 = 1                          !||
K,1,0,0                         !||
K,2,L,0                         !||
L,1,2                           !||
ET,1,BEAM189                    !||
ESIZE,,NL                       !||
SECTYPE,1, BEAM, RECT           !||
SECDATA, B,H,NB,NH              !||
SECOFFSET, USER, 0,C,           !||
LMESH,ALL                       !||
LOCAL, 11, 0, 0, 0, 0, 0, 0                        !||
CSYS,  11                                          !||
/ E O F ! = = = = = = = = = = = = = = = = = = = = = = = = = =
A R E A _ M E S H ! = = = = = = = = = = = = = = = = = = = = = = = = = =
Q2 = 1                                             !||
ET,1,PLANE183                                      !||
*USE,  ZMESHING                                    !||
*DO,PJ,1,NH+1                                      !||
*IF,ZPNTS(PJ),NE,ZPNTS(PJ+1),THEN                  !||
RECTNG,0,L,ZPNTS(PJ),ZPNTS(PJ+1)                   !||
*ENDIF                                             !||
*ENDDO                                             !||
MSHAPE,0,2D                                        !||
MSHKEY,1                                           !||
AGLUE,ALL                                          !||
LSEL,S,LOC,X,L/2                                   !||
LESIZE,  ALL,  ,  ,  NL,                           !||
LSEL,S,LOC,X,0                                     !||
LESIZE,  ALL,  ,  ,  NH,                           !||
ALLSEL,ALL                                         !||
AMESH,ALL                                          !||
LOCAL, 11, 0, 0, 0, 0, -90, 0                      !||
```

```
CSYS, 11                                    !||
/EOF!=================================
VOLUME_MESH!==================================
Q3 = 1                                      !||
ET,1,SOLID186                               !||
KEYOPT,1,2,1                                !||
*USE, ZMESHING                              !||
*DO,PJ,1,NH+1                               !||
*IF,ZPNTS(PJ),NE,ZPNTS(PJ+1),THEN           !||
BLOCK,0,L,-B/2,B/2,ZPNTS(PJ),ZPNTS(PJ+1)    !||
*ENDIF                                      !||
*ENDDO                                      !||
MSHAPE,0,3D                                 !||
MSHKEY,1                                    !||
VGLUE,ALL                                   !||
LSEL,S,LOC,X,L/2                            !||
LESIZE, ALL, , , NL,                        !||
LSEL,S,LOC,Y,0                              !||
LESIZE, ALL, , , NB,                        !||
LSEL,S,LOC,Y,B/2                            !||
LSEL,S,LOC,X,0                              !||
LESIZE, ALL, , ,NH,                         !||
ALLSEL,ALL                                  !||
VMESH,ALL                                   !||
LOCAL, 11, 0, 0, 0, 0, 0, 0, 0              !||
CSYS, 11                                    !||
/EOF!=========================================
ZMESHING!============================
STEP = H/NH                          !||
*DIM,ZPNTS,ARRAY,NH+2,1,1, , ,       !||
*VFILL,ZPNTS,DATA,                   !||
EXTFLAG  = 0                         !||
*DO,II,1,NH+1                        !||
ZT = -H/2 + (II-1)*STEP              !||
*IF,ZT,GT,C,AND,ZT-STEP,LE,C,THEN    !||
EXTFLAG = 1                          !||
```

```
ZPNTS(II) = C                        !||
*ENDIF                               !||
ZPNTS(II+EXTFLAG) = ZT               !||
*ENDDO                               !||
/EOF!================================
BC_LOADS_LINE!=========================
DL,ALL,,UY                             !||
*IF,BC,NE,2,THEN                       !||
KSEL,S,LOC,X,0                         !||
*IF,BC,EQ,0,THEN                       !||
KSEL,A,LOC,X,L                         !||
*ENDIF                                 !||
DK,ALL,ALL,0                           !||
*ELSE                                  !||
KSEL,S,LOC,X,0                         !||
KSEL,A,LOC,X,L                         !||
DK,ALL,UZ,0, , , ,UY,ROTX,ROTZ         !||
KSEL,U,LOC,X,L                         !||
DK,ALL,UZ,0, , , ,UX                   !||
*ENDIF                                 !||
ALLSEL,ALL                             !||
SFBEAM,ALL,1,PRES,LOAD*B               !||
/EOF!=================================
BC_LOADS_AREA!===========
LSEL,S,LOC,Z,H/2       !||
SFL,ALL,PRES,LOAD,     !||
*IF,BC,EQ,0,THEN       !||
LSEL,S,LOC,X,0         !||
DL,ALL, ,ALL,          !||
LSEL,S,LOC,X,L         !||
DL,ALL, ,ALL,          !||
*ELSEIF,BC,EQ,1        !||
LSEL,S,LOC,X,0         !||
DL,ALL, ,ALL,          !||
*ELSE                  !||
KSEL,S,LOC,X,0         !||
```

```
KSEL,R,LOC,Z,C          !||
DK, ALL, UY, 0,,, UX                                    !||
KSEL,S,LOC,X,L          !||
KSEL,R,LOC,Z,C          !||
DK, ALL, UY, 0,,,       !||
*ENDIF                  !||
ALLSEL,ALL              !||
/EOF!====================
BC_LOADS_VOLUME!===============
*IF,BC,EQ,0,THEN              !||
ASEL,S,LOC,X,0                !||
DA,ALL,ALL                    !||
ASEL,S,LOC,X,L                !||
DA,ALL,ALL                    !||
*ELSEIF,BC,EQ,1               !||
ASEL,S,LOC,X,0                !||
DA,ALL,ALL                    !||
*ELSE                         !||
KSEL,S,LOC,X,0                !||
KSEL,R,LOC,Z,C                !||
KSEL,R,LOC,Y,B/2              !||
DK,ALL,UY,0                   !||
LSEL,S,LOC,Z,C                !||
LSEL,R,LOC,X,0                !||
DL,ALL, ,UZ,                  !||
DL,ALL, ,UX,                  !||
LSEL,S,LOC,Z,C                !||
LSEL,R,LOC,X,L                !||
DL,ALL, ,UZ,                  !||
*ENDIF                        !||
ASEL,S,LOC,Z,H/2              !||
SFA,ALL,1,PRES,LOAD           !||
ALLSEL,ALL                    !||
/EOF!==========================
SOLVE_PLOT_BEAM!======
PLNSOL, U,Z, 0,1.0                                      !||
```

```
PRNSOL,U,Z                                                    !||
/EOF!=================
SOLVE_PLOT_3D!============
PLNSOL, U,Z, 0,1.0  ~                                         !||
PDEF, ,U,Z,AVG                                                !||
PDEF, ,U,X,AVG                                                !||
PRPATH,UX,UZ                                                  !||
/ E O F ! = = = = = = = = = = = = = = = = = = = = = = = = = = =
SOLVE_PLOT_2D!========
PLNSOL, U,Y, 0,1.0                                            !||
PDEF, ,U,Y,AVG                                                !||
PDEF, ,U,X,AVG                                                 !|
PRPATH,UX,UY                                                  !||
/EOF!=================
```

CHAPTER VIII

FROM ORGANIZATIONAL LEARNING TO MACHINE LEARNING WITH SUPERVISED, UNSUPERVISED AND REINFORCEMENT LEARNING APPROACH

MUSAB TALHA AKPINAR

(Astt. Prof. Dr), Department of Management Information Systems, Business School, Ankara Yildirim Beyazit University, Ankara, Türkiye
e-mail: takpinar@ybu.edu.tr
ORCID: 0000-0003-4651-7788

1. Introduction

From the perspective of organizational learning, the shift towards using machine learning (ML) with supervised, unsupervised, and reinforcement learning approaches can bring several benefits to an organization (Afiouni, 2019).

Supervised learning can be used to improve the efficiency and accuracy of decision-making within an organization by training models on labeled data to make predictions about new, unseen data (Vamathevan and et al., 2019; Senders and et al., 2018; Pourhomayoun & Shakibi, 2021; Jayatilake & Ganegoda, 2021). For example, a supervised learning model could be trained on sales data to predict future sales and help with inventory management.

Unsupervised learning can be used to uncover patterns and structure in an organization's data that might not be immediately obvious (Elman, 1991; Jablonka and et al., 2020; Schleder and et al., 2019; Balasubramanian and et al., 2022). For example, unsupervised learning could be used to discover hidden relationships in customer data that could inform marketing strategy.

Reinforcement learning can be used in decision-making problems that involve interactions with the environment such as resource allocation, game-theory based decision making, and recommendation systems.

Overall, the incorporation of ML with supervised, unsupervised, and reinforcement learning approaches can aid an organization in acquiring, analyzing, and utilizing data more effectively, leading to better decision making and increased efficiency (Saravanan & Sujatha, 2018; Muhammad & Yan, 2015). Furthermore, these techniques can aid organization to be more adaptive, dynamic, resilient to change and uncertainty. However, it is important to note that organizations will also need to invest in data infrastructure, human expertise and coordination, in order to effectively implement and utilize these techniques.

2. Literature review

Organizational learning is the process by which organizations develop the capacity to learn and adapt (Fiol & Lyles, 1985; Schwandt & Marquardt, 1999; Leithwood & Louis; 2021). This can include acquiring new knowledge, improving processes and decision making, and developing the skills and capabilities of employees. Machine learning is a subset of artificial intelligence that involves the use of algorithms and statistical models to enable systems to improve their performance with experience (Goldenberg and et al., 2019; Ghahramani, 2015).

Machine learning can be a powerful tool for organizational learning. For example, organizations can use machine learning to analyze large sets of data and uncover patterns and insights that might not be immediately apparent to human analysts (Kim, 2009). This can help organizations make better decisions, improve their operations, and identify new opportunities for growth and innovation.

Additionally, machine learning can be used to automate routine and repetitive tasks, allowing employees to focus on more complex and challenging work (Chui and et al., 2015; Parker & Grote, 2022; Syed and et al., 2020). This can help organizations build a more skilled and engaged workforce, which can in turn lead to improved performance and competitiveness.

Machine learning (ML) is a type of artificial intelligence that allows systems to automatically improve their performance with experience. There are several different approaches to ML, including supervised learning, unsupervised learning, and reinforcement learning (King, 2009; Kotsiantis and et al., 2007; Zdeborová, 2019; Athey, 2018).

Supervised learning is the most common type of ML, in which a model is trained on a labeled dataset, with the goal of making predictions about new, unseen data (Shokri and et al., 2017). The model is given input-output pairs

(i.e., labeled data) and the algorithm learns to map inputs to their corresponding outputs. The model is then tested on a separate dataset, known as the validation set, to determine its performance on unseen data. Examples include linear and logistic regression, decision tree, and neural networks with backpropagation (Tsochantaridis and et al., 2004).

Unsupervised learning, on the other hand, involves training a model on an unlabeled dataset, with the goal of finding patterns or structure in the data (Libbrecht & Noble, 2015). The model is not given any explicit input-output pairs to learn from, and instead must discover the underlying structure of the data on its own. Examples of unsupervised learning algorithms include k-means clustering, Principal Component Analysis (PCA), and autoencoders (Alkhayrat and et al., 2020).

Reinforcement learning is a type of ML in which a model learns to make decisions by interacting with its environment (Kaelbling et al., 1996). The model is trained to take certain actions in response to different inputs, with the goal of maximizing a reward or minimizing a penalty. Reinforcement learning is often used in decision-making problems, such as playing games or controlling robots (Brunke and et al., 2022).

It's important to note that supervised learning requires labeled data, unsupervised learning requires unlabeled data and reinforcement learning requires interaction with environment (Raina and et al., 2007). Furthermore, there are some algorithms can be applied to multiple type of ML approach and the complexity of algorithm can be increased or decreased based on the size and quality of dataset.

3. Impact of supervised machine learning to organizational learning

Supervised machine learning is a machine learning approach that involves teaching a model using labeled data, with the aim of making predictions on new and unseen data (Sommer & Gerlich, 2013). The algorithm learns to map inputs to their respective outputs based on input-output pairs provided to it. By training models on labeled data to make predictions on new and unseen data, supervised learning can be utilized to enhance the effectiveness and precision of decision-making in organizations (Kourou and et al., 2015).

In the context of organizational learning, supervised machine learning can have a significant impact (Wu and et al., 2021). One major benefit of supervised machine learning is its ability to automate routine and repetitive tasks, freeing up employees to focus on more complex and challenging work (Ramachandran

and et al., 2022). For example, a supervised learning model could be trained on sales data to predict future sales and help with inventory management. This can help organizations build a more skilled and engaged workforce, which can in turn lead to improved performance and competitiveness.

Another benefit of supervised machine learning is its ability to uncover patterns and insights in data that might not be immediately apparent to human analysts (Ma & Sun, 2020). By training models on labeled data, organizations can identify relationships and correlations that might not have been visible to human analysts. This can help organizations make better decisions, improve their operations, and identify new opportunities for growth and innovation.

Supervised machine learning can also be used to improve the accuracy and efficiency of decision-making processes within an organization (Nieto and et al., 2019). By training models on labeled data, organizations can develop predictive models that can be used to make more accurate and informed decisions. For example, a supervised learning model could be trained on customer data to predict which customers are most likely to churn, allowing organizations to take proactive measures to retain those customers (Ahmad and et al., 2019). However, there are also challenges associated with the use of supervised machine learning in organizational learning. One of the main challenges is the need for high-quality, labeled data. In order to train models effectively, organizations must have access to large amounts of high-quality data that has been labeled correctly. This can be a significant challenge, particularly for organizations that are just beginning to incorporate machine learning into their operations.

Another challenge is the need for specialized expertise. Developing and deploying effective machine learning models requires specialized expertise in areas such as data science, statistics, and computer programming (Amershi and et al., 2019). Many organizations may not have the necessary expertise in-house and may need to hire external consultants or contractors to assist with model development and deployment. In addition, there are also ethical and legal considerations associated with the use of supervised machine learning in organizational learning. For example, organizations must ensure that their models are not biased or discriminatory, and that they are not violating any privacy or data protection laws. Failure to comply with these regulations can result in significant legal and reputational consequences (Cheatham and et al., 2019).

Overall, the impact of supervised machine learning on organizational learning is significant. It has the potential to automate routine tasks, uncover

insights in data, and improve the accuracy and efficiency of decision-making processes. However, organizations must be aware of the challenges associated with incorporating supervised machine learning into their operations, including the need for high-quality data, specialized expertise, and compliance with ethical and legal regulations. By addressing these challenges, organizations can unlock the full potential of supervised machine learning and improve their performance and competitiveness.

4. Impact of unsupervised machine learning to organizational learning

Unsupervised machine learning is a subset of machine learning where the algorithm learns patterns in the data without any explicit guidance or labeled examples (Nwanganga & Chapple, 2020). Unlike supervised learning, unsupervised learning is not given a target output, but rather it tries to identify underlying patterns or structures in the data itself. The impact of unsupervised machine learning on organizational learning can be significant.

One of the most significant impacts of unsupervised machine learning on organizational learning is the ability to uncover hidden patterns or structures within large datasets (Zhou and et al., 2017). This is particularly useful for companies that collect large amounts of data but struggle to make sense of it. Unsupervised machine learning algorithms can analyze the data, identify patterns, and group similar data points together (Sarker, 2021). This can lead to new insights and understanding of the data, which can inform business decisions and improve organizational performance. Another important impact of unsupervised machine learning on organizational learning is its ability to identify anomalies or outliers in the data (Al-amri and et al., 2021). This is particularly useful in industries where safety or security is a concern. Unsupervised machine learning algorithms can identify unusual patterns in the data, which may indicate a safety or security breach. This can help organizations respond quickly to potential threats and prevent them from causing harm.

Unsupervised machine learning can also be used for clustering, which is the process of grouping similar data points together based on their characteristics (Wang and et al., 2023). This can be useful for identifying customer segments or for personalized marketing. By grouping customers based on their behavior or preferences, organizations can tailor their marketing messages and offers to specific groups, which can increase sales and customer satisfaction (Alzoubi and et al., 2022). Furthermore, unsupervised machine learning can help organizations automate processes that would otherwise be too time-consuming or difficult

to do manually. For example, unsupervised machine learning algorithms can be used to classify and organize large amounts of text data, such as customer feedback or social media posts. This can help organizations identify trends and sentiment around their products or services, which can inform business decisions and improve customer experience.

In summary, the impact of unsupervised machine learning on organizational learning is significant. By uncovering hidden patterns and structures within large datasets, identifying anomalies or outliers, clustering similar data points, and automating processes, organizations can gain new insights and understanding of their data. This can inform business decisions, improve organizational performance, and ultimately lead to a competitive advantage.

5. Impact of reinforcement learning to organizational learning

Reinforcement learning (RL) is a type of machine learning in which an algorithm learns to make decisions by interacting with its environment and receiving feedback in the form of rewards or penalties (Shin and et al., 2019). In RL, an agent learns by trial and error, improving its decision-making capabilities over time through continuous learning (Hook and et al., 2021). The impact of RL on organizational learning can be significant, particularly in industries that involve complex decision-making processes. For example, in the finance industry, RL can be used to optimize investment strategies or to identify and manage risk.

One of the primary benefits of RL in organizational learning is its ability to enable autonomous decision-making (Weiner and et al., 2021). With RL, an agent can learn to make decisions on its own, without the need for human intervention (Zhu and et al., 2020). This can be particularly useful in industries that require fast decision-making or that involve high-risk situations, such as emergency response or military operations. Another benefit of RL in organizational learning is its ability to adapt to changing environments (Sturm and et al., 2021). RL algorithms are designed to learn from experience, which means that they can adapt to changes in their environment and adjust their decision-making accordingly. This adaptability is particularly useful in industries that are subject to rapid change, such as technology or healthcare.

One potential downside of RL in organizational learning is the potential for unintended consequences (Nian and et al., 2020). Because RL agents learn by trial and error, they may make decisions that have unintended consequences,

particularly if the reward or penalty structure is not well-designed. In some cases, this can lead to suboptimal decision-making or even ethical issues. To mitigate these risks, it is important to carefully design the reward or penalty structure for RL agents. Additionally, human oversight and intervention may be necessary to ensure that RL agents are making decisions that align with organizational values and goals (Leike and et al., 2018).

Overall, the impact of RL on organizational learning is significant and growing. As RL technology continues to advance, it is likely that more and more industries will begin to adopt it as a way to optimize decision-making and improve performance. However, as with any technology, it is important to carefully consider the potential benefits and risks before implementing RL in organizational learning.

6. Conclusion

In conclusion, machine learning has brought new methods for managing knowledge and has the potential to significantly impact organizational learning (Tortorella and et al., 2020). The three types of machine learning - supervised, unsupervised, and reinforcement learning - each have their own unique strengths and can be used to improve decision-making, uncover patterns and relationships in data, and enable systems to learn from experience. Incorporating machine learning with these approaches can aid organizations in acquiring, analyzing, and utilizing data more effectively, leading to better decision-making and increased efficiency (Sarker, 2021; Ahmed and et al., 2020). However, it is important for organizations to invest in data infrastructure, human expertise, and coordination to effectively implement and utilize these techniques. Overall, the integration of machine learning with organizational learning has the potential to make organizations more adaptive, dynamic, and resilient to change and uncertainty. The shift from organizational learning to machine learning (ML) can bring several benefits to an organization (Beer and et al., 2005).

- ML allows organizations to process and analyze large amounts of data quickly and accurately, which can lead to better decision-making and increased efficiency. For example, an ML model could be trained on past customer data to predict future behavior and inform marketing strategy.
- ML can also help organizations identify patterns and relationships in data that might not be immediately obvious to human analysts, leading to new insights and opportunities.

• Additionally, ML can help organizations automate tasks that would be time-consuming or difficult for humans to perform, such as image or speech recognition, natural language processing and anomaly detection.

• Furthermore, ML can aid organizations in being more adaptive to change, dynamic and resilient to uncertainty, by providing real-time analytics, prediction, and decision-making capabilities.

• However, it is important to note that in order for organizations to effectively implement and utilize ML, they will need to invest in data infrastructure, human expertise and coordination. Furthermore, the ethical and legal aspect of ML usage and the potential impact on workforce should be taken into consideration as well.

In summary, the shift from organizational learning to machine learning can bring significant benefits to an organization, but requires significant investments in data infrastructure, human expertise and coordination in order to effectively implement and utilize these techniques.

7. Future Studies

There are also areas in which machine learning can be applied to measure, assess, and improve organizational learning. One way can be using ML models to predict the performance of an employee, team or organization and using the prediction to assess the potential impact of different learning and development initiatives (Hong and et al., 2020; Fallucchi and et al., 2020). Another way is the use of natural language processing (NLP) to extract insights from unstructured data, such as emails, chat logs, and social media posts, to understand employee attitudes and feedback about organizational learning and development initiatives.

It's also worth to mention, that although ML can be a powerful tool for organizational learning, it's not a panacea and it's important for organizations to have a clear understanding of the limits and potential biases of the models they are using and have a clear plan for addressing these concerns (March & Olsen, 1975).

Here are some suggestions for further studies that could be conducted on this topic, specifically focusing on organizations:

• Investigate the impact of specific organizational structures and policies on employee burnout rates. For example, compare the burnout rates of employees working in hierarchical organizations versus those working in more democratic, flat structures.

• Examine the effectiveness of various burnout prevention strategies implemented by organizations, such as providing mental health resources, implementing flexible work schedules, and offering employee wellness programs.

• Conduct research on the relationship between leadership styles and employee burnout. For example, study the differences in burnout rates among employees whose managers exhibit transactional leadership behaviors (rewarding or punishing based on performance) versus those whose managers exhibit transformational leadership behaviors (inspiring and motivating employees to achieve their best).

• Explore the impact of organizational culture on employee burnout rates. Research could investigate how cultures that prioritize work-life balance and employee well-being compare to those that prioritize productivity and long work hours.

• Analyze the role of technology in contributing to or preventing employee burnout. Specifically, research could examine how organizations can use technology to promote work-life balance, reduce employee stress, and improve overall job satisfaction.

These are just a few potential areas of research that could be pursued to further understand the relationship between organizations and employee burnout. By investigating these topics, organizations can better understand how to support their employees and promote a healthy work environment.

8. Reference

Afiouni, R. (2019). Organizational learning in the rise of machine learning.

Ahmad, A. K., Jafar, A., & Aljoumaa, K. (2019). Customer churn prediction in telecom using machine learning in big data platform. Journal of Big Data, 6(1), 1-24.

Ahmed, Z., Mohamed, K., Zeeshan, S., & Dong, X. (2020). Artificial intelligence with multi-functional machine learning platform development for better healthcare and precision medicine. Database, 2020.

Al-amri, R., Murugesan, R. K., Man, M., Abdulateef, A. F., Al-Sharafi, M. A., & Alkahtani, A. A. (2021). A review of machine learning and deep learning techniques for anomaly detection in IoT data. Applied Sciences, 11(12), 5320.

Alkhayrat, M., Aljnidi, M., & Aljoumaa, K. (2020). A comparative dimensionality reduction study in telecom customer segmentation using deep learning and PCA. Journal of Big Data, 7, 1-23.

Alzoubi, H., Alshurideh, M., Kurdi, B., Akour, I., & Aziz, R. (2022). Does BLE technology contribute towards improving marketing strategies, customers' satisfaction and loyalty? The role of open innovation. International Journal of Data and Network Science, 6(2), 449-460.

Amershi, S., Begel, A., Bird, C., DeLine, R., Gall, H., Kamar, E., ... & Zimmermann, T. (2019, May). Software engineering for machine learning: A case study. In 2019 IEEE/ACM 41st International Conference on Software Engineering: Software Engineering in Practice (ICSE-SEIP) (pp. 291-300). IEEE.

Athey, S. (2018). The impact of machine learning on economics. In The economics of artificial intelligence: An agenda (pp. 507-547). University of Chicago Press.

Balasubramanian, N., Ye, Y., & Xu, M. (2022). Substituting human decision-making with machine learning: Implications for organizational learning. Academy of Management Review, 47(3), 448-465.

Beer, M., Voelpel, S. C., Leibold, M., & Tekie, E. B. (2005). Strategic management as organizational learning: Developing fit and alignment through a disciplined process. Long Range Planning, 38(5), 445-465.

Brunke, L., Greeff, M., Hall, A. W., Yuan, Z., Zhou, S., Panerati, J., & Schoellig, A. P. (2022). Safe learning in robotics: From learning-based control to safe reinforcement learning. Annual Review of Control, Robotics, and Autonomous Systems, 5, 411-444.

Carleo, G., Cirac, I., Cranmer, K., Daudet, L., Schuld, M., Tishby, N., ... & Zdeborová, L. (2019). Machine learning and the physical sciences. Reviews of Modern Physics, 91(4), 045002.

Cheatham, B., Javanmardian, K., & Samandari, H. (2019). Confronting the risks of artificial intelligence. McKinsey Quarterly, 2(38), 1-9.

Chui, M., Manyika, J., & Miremadi, M. (2015). Four fundamentals of workplace automation. McKinsey Quarterly, 29(3), 1-9.

Elman, J. L. (1991). Distributed representations, simple recurrent networks, and grammatical structure. Machine learning, 7(2), 195-225.

Fallucchi, F., Coladangelo, M., Giuliano, R., & William De Luca, E. (2020). Predicting employee attrition using machine learning techniques. Computers, 9(4), 86.

Fiol, C. M., & Lyles, M. A. (1985). Organizational learning. Academy of management review, 10(4), 803-813.

Ghahramani, Z. (2015). Probabilistic machine learning and artificial intelligence. Nature, 521(7553), 452-459.

Goldenberg, S. L., Nir, G., & Salcudean, S. E. (2019). A new era: artificial intelligence and machine learning in prostate cancer. Nature Reviews Urology, 16(7), 391-403.

Hong, X., Lin, X., Fang, L., Gao, Y., & Li, R. (2022). Application of machine learning models for predictions on cross-border merger and acquisition decisions with ESG characteristics from an ecosystem and sustainable development perspective. Sustainability, 14(5), 2838.

Hook, J., El-Sedky, S., De Silva, V., & Kondoz, A. (2021). Learning data-driven decision-making policies in multi-agent environments for autonomous systems. Cognitive Systems Research, 65, 40-49.

Jablonka, K. M., Ongari, D., Moosavi, S. M., & Smit, B. (2020). Big-data science in porous materials: materials genomics and machine learning. Chemical reviews, 120(16), 8066-8129.

Jayatilake, S. M. D. A. C., & Ganegoda, G. U. (2021). Involvement of machine learning tools in healthcare decision making. Journal of Healthcare Engineering, 2021.

Kaelbling, L. P., Littman, M. L., & Moore, A. W. (1996). Reinforcement learning: A survey. Journal of artificial intelligence research, 4, 237-285.

Kim, D. H. (2009). The link between individual and organizational learning. In The strategic management of intellectual capital (pp. 41-62). Routledge.

King, D. E. (2009). Dlib-ml: A machine learning toolkit. The Journal of Machine Learning Research, 10, 1755-1758.

Kotsiantis, S. B., Zaharakis, I., & Pintelas, P. (2007). Supervised machine learning: A review of classification techniques. Emerging artificial intelligence applications in computer engineering, 160(1), 3-24.

Kourou, K., Exarchos, T. P., Exarchos, K. P., Karamouzis, M. V., & Fotiadis, D. I. (2015). Machine learning applications in cancer prognosis and prediction. Computational and structural biotechnology journal, 13, 8-17.

Leike, J., Krueger, D., Everitt, T., Martic, M., Maini, V., & Legg, S. (2018). Scalable agent alignment via reward modeling: a research direction. arXiv preprint arXiv:1811.07871.

Leithwood, K., & Louis, K. S. (2021). Organizational learning in schools: An introduction. In Organizational learning in schools (pp. 1-14). Taylor & Francis.

Libbrecht, M. W., & Noble, W. S. (2015). Machine learning applications in genetics and genomics. Nature Reviews Genetics, 16(6), 321-332.

Ma, L., & Sun, B. (2020). Machine learning and AI in marketing–Connecting computing power to human insights. International Journal of Research in Marketing, 37(3), 481-504.

March, J. G., & Olsen, J. P. (1975). The uncertainty of the past: Organizational learning under ambiguity. European journal of political research, 3(2), 147-171.

Muhammad, I., & Yan, Z. (2015). SUPERVISED MACHINE LEARNING APPROACHES: A SURVEY. ICTACT Journal on Soft Computing, 5(3).

Nian, R., Liu, J., & Huang, B. (2020). A review on reinforcement learning: Introduction and applications in industrial process control. Computers & Chemical Engineering, 139, 106886.

Nieto, Y., Gacía-Díaz, V., Montenegro, C., González, C. C., & Crespo, R. G. (2019). Usage of machine learning for strategic decision making at higher educational institutions. IEEE Access, 7, 75007-75017.

Nwanganga, F., & Chapple, M. (2020). Practical machine learning in R. John Wiley & Sons.

Parker, S. K., & Grote, G. (2022). Automation, algorithms, and beyond: Why work design matters more than ever in a digital world. Applied Psychology, 71(4), 1171-1204.

Pourhomayoun, M., & Shakibi, M. (2021). Predicting mortality risk in patients with COVID-19 using machine learning to help medical decision-making. Smart Health, 20, 100178.

Raina, R., Battle, A., Lee, H., Packer, B., & Ng, A. Y. (2007, June). Self-taught learning: transfer learning from unlabeled data. In Proceedings of the 24th international conference on Machine learning (pp. 759-766).

Ramachandran, K. K., Mary, A. A. S., Hawladar, S., Asokk, D., Bhaskar, B., & Pitroda, J. R. (2022). Machine learning and role of artificial intelligence in optimizing work performance and employee behavior. Materials Today: Proceedings, 51, 2327-2331.

Saravanan, R., & Sujatha, P. (2018, June). A state of art techniques on machine learning algorithms: a perspective of supervised learning approaches in data classification. In 2018 Second International Conference on Intelligent Computing and Control Systems (ICICCS) (pp. 945-949). IEEE.

Sarker, I. H. (2021). Machine learning: Algorithms, real-world applications and research directions. SN computer science, 2(3), 160.

Schleder, G. R., Padilha, A. C., Acosta, C. M., Costa, M., & Fazzio, A. (2019). From DFT to machine learning: recent approaches to materials science–a review. Journal of Physics: Materials, 2(3), 032001.

Schwandt, D., & Marquardt, M. J. (1999). Organizational learning. CRC Press.

Senders, J. T., Staples, P. C., Karhade, A. V., Zaki, M. M., Gormley, W. B., Broekman, M. L., ... & Arnaout, O. (2018). Machine learning and neurosurgical outcome prediction: a systematic review. World neurosurgery, 109, 476-486.

Shin, J., Badgwell, T. A., Liu, K. H., & Lee, J. H. (2019). Reinforcement learning–overview of recent progress and implications for process control. Computers & Chemical Engineering, 127, 282-294.

Shokri, R., Stronati, M., Song, C., & Shmatikov, V. (2017, May). Membership inference attacks against machine learning models. In 2017 IEEE symposium on security and privacy (SP) (pp. 3-18). IEEE.

Sommer, C., & Gerlich, D. W. (2013). Machine learning in cell biology–teaching computers to recognize phenotypes. Journal of cell science, 126(24), 5529-5539.

Stevens, L. M., Mortazavi, B. J., Deo, R. C., Curtis, L., & Kao, D. P. (2020). Recommendations for reporting machine learning analyses in clinical research. Circulation: Cardiovascular Quality and Outcomes, 13(10), e006556.

Sturm, T., Gerlach, J. P., Pumplun, L., Mesbah, N., Peters, F., Tauchert, C., ... & Buxmann, P. (2021). Coordinating Human and Machine Learning for Effective Organizational Learning. MIS Quarterly, 45(3).

Syed, R., Suriadi, S., Adams, M., Bandara, W., Leemans, S. J., Ouyang, C., ... & Reijers, H. A. (2020). Robotic process automation: contemporary themes and challenges. Computers in Industry, 115, 103162.

Tortorella, G. L., Vergara, A. M. C., Garza-Reyes, J. A., & Sawhney, R. (2020). Organizational learning paths based upon industry 4.0 adoption: An empirical study with Brazilian manufacturers. International Journal of Production Economics, 219, 284-294.

Tsochantaridis, I., Hofmann, T., Joachims, T., & Altun, Y. (2004, July). Support vector machine learning for interdependent and structured output spaces. In Proceedings of the twenty-first international conference on Machine learning (p. 104).

Vamathevan, J., Clark, D., Czodrowski, P., Dunham, I., Ferran, E., Lee, G., ... & Zhao, S. (2019). Applications of machine learning in drug discovery and development. Nature reviews Drug discovery, 18(6), 463-477.

Wang, H., Feil, J. H., & Yu, X. (2023). Let the data speak about the cut-off values for multidimensional index: Classification of human development index with machine learning. Socio-Economic Planning Sciences, 101523.

Weiner, J., Francois, C., Stone-Johnson, C., & Childs, J. (2021, January). Keep safe, keep learning: principals' role in creating psychological safety and organizational learning during the COVID-19 pandemic. In Frontiers in Education (Vol. 5, p. 618483). Frontiers Media SA.

Wu, X., Zheng, W., Chen, X., Zhao, Y., Yu, T., & Mu, D. (2021). Improving high-impact bug report prediction with combination of interactive machine learning and active learning. Information and Software Technology, 133, 106530.

Zhou, L., Pan, S., Wang, J., & Vasilakos, A. V. (2017). Machine learning on big data: Opportunities and challenges. Neurocomputing, 237, 350-361.

Zhu, H., Yu, J., Gupta, A., Shah, D., Hartikainen, K., Singh, A., ... & Levine, S. (2020). The ingredients of real-world robotic reinforcement learning. arXiv preprint arXiv:2004.12570.